NIWA
Taihoro Nukurangi

Seabird distribution modelling for the 2025 southern hemisphere spatially explicit fisheries risk assessment

Prepared for Shearwater Analytics Ltd.

May 2025

Climate, Freshwater & Ocean Science

Prepared by:
Jennifer Devine

For any information regarding this report please contact:

Jennifer Devine
Fisheries, senior scientist

+64 3 545 7880
jennifer.devine@niwa.co.nz

National Institute of Water & Atmospheric Research Ltd
PO Box 893
Nelson 7040

Phone +64 3 548 1715

NIWA CLIENT REPORT No: 2025159NE
Report date: May 2025
NIWA Project:

Revision	Description	Date
Version 0.1	Draft in preparation/in review	26 May 2025
Version 1.0	Final version sent to client	10 June 2025

Quality Assurance Statement		
	Reviewed by:	Darren Stevens
	Formatting checked by:	Victoria McIntyre
	Approved for release by:	Richard O'Driscoll

Contents

Executive summary

This report updates the distribution maps for sixteen albatross and petrel taxa (Table 1) for the 2025 spatially explicit fisheries risk assessment model (SEFRA) for the CCSBT pelagic longline fisheries on seabirds.

Tracking data for most species were requested from individual data owners via Bird Life International; some tracking data were also received directly from the New Zealand Department of Conservation (DOC). A review of the original distribution maps by world experts identified key tracking datasets to be added and emphasis was given to obtaining those, with mixed success. This update to the models weighted the relative densities by mean colony size, which improved the distributions for all species.

Seabird data distributions were determined using spatial generalised additive models (GAMs) that included a 3-dimensional spatiotemporal spline model, which smoothed simultaneously across position and date, fitted with a Tweedie distribution, where the estimated Tweedie parameter was between 1–2, indicating a compound Poisson-gamma distribution. All models explained between 67–91% of the deviance. Weighting the tracks directly by colony size produced better fits (in terms of deviance explained and residual patterns) than models that did not include weighting. This approach is also preferred on a theoretical basis, by reducing bias in observed distributions at a population level resulting from differing levels of tracking data at a colony level. The models fit by including colony size as an offset, weighting each observation's contribution to the likelihood, or by including colony name as an additional factor in the model produced much poorer fits than directly scaling the relative density by mean colony size, i.e., residual patterns were worse and extreme densities were predicted at the margins of the modelled spatial range (e.g. where no data existed).

Tracking data were not obtained for all the major breeding colonies for six of the assessed seabird taxa. For some of these colonies, quarterly predictions of spatial count were available from the study by Carneiro et al. (2020). The colonies that needed augmentation made up 20% of the population for Sooty albatross (Tristan da Cunha) and Atlantic yellow-nosed albatross (Gough), while size of the colonies for the other four species ranged between 1–11% of the total population.

1 Background

This report updates the distribution maps for sixteen albatross and petrel taxa (Table 1) for the 2025 spatially explicit fisheries risk assessment model (SEFRA) for the CCSBT pelagic longline fisheries on seabirds.

Table 1: Albatross and petrel taxa updated for the 2025 risk assessment.

Common name	Scientific name
Gibson's albatross	*Diomedea antipodensis gibsoni*
Wandering albatross	*Diomedea exulans*
Southern royal albatross	*Diomedea epomophora*
Atlantic yellow-nosed albatross	*Thalassarche chlororhynchos*
Black-browed albatross	*Thalassarche melanophris*
Campbell black-browed albatross	*Thalassarche impavida*
Shy albatross	*Thalassarche cauta*
Grey-headed albatross	*Thalassarche chrysostoma*
Southern Buller's albatross	*Thalassarche bulleri bulleri*
Northern Buller's albatross	*Thalassarche bulleri platei*
Sooty albatross	*Phoebetria fusca*
Light-mantled sooty albatross	*Phoebetria palpebrata*
Grey petrel	*Procellaria cinerea*
Black petrel	*Procellaria parkinsoni*
Westland petrel	*Procellaria westlandica*
White-chinned petrel	*Procellaria aequinoctialis*

2 Methods

2.1 Tracking data

Tracking data for most species in Table 1 were requested from individual data owners via Bird Life International; some tracking data were also received directly from the New Zealand Department of Conservation (DOC) (Table 2). A review of the original distribution maps (unpublished) by world experts identified key tracking datasets to be added and emphasis was given to obtaining those, with mixed success. Because the risk assessment model is currently only for adult birds, irrespective of breeding status, tracking data were included only for adults or where life stage was not known.

2.2 Data grooming

Tracking data were groomed following methods similar to those by Carneiro et al. (2020). Gaps exceeding 24 hours were discarded by splitting the deployment into separate tracks. Each track was interpolated regularly in time to obtain points that were equally spaced. Any points falling on land or where speed of bird was in excess of 100 km per hour were removed. Tracks that incorrectly crossed the 180° or 360° line were manually corrected. All points were then reassigned positions within a 0.25° lat-lon grid cell.

Each track was handled individually. Because different tag types report data differently and to ensure tag type did not have influence on the model, each point along the track was weighted by the time between reports (half the time from the previous observation + half the time to the next observation). Weighted observations were converted from time in seconds to days. This then produced a weighted count per day per track for a given 0.25° lat-lon grid cell and a given month. This weighting did not remove issues that may occur if a tag type lasts longer, i.e., tracks with longer time series will have more data. The observations in a cell were then summed and divided by the number of days spent in that cell in that month. Values were then standardised by dividing by the mean (values were between 0 and 1). The relative density of each track was than weighted by the mean colony size (average number of breeding pairs) (Table 3), noting that various methods of weighting the relative densities by colony size both within the spatial models (i.e., weighting each observation's contribution to the likelihood) or by directly weighting the data (as done here) were assessed for best fit before applying the chosen weighting method. If only one colony was present, data were not weighted by mean colony size (e.g., Campell black-browed albatross, Westland petrel).

After each track was standardised, all values for all tracks in each cell and month were summed to create a relative density of birds in each 0.25° lat-lon grid cell for a given month. By standardising each track prior to aggregating, the characteristics of a few, such as those birds that behaved differently, did not dominate in the model. Using standardised mean weighted counts eliminated the need to include a random effect in the model, which greatly sped up computation time, a necessity with the number of birds and lat-lon cells that were modelled.

Data were autocorrelated because each observation in a track was not independent (an observation at time *t* was correlated to the observation at *t*-1), but each complete track was treated independently (i.e., each bird behaved independently).

2.3 Spatial models

Seabird data distributions were determined using spatial generalised additive models (GAMs) that included a 3-dimensional tensor product smoother that smooths simultaneously across a location (latitude and longitude) and time (month). Smoother specifications treat space and time as being dissimilar, by using different smoothing parameters to push the 2-dimensional spatial smoother through time, where the smoother on the time component is fit with a cubic regression spline (see Marra et al. 2011). The temporal spline was specified to treat December and January as if they were next to each other in time; hence, the predicted smoother was constrained in December to be near the predicted smoother in January. The spatial smoother (the 2-dimensional smooth on latitude and longitude) was fit using a Gaussian process (gp) smoother because it can deal with spatial autocorrelation better than most other types of smoothers, while still varying smoothly within the space dimension (Marra et al. 2011); cyclic smoothers for the spatial component may sometimes cause problems and result in poor fits, with no structure (Wood 2017). When distributions needed to wrap around the world, a cyclic smooth on longitude was often found to be a better fit.

Models were fitted to tracking data aggregated to a 1-degree cell resolution using the '*bam*' function within the *mgcv* R package (Wood 2003, 2017) and a Tweedie distribution. Tweedie distributions are a subfamily of exponential dispersion models that have the ability to replicate a wide range of distributions via the power function and were preferred because they perform well when fitting to data that are positive, continuous, and contain many zero observations (Jørgensen 1987). Tweedie distributions, model fits, residual patterns, percentage deviance explained, plots of partial fits, and relative importance of parameters were inspected, and the best model was chosen. Longitude was typically in 0° to 360° space to keep positions crossing 180° near to each other, unless otherwise specified. For birds that had a circumpolar distribution, the spatial spline was specified to wrap around the globe, i.e., treat 0° and 360° near to each other in space.

Expected densities were predicted into a 1-degree cell resolution spatial grid for each month, but often extremely small values were predicted at the margins of the distribution, which caused e.g., densities to be predicted across continental boundaries where species were known not to occur, such as across the southern tip of South America. A soap film smoother was tested, which distorts the film towards the data of highest occurrence; these smooths were constructed to not cross boundary features, such as continents. However, this did not fully resolve the issue. A manual soap film boundary was thus constructed, where values that were less than the 40th percentile were set to 0 (values were less than 10^{-5}). Data were then aggregated at a 5 ° lat-lon resolution. To remove data where only a few 1 ° lat-lon cells contributed to the 5 ° lat-lon cell, densities below the 40th percentile were again set to 0. This resolved issues at the margins of the predicted distribution, such that predictions did not cross continents.

Tracking data were not obtained for all the major breeding colonies of all the assessed seabird taxa (Table 3). For some of these colonies, quarterly predictions of spatial count were available from the study by Carneiro et al. (2020). For many taxa, the predictions of Carneiro et al. (2020) were representative of juveniles as well as at-sea foraging adults, whereas the current analysis was based on adult data, although Carneiro et al. (2020) 'noted that the spatial foraging patterns of each age stage were often not very different'. The Carneiro et al. (2020) study reported that their predictions were representative of density, but from closer inspection they were representative of mean count per 5-degree grid cell (i.e., not accounting for the area of each cell) and, so, were in a comparable format to the spatial predictions from the current study.

As such, it was decided to use the Carneiro et al. (2020) spatial predictions to plug some of the gaps in tracking data by colony (Table 3). This was achieved by merging the predictions from the current study with those of Carneiro et al. (2020) after these had first been rescaled for colony size based on the most recent estimate of breeding pairs. For each species for which the Carneiro et al. (2020) layers were used, this was achieved as follows:

1. Reproject the Carneiro layers to match the projection used for making predictions in the current study (coordinate reference system = "+proj=laea +lat_0=-90 +lon_0=170").

2. Rescale the layers from Carneiro et al. (2020) and the current study to sum to the total estimated adult population size for the respective colony, calculated as the total number of breeding pairs for the colony.

3. For each month, sum all rasters across all colonies for which there was a prediction from Carneiro et al. (2020) or from the current study. As per the description given by Carneiro et al. (2020) for which the layers were for quarterly periods, the summer prediction was used for the months of December, January and February, autumn = March, April and May, winter = June, July and August, and spring = September, October and November.

4. Rescale the monthly rasters so that each sums to 1.

3 Results

3.1 Tracking data

Tracking data were obtained for many of the main breeding colonies for most of the 16 species (Tables 2–3). The amount of data received was an improvement over the previous distribution maps (Devine et al. in press), where some missing colonies made up to 58% of the breeding pairs. Spatial predictions from Carneiro et al. (2020) augmented the predicted distributions of six species. Augmentation was because data from breeding colonies were missing for Gibson's albatross (Auckland Islands), grey-headed albatross (PEI), light-mantled albatross (PEI), and sooty albatross (PEI), while information on the remaining colonies was missing for only some of the months. The information used from Carneiro et al. (2020) for Sooty albatross (Tristan da Cunha) and Atlantic yellow-nosed albatross (Gough) made up 20% of the breeding pairs, while the size of the colonies for the other four species ranged between 1–11% (Table 3).

Table 2: Information on tracking data obtained, including number of datasets used (of those available in BirdLife International), the dataset identification number, and number of tracks per colony and life stage. Track duration is the mean (standard deviation) in hours; NA indicates not enough data to estimate. Note that while permission to data had been granted, not all data were included in the modelling but are included here for full transparency. Temporal coverage does not include information from juvenile or immature birds. PEI refers to Prince Edward Island. Juv indicates juvenile, Imm indicates immature.

Common name	No. used	Dataset id by site	No. tracks by life stage	No. tracks per colony	Track duration (hrs)	Temporal coverage
Gibson's albatross	3[†]	Adams: DOC[†]	Adult: 41 Juvenile: 22	Adams: 63	Adult: 3262 (1576) Juvenile: 6427 (2248)	January–September
Wandering albatross	43 (of 45)	Kerguelen: 435, 1318, 1320 Crozet: 436, 437, 1133, 1134, 1135, 1136, 1137, 1138, 1319, 1321, 1322 South Georgia: 460, 461, 462, 463, 473, 1387, 1394, 1395, 1405, 1885, 1888, 1889, 1890, 1891, 1892, 1893, 1895, 1896, 2005, 2006, 2272 Macquarie: 412 Marion Island (PEI): 465, 1513, 1516, 1517, 1528, 2210 Non-breeding/site unknown: 464	Adult: 1766 Unknown: 4 Fledgling: 19 Juvenile: 78 Immature: 115 Juv/Imm: 13	Iles Kerguelen: 89 Iles Crozet: 636 Ile de la Possession: 13 Bird Island (SGSSI): 1089 Marion Island: 153 Macquarie Island: 8 Non-breeding/site unknown: 7	Adult: 1741 (4035) Unknown: 451 (208) Fledgling: 5801 (3462) Juvenile: 2502 (2425) Immature: 3908 (3361) Juv/Imm: 4040 (2050)	Iles Kerguelen: all months Iles Crozet: all months Ile de la Possession: NA Bird Island (SGSSI): all months Marion Island: Jan–Sept Macquarie Island: Dec–Mar Non-breeding/site unknown: Aug–Dec
Southern royal albatross	4 (of 4)	Campbell Islands: 431, 556, 2246, 2266	Adult: 56 Unknown: 10	Campbell: 66	Adult: 171501 (129635) Unknown: 296 (89)	All months
Atlantic yellow-nosed albatross	9 (of 10)	At sea: 1412, 1560 Gough Island: 700, 1103, 1104, 1455 Inaccessible Island: 1506 Nightingale: 1105, 1504	Adult: 128 Unknown: 7 Immature: 3	At sea: 11 Gough Island: 81 Inaccessible Island: 18 Nightingale: 28	Adult: 585 (438) Unknown: 350 (335) Immature: 787 (796)	At sea: Oct–May Gough Island: Oct–Jan Inaccessible Island: Oct–Nov Nightingale: Oct–Nov
Grey-headed albatross	21 (of 26)	Marion Island/PEI: 1508, 1509, 1514, 1515, 1527, 2208 Islas Ildefonso: 485 Campbell Islands: 430, 1082, 2173 Islas Diego Ramirez: 484, 486 South Georgia: 459, 494, 495, 1383, 1390, 1391, 1845 Macquarie Island: 409, 496	Adult: 782 Juvenile: 28 Fledgling: 1	Bird Island: 451 Campbell Island: 91 Islas Diego Ramirez: 67 Islas Ildefonso: 1 Macquarie Island: 10 Marion Island: 191	Adult: 1689 (4375) Juvenile: 1870 (1314) Fledgling: 1228 (NA)	Bird Island: all months Campbell Island: all months Islas Diego Ramirez: Nov –Feb Islas Ildefonso: November Macquarie Island: Nov –Jan Marion Island: all months

Common name	No. used	Dataset id by site	No. tracks by life stage	No. tracks per colony	Track duration (hrs)	Temporal coverage
Southern Buller's albatross	3	Solander: 1 (DOC)† Snares: 2 (DOC)†	Adult: 56	Solander: 20 Snares: 36	Adults: 5813 (3273)	Solander: Mar–Aug Snares: all months
Northern Buller's albatross	3	Motuhara: 2 (DOC)† Chatham Island/Pyramid: 644	Adult: 81	Motuhara: 79 The Pyramid: 2	Adult: 7484 (2351)	Motuhara: all months The Pyramid: November
Shy albatross	9 (of 9)	Albatross Island: 414, 440, 1378, 1381 Pedra Branca: 416, 442 The Mewstone: 415, 441, 1379	Adult: 171 Fledgling: 26 Juvenile: 6 Juv/Imm: 6	Albatross Island: 179 Pedra Branca: 11 The Mewstone: 20	Adult: 377 (1294) Fledgling: 697 (470) Juvenile: 2944 (1012) Juv/Imm: 2278 (315)	Albatross Island: all months Pedra Branca: Mar–Apr, Nov–Dec The Mewstone: Nov–Aug
Campbell black-browed albatross	2 (of 2)	Campbell Islands: 429, 2172	Adult: 78	Campell Island: 78	Adult: 7479 (3013)	All months
Black-browed albatross	34 (of 46)	Kerguelen: 426, 1295, 1296, 1297 South Georgia: 457, 492, 493, 1382, 1388, 1389, 1537, 2004, 2225 Islas Diego Ramirez: 483, 487 Falkland Island/Islas Malvinas: 488, 489, 490, 491, 594, 600, 602, 603, 604, 685, 899, 901, 1448, 1451, 1454 Islas Albatros: 2275, 2276 Macquarie Island: 408, 445	Adult: 2168 Fledgling: 2 Juvenile: 13 Immature: 276 Juv/Imm: 3	Beauchene Island: 60 Bird Island: 826 Iles Kerguelen: 236 Islas Diego Ramirez: 115 Islas Albatros: 21 Jeanne d'Arc Peninsula: 26 Macquarie Island: 9 New Island: 700 Saunders Island: 253 Steeple Jason: 216	Adult: 1549 (3133) Fledgling: 2157 (345) Juvenile: 1119 (945) Immature: 525 (1952) Juv/Imm: 2395 (473)	Beauchene Island: Feb–Apr, Oct–Dec Bird Island: all months Iles Kerguelen: all months Islas Diego Ramirez: all months except January and September Islas Albatros: all months Jeanne d'Arc Peninsula: Feb, Nov-Dec Macquarie Island: Nov–Jan New Island: all months Saunders Island: all months Steeple Jason: all months
Sooty albatross	13 (of 13)	Marion Island: 651, 1512, 1529, 2209 Crozet: 425, 1313 Ile Amsterdam: 606, 1312 Tristan da Cunha: 1292 Gough Island: 420, 424, 1290 Prince Edward Island: 835	Adult: 311 Unknown: 10 Juvenile: 18	Marion Island: 193 Crozet: 50 Ile Amsterdam: 16 Tristan da Cunha: 3 Gough Island: 75 Prince Edward Island: 2	Adult: 1057 (1766) Unknown: 3150 (1556) Juvenile: 3527 (3511)	Marion Island: all months Crozet: all months Ile Amsterdam: Dec–Aug Tristan da Cunha: Oct–Dec Gough Island: all months Prince Edward Island: Mar–Sept

Common name	No. used	Dataset id by site	No. tracks by life stage	No. tracks per colony	Track duration (hrs)	Temporal coverage
Light-mantled sooty albatross	15 (of 16) + 1[†]	Macquarie Island: 413, 443 South Georgia: 444, 1384 Marion/PEI: 649, 650, 833, 1511, 1530 Heard Island: 661 Crozet: 1306, 1604 Kerguelen: 1309, 1605 Campbell Island: 2245, 1 (DOC)[†]	Adult: 165 Unknown: 1 Juvenile: 7	Macquarie Island: 14 Bird Island: 62 Heard Island: 6 Crozet: 8 Kerguelen: 3 Campbell Island: 20 Canyon des Sourcils Noirs: 5 Ile de la Possession: 7 Marion Island: 48	Adult: 17802 (63904) Unknown: 2600 (NA) Juvenile: 2207 (1429)	Macquarie Island: Nov–Jan Bird Island: Dec–Apr Heard Island: Dec–Mar Crozet: Jan–Apr Kerguelen: NA Campbell Island: all months Canyon des Sourcils Noirs: all months Ile de la Possession: all months Marion Island: all months
Grey petrel	4 (of 4) + 1[‡]	Antipodes: 634 Gough: 1288, 1[‡] Kerguelen: 1298, 1608 Marion: 1[‡]	Adult: 59 Unknown: 75	Antipodes Islands: 49 Gough Island: 31 Ile Mayes: 37 Iles Kerguelen: 7 Marion Island: 10	Adult: 5640 (4367) Unknown: 5345 (4481)	Antipodes Islands: all months Gough Island: all months Ile Mayes: Apr–Feb Iles Kerguelen: Apr–Jun Marion Island: all months
Black petrel	5 (of 5) + 1[†]	Little Barrier: 659 Great barrier: 658, 949, 951, 2268, 1[†]	Adult: 83 Unknown: 80 Juvenile: 13	Little Barrier Island: 13 Great Barrier Island: 163	Adult: 3819 (3508) Unknown: 2276 (2562) Juvenile: 1178 (989)	Little Barrier Island: all months Great Barrier Island: all months
Westland petrel	6 (of 7)	Punakaiki: 448, 683, 1449, 1819, 2236, 2237	Adult: 333	Punakaiki: 333	Adult: 2837 (4004)	All months
White-chinned petrel	20 (of 20)	Crozet: 434, 1314, 1606 Kerguelen: 1317, 1607 South Georgia: 438, 439, 1386, 1396, 1500, 1558, 2032 Antipodes: 627, 635, 2260 Marion Island: 1582, 1592 New Island: 2029 Falkland Island/Kidney Island: 2030 Adams Island: 2024	Adult: 315 Unknown: 77 Juvenile: 26	Adams Island: 102 Antipodes Islands: 68 Bird Island: 102 Iles Crozet: 47 Kidney Island: 9 Marion Island: 31 New Island: 5	Adult: 4377 (5373) Unknown: 2337 (1852) Juvenile: 874 (835)	Adams Island: Apr–Feb Antipodes Islands: all months Bird Island: all months Iles Crozet: all months Kidney Island: all months except Mar Marion Island: all months New Island: all months except Mar (1 track in Sept)

[†] Data were provided by the New Zealand Department of Conservation (DOC).

[‡] Data were provided by Jaimie Cleeland.

Table 3: Source of spatial information for the major breeding colonies of the assessed seabird taxa, the mean colony size (number of breeding pairs), whether tracking data were available (in BirdLife International) from the colony for the previous (2023) or current (2025) distribution mapping (adult or unknown age tracks only), and whether maps were available from Carneiro et al. (2020). '*' indicates which of these sources was used to make the final spatial distribution layer of each respective taxon, noting that permission had not been obtained to use some data. No spatial information was available for some colonies and these colonies were thus not represented by the spatial layers produced by this assessment. The number of tracks may not match Table 2 because some tracks were removed during grooming or colony site was unknown.

Common name	Colony	Mean colony size	Tracking 2023	Tracking 2025	Carneiro
Gibson's albatross	Disappointment	244			
	Adams	4 181	PTT 12*; GPS 0; GLS 0	PTT 41*; GPS 0; GLS 0	Y*‡
Wandering albatross	South Georgia (Islas Georgias del Sur)	1 278	PTT 12*; GPS 66*; GLS 170*	PTT 229*; GPS 521*; GLS 170*	Y
	Prince Edward	1 600			
	Marion	2 668	PTT 3*; GPS 34*; GLS 0	PTT 3*; GPS 150*; GLS 0	
	Crozet	2 324	PTT 479*; GPS 29*; GLS 98*	PTT 479*; GPS 29*; GLS 98*	Y
	Kerguelen	2 252	PTT 44*; GPS 0; GLS 23*	PTT 44*; GPS 0; GLS 23*	Y
	Macquarie	8	PTT 12; GPS 0; GLS 4	PTT 4*; GPS 0; GLS 4	
Southern royal albatross	Enderby	47			
	Motu Ihupuku/Campbell	5 767	PTT 17*; GPS 0; GLS 0	PTT 52*; GPS 0; GLS 14*	
Atlantic yellow-nosed albatross	Tristan da Cunha	15 250			
	Inaccessible	2 000	PTT 0; GPS 18*; GLS 0	PTT 0; GPS 18*; GLS 0	
	Nightingale	4 000	PTT 0; GPS 28*; GLS 0	PTT 0; GPS 28*; GLS 0	
	Gough	5 300	PTT 7*; GPS 74*; GLS 113	PTT 7*; GPS 74*; GLS 113	Y*
	Middle & Stoltenhoff	250			
Grey-headed albatross	South Georgia (Islas Georgias del Sur)	18 475	PTT 30*; GPS 64*; GLS 53*	PTT 302*; GPS 64*; GLS 53*	Y
	Islas Diego Ramirez	18 358	PTT 50*; GPS 0; GLS 0	PTT 67*; GPS 0; GLS 0	
	Prince Edward	1 506			Y*
	Marion	8 180	PTT 6; GPS 86*; GLS 25	PTT 6; GPS 191*; GLS 25	
	Crozet	6 319			
	Kerguelen	6 445			

Common name	Colony	Mean colony size	Tracking 2023	Tracking 2025	Carneiro
	Macquarie	100	PTT 9; GPS 5; GLS 2	PTT 9*; GPS 5; GLS 2	
	Campbell	3 672	PTT 5*; GPS 24*; GLS 0	PTT 5*; GPS 24*; GLS 64*	
	Islas Ildefonso	NA	PTT 1; GPS 0; GLS 0	PTT 1*; GPS 0; GLS 0	
Southern Buller's albatross[§]	Hautere/Solander	4 793	PTT 452*; GPS 97*; GLS 102*	PTT 20*; GPS 0; GLS 0	
	Tini Heke/Snares	8 700	PTT 452*; GPS 97*; GLS 102*	PTT 3*; GPS 5*; GLS 28*	Y
Northern Buller's albatross[§]	Motuhara/Forty-fours	16 081	PTT 452*; GPS 97*; GLS 102*	PTT 10*; GPS 2*; GLS 69*	
	Rangitatahi/Sisters	3 273			
Shy albatross	Albatross Island	5 585	PTT 55*; GPS 0; GLS 0	PTT 55*; GPS 103*; GLS 0	
	Pedra Branca	90	PTT 6; GPS 0; GLS 0	PTT 6*; GPS 0; GLS 0	
	Mewstone	9 660	PTT 5*; GPS 0; GLS 0	PTT 5*; GPS 0; GLS 0	
Campbell black-browed albatross	Motu Ihupuku/Campbell	14 129	PTT 10*; GPS 0; GLS 0	PTT 10*; GPS 0; GLS 68*	
Black-browed albatross	Falklands (Islas Malvinas)	474 219	PTT 200*; GPS 2*; GLS 201*	PTT 200*; GPS 485*; GLS 252*	Y
	South Georgia (Islas Georgias del Sur)	55 119	PTT 358*; GPS 180*; GLS 182*	PTT 363*; GPS 209*; GLS 226*	Y
	Islas Diego de Almagro	15 594	PTT 13; GPS 0; GLS 0	PTT 13; GPS 0; GLS 0	
	Islotes Evangelistas	4 818			
	Islas Diego Ramirez	61 749	PTT 13*; GPS 0; GLS 15*	PTT 100*; GPS 0; GLS 15*	Y*
	Islas Ildefonso	54 284	PTT 26; GPS 0; GLS 0	PTT 26; GPS 0; GLS 0	
	Islote Albatros	104	PTT 0; GPS 38; GLS 0	PTT 0; GPS 19*; GLS 0	
	Islote Leonard	545			
	Crozet	710			
	Kerguelen	2 880	PTT 58*; GPS 0; GLS 202*	PTT 58*; GPS 0; GLS 202*	Y
	Heard	600	PTT 10; GPS 0; GLS 0	PTT 10; GPS 0; GLS 0	
	Macquarie, Bishop & Clerk	192	PTT 9; GPS 5; GLS 2	PTT 7*; GPS 5; GLS 2	
	New Zealand Subantarctic	146			
Sooty albatross	Gough	3 750	PTT 6*; GPS 13*; GLS 56*	PTT 6*; GPS 13*; GLS 56*	

Common name	Colony	Mean colony size	Tracking 2023	Tracking 2025	Carneiro
	Inaccessible	500			
	Nightingale	150			
	Stoltenhoff	37			
	Tristan da Cunha	2 675	PTT 0; GPS 3*; GLS 0	PTT 0; GPS 3*; GLS 0	Y*
	Prince Edward	1 500	PTT 2*; GPS 0; GLS 0	PTT 2*; GPS 0; GLS 0	Y*
	Marion	2 000	PTT 10*; GPS 59*; GLS 0	PTT 10*; GPS 183*; GLS 0	
	Crozet	2 144	PTT 41*; GPS 0; GLS 0	PTT 41*; GPS 0; GLS 0	
	Amsterdam	394	PTT 7*; GPS 0; GLS 0	PTT 7*; GPS 0; GLS 0	
Light-mantled sooty albatross	South Georgia (Islas Georgias del Sur)	5 000	PTT 42*; GPS 20; GLS 0	PTT 42*; GPS 20*; GLS 0	
	Prince Edward	150			Y*
	Marion	268	PTT 10*; GPS 10*; GLS 0	PTT 10*; GPS 38*; GLS 0	
	Crozet	2 159	PTT 4*; GPS 0; GLS 7*	PTT 4*; GPS 0; GLS 7*	
	Kerguelen	4 000	PTT 0; GPS 0; GLS 5*	PTT 0; GPS 0; GLS 5*	
	Heard	350	PTT 6; GPS 0; GLS 0	PTT 6*; GPS 0; GLS 0	
	Macquarie	2 150	PTT 4*; GPS 0; GLS 3	PTT 14*; GPS 0; GLS 3	
	Maukahuka/Auckland	5 000			
	Motu Ihupuku/Campbell	1 600	PTT 20; GPS 0; GLS 0	PTT 20*; GPS 0; GLS 0	
	Moutere Mahue/Antipodes	250			
Grey petrel	Gough	17 500	PTT 0; GPS 15*; GLS 16*	PTT 0; GPS 15*; GLS 16*	Y
	Prince Edward & Marion	5 000	PTT 0; GPS 0; GLS 10*	PTT 0; GPS 0; GLS 10*	Y
	Crozet	5 500			
	Kerguelen	3 400	PTT 7*; GPS 0; GLS 37*	PTT 7*; GPS 0; GLS 37*	
	Amsterdam	7			
	Macquarie	252			
	Motu Ihupuku/Campbell	98			
	Moutere Mahue/Antipodes	73 860	PTT 0; GPS 0; GLS 49*	PTT 0; GPS 0; GLS 49*	

Common name	Colony	Mean colony size	Tracking 2023	Tracking 2025	Carneiro
Black petrel	Hauturu-o-Toi/Little Barrier	620	PTT 0; GPS 0; GLS 13*	PTT 0; GPS 0; GLS 13*	Y[†]
	Aotea/Great Barrier	4 836	PTT 0; GPS 30*; GLS 0	PTT 0; GPS 30*; GLS 112*	Y[†]
Westland petrel	Punakaiki	6 223	PTT 20*; GPS 142*; GLS 8*	PTT 20*; GPS 158*; GLS 151*	Y
White-chinned petrel	South Georgia (Islas Georgias del Sur)	773 150	PTT 23; GPS 15; GLS 42	PTT 23*; GPS 15*; GLS 51*	Y
	Prince Edward	12 000			Y
	Marion	24 000	PTT 0; GPS 21*; GLS 10*	PTT 0; GPS 21*; GLS 10*	
	Crozet	44 428	PTT 33*; GPS 0; GLS 10*	PTT 33*; GPS 0; GLS 10*	
	Kerguelen	234 000	PTT 21*; GPS 0; GLS 24*	PTT 21*; GPS 0; GLS 24*	
	Disappointment	153 000			
	Adams	28 300	PTT 0; GPS 0; GLS 102	PTT 0; GPS 0; GLS 102*	
	Motu Ihupuku/Campbell	22 000			
	Moutere Mahue/Antipodes	26 400	PTT 0; GPS 0; GLS 61*	PTT 0; GPS 0; GLS 66*	Y
	New Island/Kidney Island[§]	55	PTT 0; GPS 0; GLS 14	PTT 0; GPS 0; GLS 14*	

[‡] Distribution map was named Auckland Islands.

[†] Data from both colonies were merged into one distribution map.

[§] Breeding pairs from (Reid et al. 2007).

[§] Previous distribution maps did not differentiate between the two species.

3.2 Spatiotemporal models

The best models for all species included a 3-dimensional spatiotemporal spline model, which smoothed simultaneously across position and date, fitted with a Tweedie distribution, where the estimated Tweedie parameter was between 1–2, indicating a compound Poisson-gamma distribution (Table 4). Weighting the tracks directly by colony size produced better fits (in terms of deviance explained and residual patterns) than models that did not include weighting. This approach is also preferred on a theoretical basis, in reducing bias in observed distributions at a population level resulting from differing levels of tracking data at a colony level. The models fit by including colony size as an offset, weighting each observation's contribution to the likelihood, or by including colony name as an additional factor in the model produced much poorer fits than directly scaling the relative density by mean colony size, i.e., residual patterns were worse and extreme densities were predicted at the margins of the modelled spatial range (e.g. where no data existed). All models explained between 67–91% of the deviance.

Modelled predicted relative mean density by month and 5-degree grid cell are shown by species below, while the Appendices A–P include:

- A spatial plot of all ungroomed tracking data locations for all life stages obtained by this study, using separate colours for each colony;
- A spatial plot of all groomed and interpolated tracking data locations for only adults (or where life stage was not specified), using separate colours for each track;
- A spatial plot of the density of processed tracking data locations by month, aggregated by 1-degree grid cell; and
- Model diagnostic plots, including a quantile-quantile plot and model residuals plotted spatially.

Table 4: Model formulation including information on the type of splines and smooth terms, estimated Tweedie parameter, and percent deviation explained. 'te' indicates a tensor product smooth, 'gp' is a Gaussian process smooth, 'cc' is a cyclic cubic regression spline, and 'cs' is the shrinkage version of a cubic regression spline, where both 'cc' and 'cs' splines are a type of penalized cubic regression spline whose endpoints match (i.e., first and last values are considered near to each other in space or time).

Species	Tweedie ρ	Model formulation	% Dev.
Gibson's albatross	1.440	~ te(lat, lon, month, d = c(2, 1), bs = c("gp","cc"), k=c(3,8,4))	87.9
Wandering albatross	1.544	~ te(lat, lon, month, d = c(1,1, 1), bs = c("gp","cc","cc"), k=c(7, 28, 6))	81.0
Southern royal albatross	1.530	~ te(lat, lon, month, d = c(2, 1), bs = c("gp"), k=c(4, 12, 5))	77.6
Atlantic yellow-nosed albatross	1.532	~ te(lat, lon, month, d = c(2, 1), bs = c("gp","cc"), k=c(5, 3, 4))	85.9
Black-browed albatross	1.695	~ te(lat, lon, month, d = c(1, 1, 1), bs = c("cs","cc","cc"), k=c(7, 20, 7))	91.0
Campbell black-browed albatross	1.321	~ te(lat, lon, month, d = c(2, 1), bs = c("cs","cc"), k=c(4, 12, 4))	69.1
Shy albatross	1.628	~ te(lat, lon, month, d = c(2, 1), bs = c("gp","cc"), k=c(3, 3, 3))	87.8
Grey-headed albatross	1.587	~ te(lat, lon, month, d = c(1, 1, 1), bs = c("gp","cc", "cc"), k=c(7, 18, 8))	86.9
Southern Buller's albatross	1.364	~ te(lat, lon, month, d = c(2, 1), bs = c("gp","cc"), k=c(4, 8, 5))	67.1
Northern Buller's albatross	1.308	~ te(lat, lon, month, d = c(2, 1), bs = c("gp","cc"), k=c(4, 8, 3))	73.8
Sooty albatross	1.520	~ te(lat, lon, month, d = c(2, 1), bs = c("gp", "cc"), k=c(5, 12, 4))	77.0
Light-mantled sooty albatross	1.645	~ te(lat, lon, month, d = c(1, 1, 1), bs = c("gp", "cc", "cc"), k = c(7, 13, 7))	78.5
Grey petrel	1.583	~ te(lat, lon, month, d = c(1, 1, 1), bs = c("gp","cc", "cc"), k=c(6, 15, 6))	72.2
Black petrel	1.457	~ te(lat, lon, month, d = c(2, 1), bs = c("gp","cc"), k=c(5, 7, 4))	73.7
Westland petrel	1.522	~ te(lat, lon, month, d = c(1, 1, 1), bs = c("gp","cc", "cc"), k = c(4, 12, 6))	85.0
White-chinned petrel	1.631	~ te(lat, lon, month, d = c(1, 1, 1), bs = c("gp","cc", "cc"), k = c(4, 11, 5))	68.3

3.3 Species-specific results

3.3.1 Gibson's albatross

Datasets received were from the New Zealand Department of Conservation (DOC). Four additional datasets held by BirdLife International that were identified as Gibson's albatross were requested, but no response was received. These data included tracks that extended along the southern coast of Australia and slightly to the west of Australia, which would have expanded the predicted distribution for several months, but noting that it was difficult to determine whether two of these datasets may have already been among those received from the New Zealand DOC. Of the received data, no data were from the October–December period and tracks were very limited in January and September.

Distribution maps fitted from the data indicated a slight westward movement, along the southern coast of Australia in June–November (Figure 1). The Carneiro et al. (2020) distribution maps for the Auckland Island colony (all four quarters) were used to augment the spatial distribution, which extended the distribution along the southern coast of Australia in most months (Figure 2).

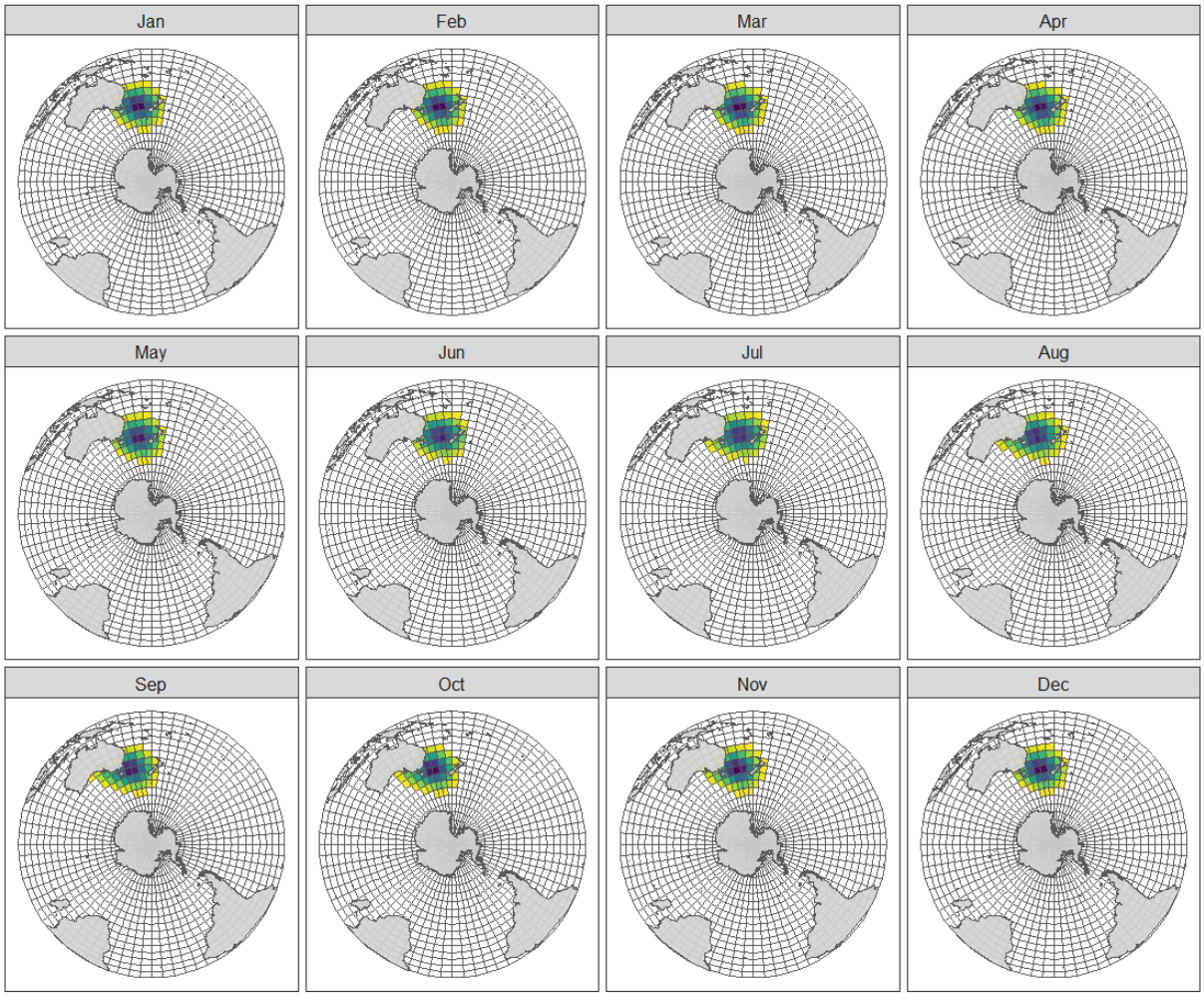

Figure 1: Gibson's albatross (*Diomedea antipodensis gibsoni*) predicted distribution by month. Yellow indicates low densities, and dark blue indicates high densities.

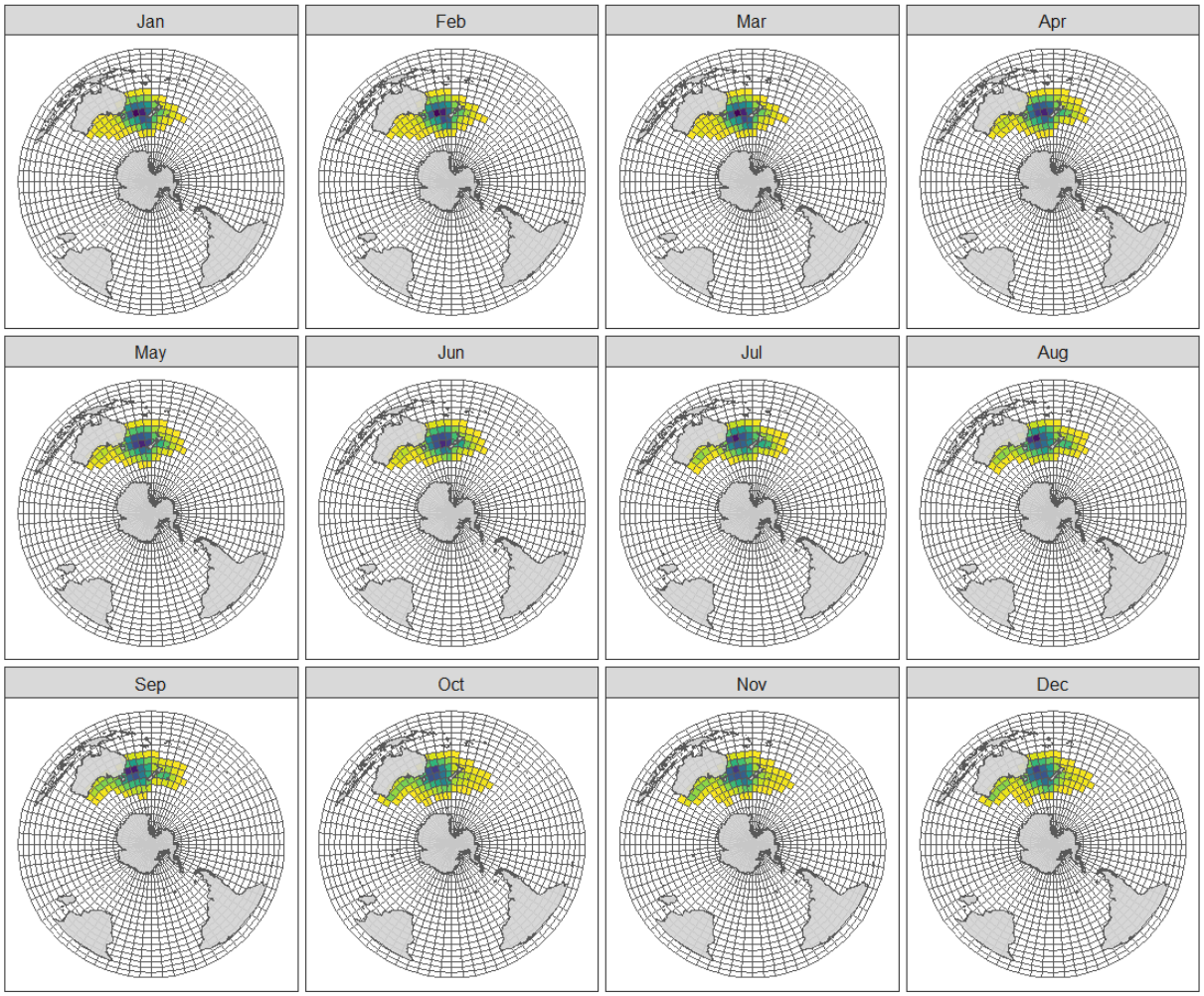

Figure 2: Gibson's albatross (*Diomedea antipodensis gibsoni*) predicted distribution by month, after augmentation with the Auckland Island colony distribution maps of Carneiro et al. (2020). Yellow indicates low densities, and dark blue indicates high densities.

3.3.2 Wandering albatross

A response to data requests was not received for only two datasets (of 45) that were requested through BirdLife International. All datasets identified by the external review, including data from the South Atlantic Ocean (e.g., South Georgia) were received. Of the received data, data were available from the Macquarie colony only from December–March, and from the Marion Island colony for January–September; all other colonies had coverage over all months.

Distribution maps fitted from the data indicated a circumpolar distribution for all months except February–March, with densest concentrations in the south Atlantic (Falklands/South Georgia area) and south Indian Oceans (Figure 3). The distribution was weighted (as a result of including weighting by the mean colony size) towards the Marion, Crozet, and Kerguelen colonies in the south Indian Ocean; these colonies make up approximately 70% of the population. The Carneiro et al. (2020) distribution maps were not used to augment the predicted distribution.

Figure 3: Wandering albatross (*Diomedea exulans*) predicted distribution by month. Yellow indicates low densities, and dark blue indicates high densities.

3.3.3 Southern royal albatross

The external review (Edwards et al. 2025, Table A.6) identified that additional datasets were required because the previous analysis (Devine et al. in press) did not capture the circumpolar distribution of this species. Requests to use all datasets available in BirdLife International were granted for the update, which provided information on the distribution across the south Pacific Ocean for most months (Figure 4). Coverage of all months was good, but very few of the adult tracks circumnavigated the globe, which meant that the distribution of the species was limited except in the south Pacific Ocean region.

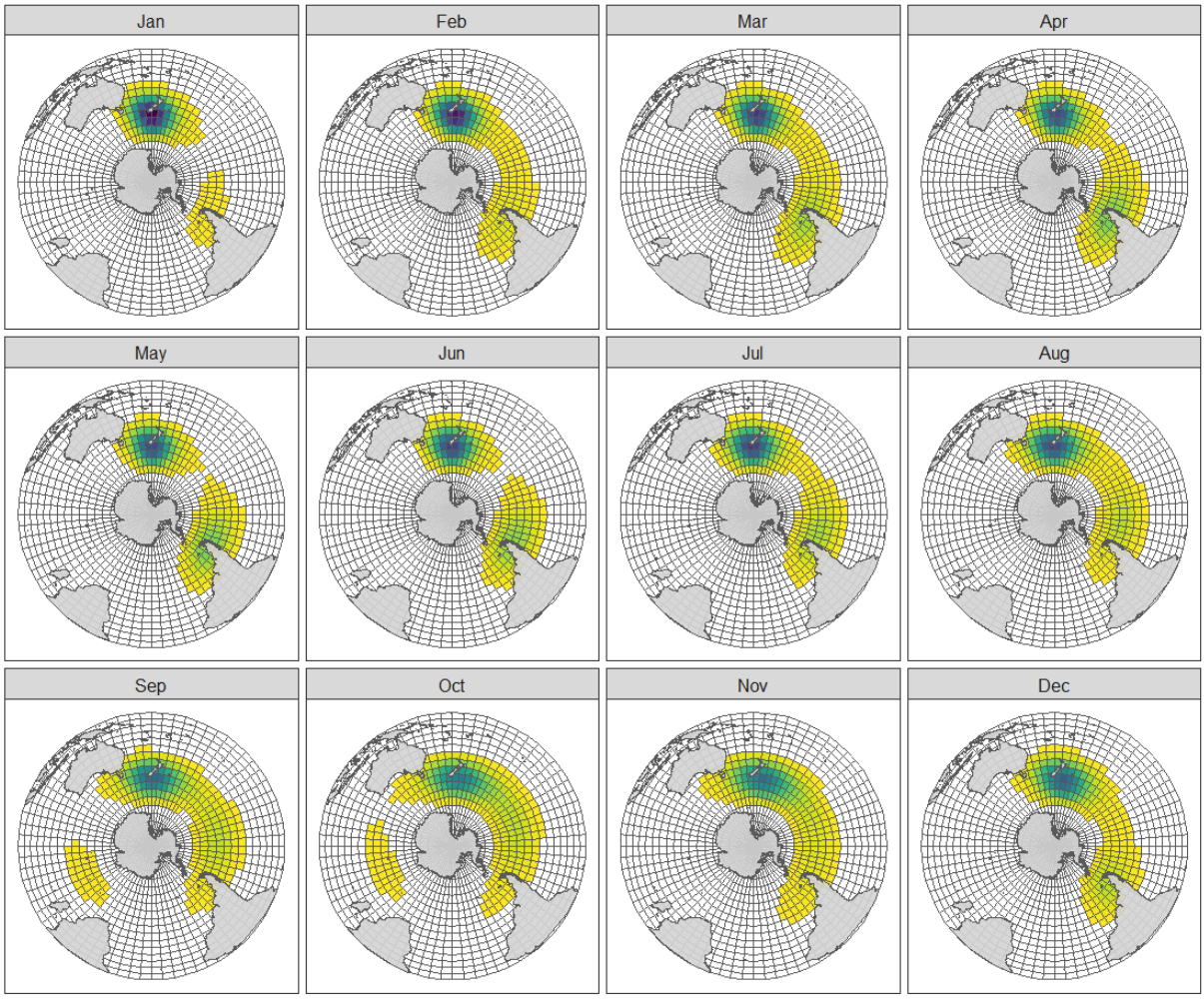

Figure 4: Southern royal albatross (*Diomedea epomophora*) predicted distribution by month. Yellow indicates low densities, and dark blue indicates high densities.

3.3.4 Atlantic yellow-nosed albatross

Additional datasets were required because the previous analysis did not capture the spatiotemporal movement across the south Atlantic Ocean or take into account known foraging areas, e.g., Benguela upwelling zone (see Table A.6 in Edwards et al. 2025). Requests to use all datasets available in BirdLife International were granted for all but one dataset (Table 2). No tracking data were available in June to September (all colonies) or for the main breeding colony (Tristan da Cunha). Convergence was an issue with this model, which was solved by adjusting the weighting (mean colony size) to be the mean of the colonies in the data instead of the mean of all known breeding colonies (i.e., removing Tristan da Cunha and Middle & Stoltenhoff) (Table 3).

The monthly distribution maps indicated an eastward movement across the south Atlantic Ocean, beginning in August, with a return to South America by April (Figure 5). Carneiro et al. (2020) distributions were used to augment the predicted distributions for the Gough breeding colony for all months except October–December, i.e., omitting months when the available tracking data had good coverage (Table 3, Figure 6). This augmentation meant that a proportion of the population remained at the coast of Africa in April–July (i.e., in the Benguela upwelling zone) and around Gough Island in the first three quarters of the calendar year (Figure 6).

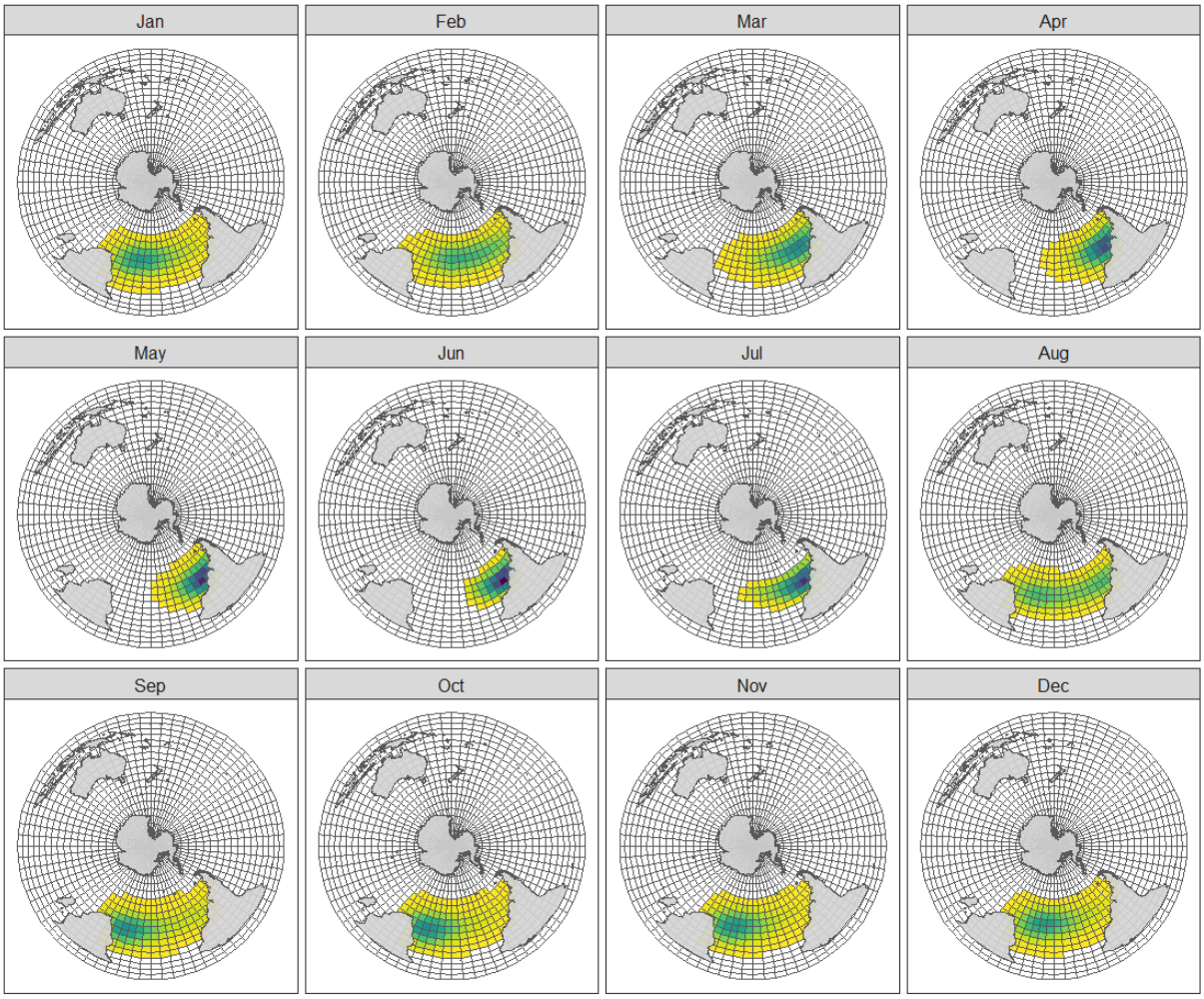

Figure 5: Atlantic yellow-nosed albatross (*Thalassarche chlororhynchos*) predicted distribution by month. Yellow indicates low densities, and dark blue indicates high densities.

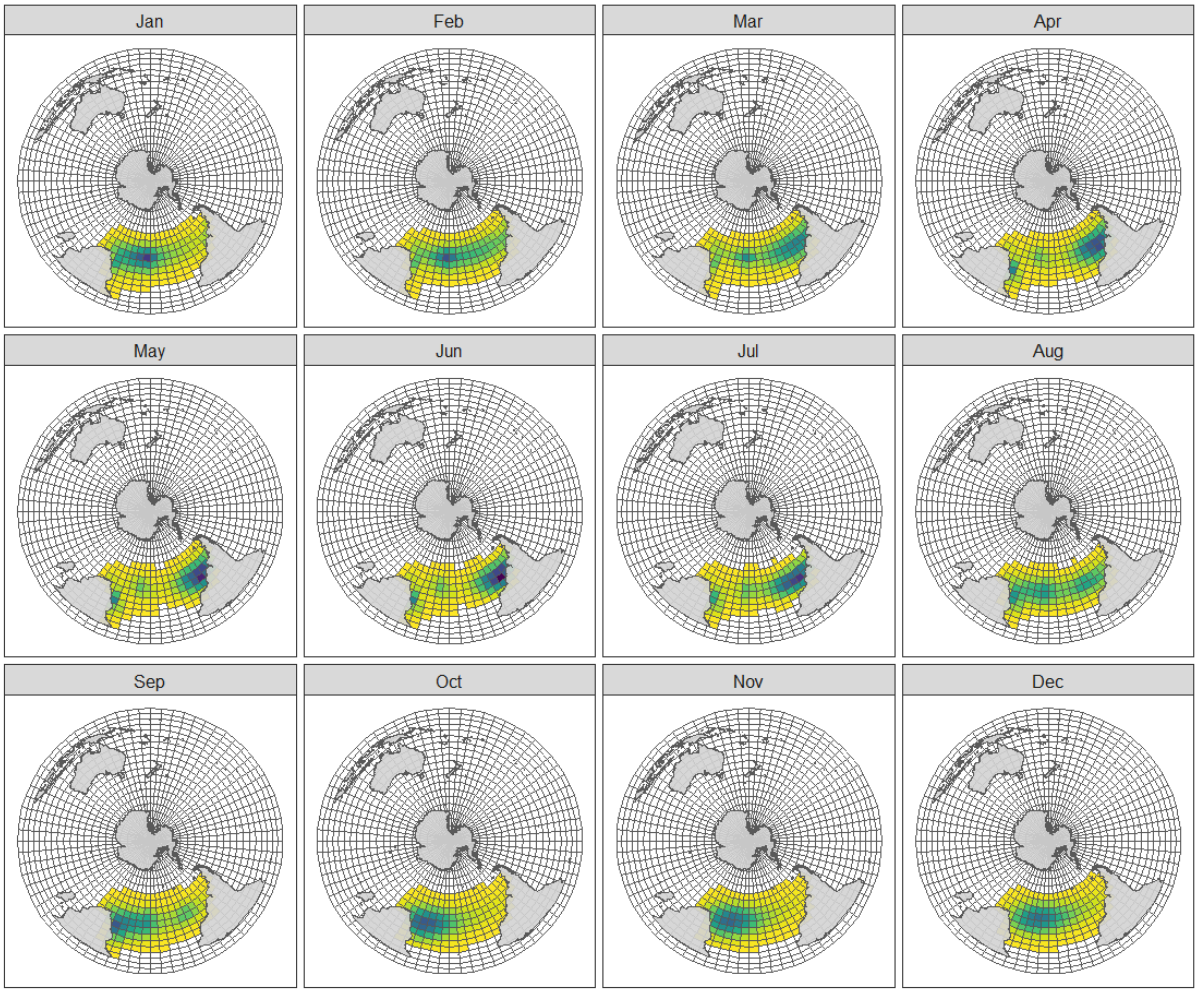

Figure 6: Atlantic yellow-nosed albatross (*Thalassarche chlororhynchos*) predicted distribution by month, after augmentation with the Gough Island colony distribution maps of Carneiro et al. (2020). Yellow indicates low densities, and dark blue indicates high densities.

3.3.5 Black-browed albatross

The external review of the previous distribution modelling (Devine et al. in press) noted the lack of tracking data from key colonies, including the Falkland Islands and southern Chile, and noted an additional 12 tracking datasets held by BirdLife International that would improve the distributions. Of those identified datasets, 9 were made available by data owners for the update, resulting in 34 (of 46) datasets being included (Table 2). In the available tracking data, a northward truncation in the south Indian Ocean was apparent (see Appendix E). Tracking data were available for most major colonies for all months but was sparse for the Islas Diego Ramirez colony (Table 3).

The additional tracking data improved the updated distribution maps, particularly in the south Indian and Atlantic Ocean sectors, and down-weighted the distribution towards the Australian Bight (Figure 7). The modelled distributions were circumpolar for May only but augmenting with the Islas Diego Ramirez colony maps from Carneiro et al. (2020) improved the distributions for the south Pacific region for all months (Figure 8).

Figure 7: Black-browed albatross (*Thalassarche melanophris*) predicted distribution by month. Yellow indicates low densities, and dark blue indicates high densities.

Figure 8: Black-browed albatross (*Thalassarche melanophris*) predicted distribution by month, after augmentation with the Islas Diego Ramirez colony distribution maps of Carneiro et al. (2020). Yellow indicates low densities, and dark blue indicates high densities.

3.3.6 Campbell black-browed albatross

The previous version included data from only February. An additional dataset was identified as necessary by the expert review and was included in the update (Table 2). This expanded coverage to all months and included a few tracks in the south Atlantic and Indian Ocean regions. This appeared to be one bird that flew south of South America, crossed the Atlantic, flew to Antarctica, and then returned to the southern Tasman Sea. Because of the low relative densities in these cells, they were not adequately modelled (see Appendix F). The final distribution map indicated a distribution localised to the south of New Zealand October–February, with distribution both westward into the south Indian Ocean and eastward, towards South America, the rest of the year (Figure 9).

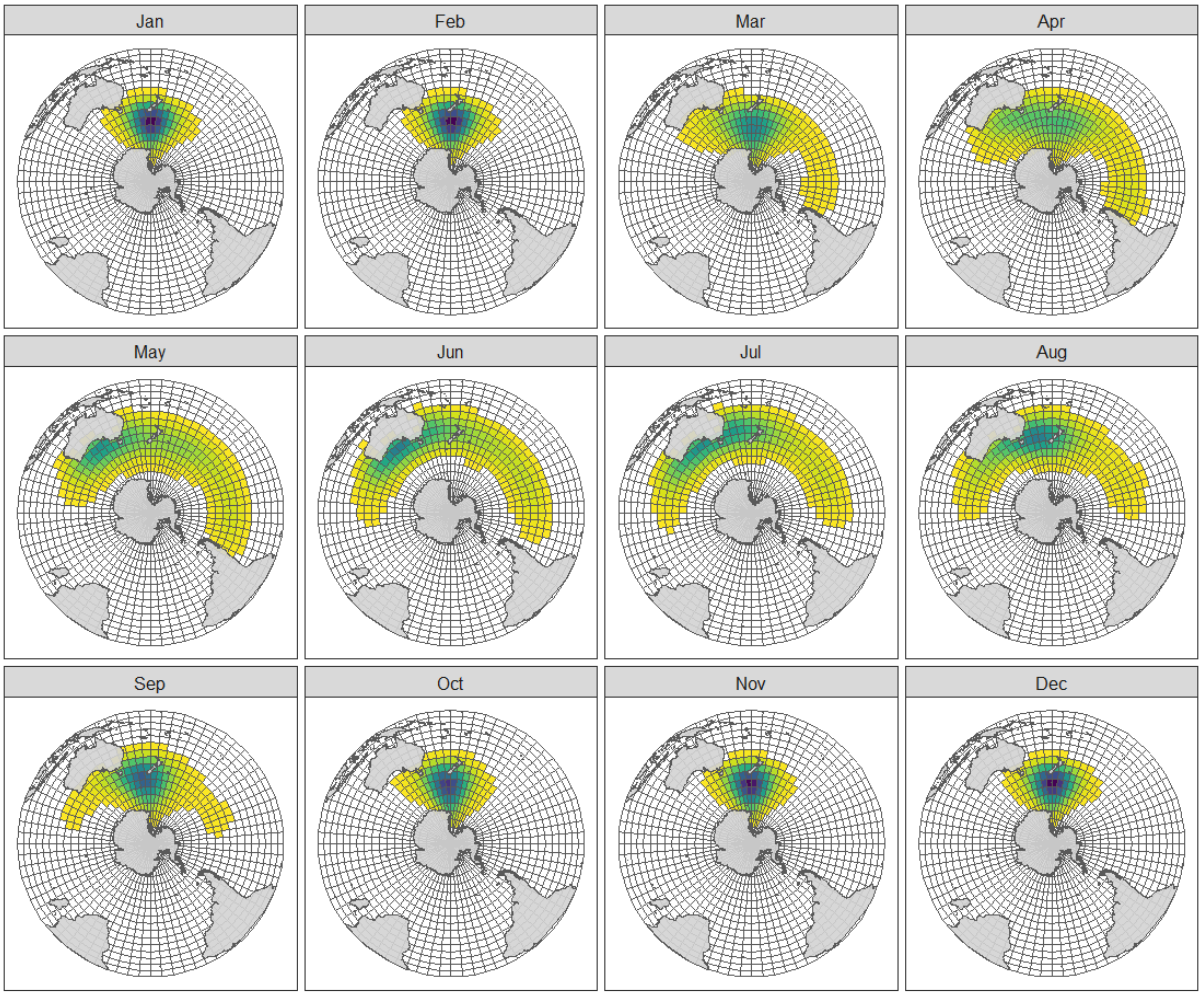

Figure 9: Cambell black-browed albatross (*Thalassarche impavida*) predicted distribution by month. Yellow indicates low densities, and dark blue indicates high densities.

3.3.7 Shy albatross

The review by international experts identified six additional datasets that would improve the distribution maps and included some wide-ranging tracks. Permission to use those data were given (Table 2). The review also noted that known foraging areas in the Indian Ocean, and off the east coast of South Africa were absent, but these tracking data were from juveniles and thus not included in the analysis (see Appendix G). Data for adults were only from the area around Tasmania and southern coastal Australia. This meant that the updated predicted monthly distribution did not differ greatly from the previous version except that tracks from Mewstone Island (the largest colony) were included (Figure 10, see Appendix G).

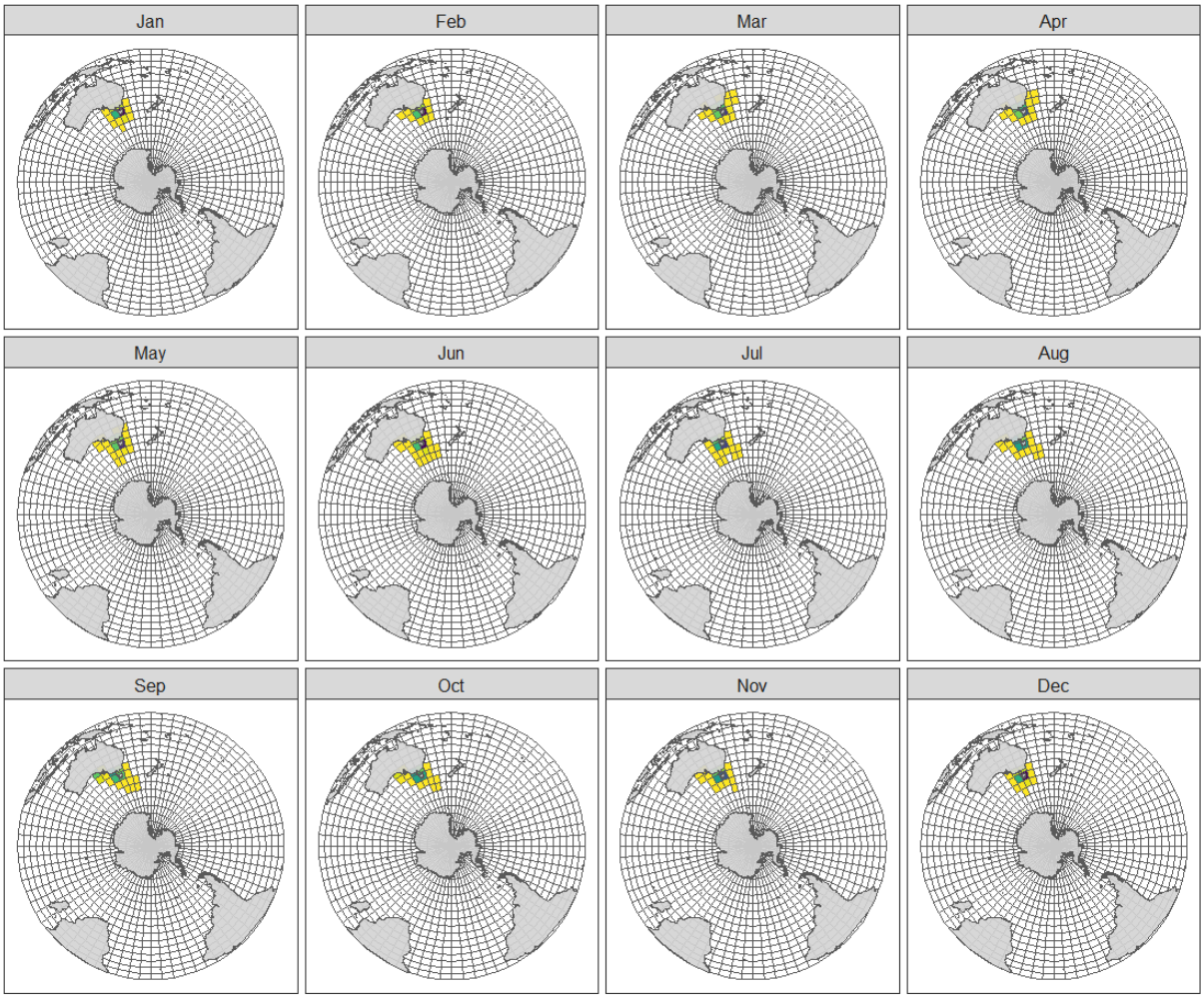

Figure 10:Shy albatross (*Thalassarche cauta*) predicted distribution by month. Yellow indicates low densities, and dark blue indicates high densities.

3.3.8 Grey-headed albatross

The review by international experts noted additional datasets that would improve the updated distribution maps and included some poorly represented colonies. Permission to use four of these datasets were given, which included the Islas Diego Ramirez, South Georgia, and Marion Island colonies (Table 2), but permission was not received to use other data identified as being key from Macquarie and Marion Islands.

Predicted distributions were largely circumpolar, but with some notable gaps in the distribution in the south Indian Ocean region between March–May (Figure 11). Augmentation with the Prince Edward Island colony maps from Carneiro et al. (2020) indicated a low-density circumpolar distribution in all months (Figure 12).

Figure 11: Grey-headed albatross (*Thalassarche chrysostoma*) predicted distribution by month. Yellow indicates low densities, and dark blue indicates high densities.

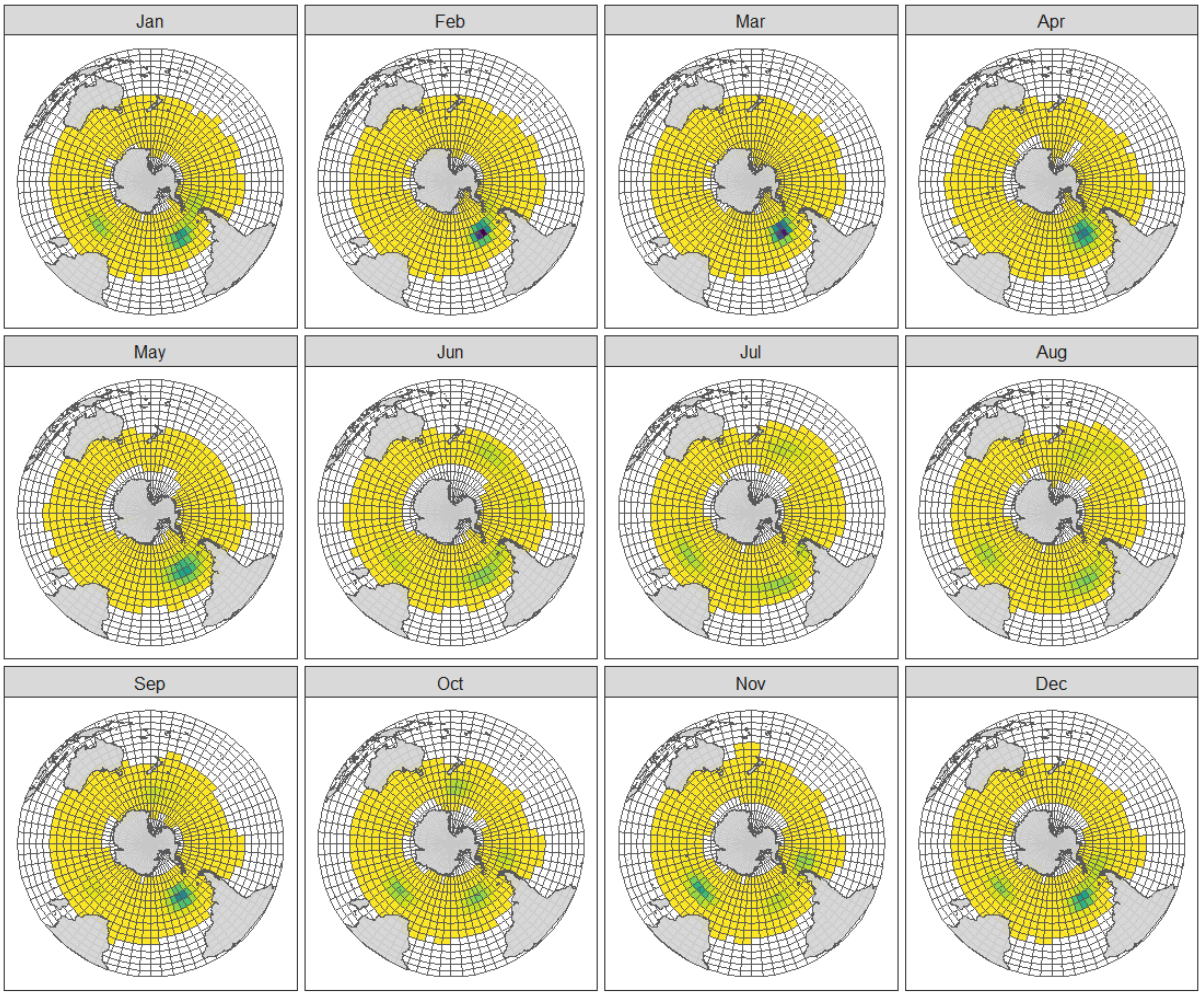

Figure 12: Grey-headed albatross (*Thalassarche chrysostoma*) predicted distribution by month, after augmentation with the Prince Edward Island colony distribution maps of Carneiro et al. (2020). Yellow indicates low densities, and dark blue indicates high densities.

3.3.9 Southern Buller's albatross

The previous analysis (Devine et al. in press) could not differentiate between Northern and Southern Buller's albatross because many of the tracking datasets held by BirdLife International did not differentiate between the two subspecies. The New Zealand DOC provided subspecies-specific tracking data to enable each to be modelled (Table 2). Tracking data from the Snares colony was missing information for December through March, and from Solander for September–February. Despite missing information for these months, the predicted distribution showed birds leaving South America and migrating to New Zealand for the breeding season, a pattern that was similar to that reported by Fischer et al. (2023) (Figure 13). Augmentation with the Carneiro et al. (2020) maps for the four missing months indicated a lower density of birds were at the breeding grounds in December–March (not shown) than the non-augmented maps. The decision was made to not use the augmented maps.

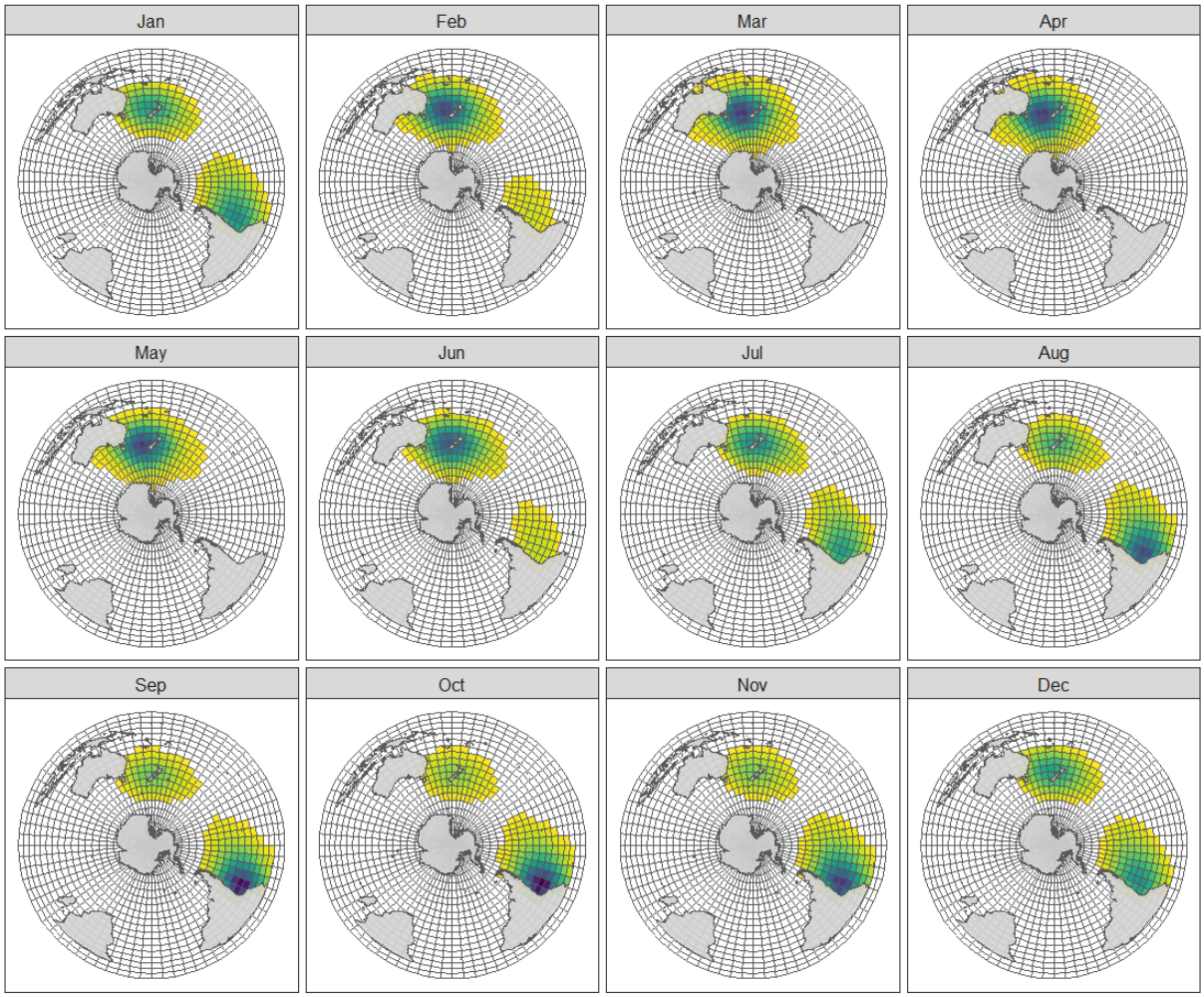

Figure 13: Southern Buller's albatross (*Thalassarche bulleri bulleri*) predicted distribution by month. Yellow indicates low densities, and dark blue indicates high densities.

3.3.10 Northern Buller's albatross

All provided tracking data were from the larger of the two colonies (i.e., Motuhara) (Tables 2–3). Increasing the number of knots in the spatiotemporal smoother made no improvement to the predicted distribution; the model was not able to completely shift all birds from around New Zealand to the South American coast in August (Figure 14).

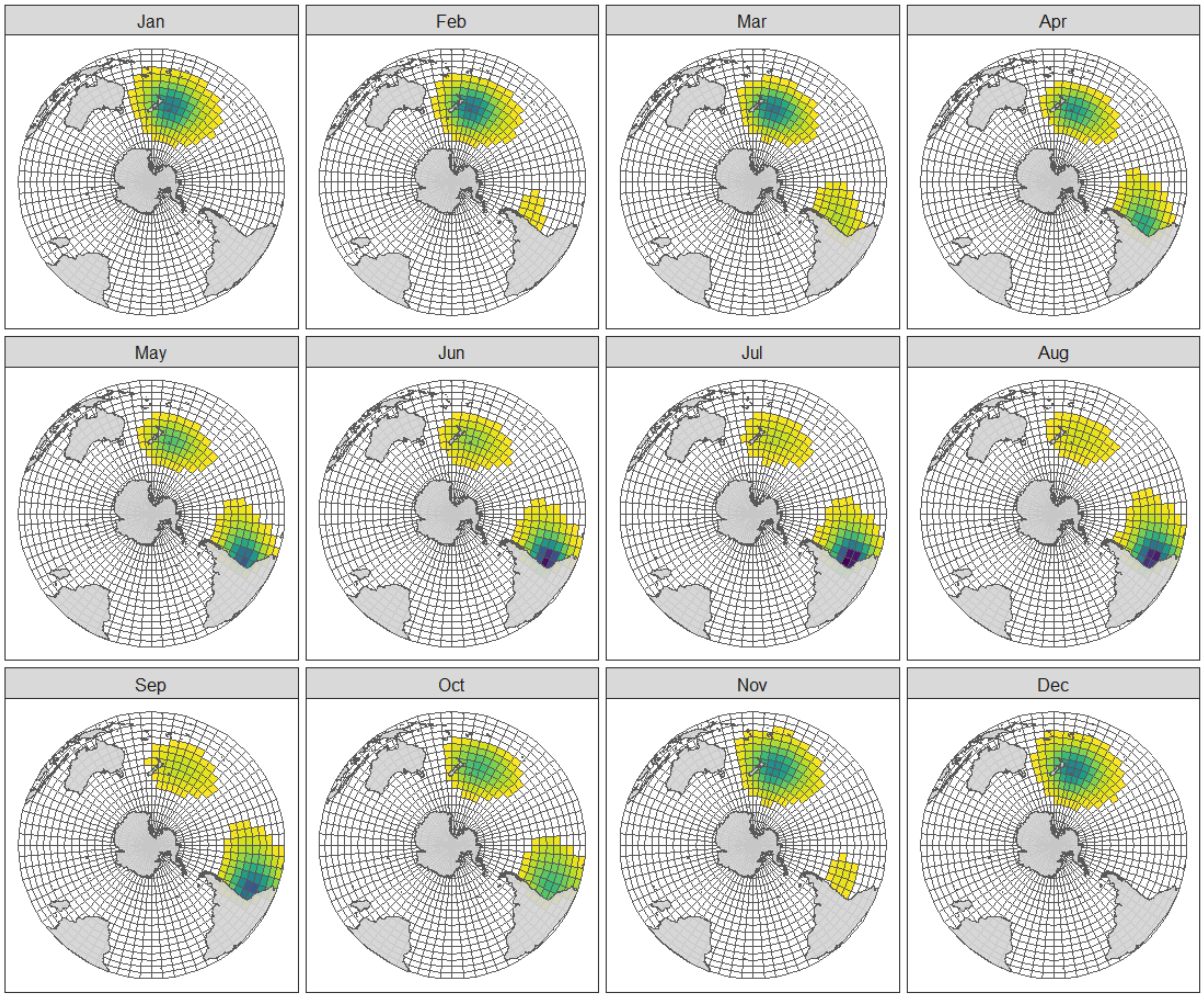

Figure 14: Northern Buller's albatross (*Thalassarche bulleri platei*) predicted distribution by month. Yellow indicates low densities, and dark blue indicates high densities.

3.3.11 Sooty albatross

Two additional tracking datasets were approved for use for this update, which meant that all available datasets were used (Table 2). Care was taken to use only data identified as sooty albatross, taking into consideration a comment from the external review (see Table A.6 in Edwards et al. 2025). Tracking data included only a few tracks in July and September for the Prince Edward Island colony (2 tracks in total), and no information January–October for the Tristan da Cunha colony (3 tracks in total). Because of this and the low number of tracks for two of the larger colonies, the Carneiro et al. (2020) maps were used to augment the predicted distributions (all months) for these two colonies. This resulted in more eastward distributions in the south Indian Ocean between September and March, and a more westward distribution September–March in the South Atlantic (Figures 15–16).

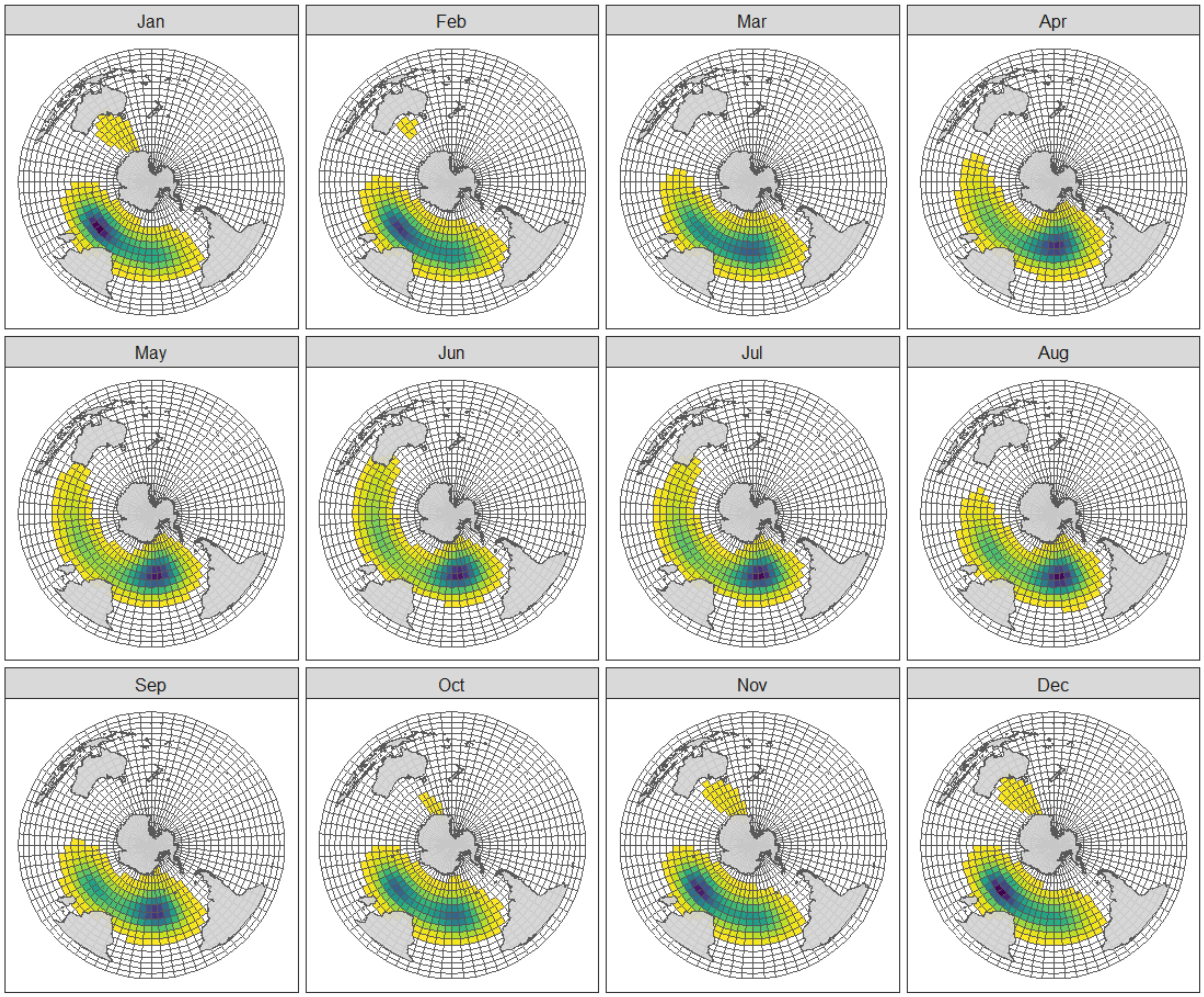

Figure 15: Sooty albatross (*Phoebetria fusca*) predicted distribution by month. Yellow indicates low densities, and dark blue indicates high densities.

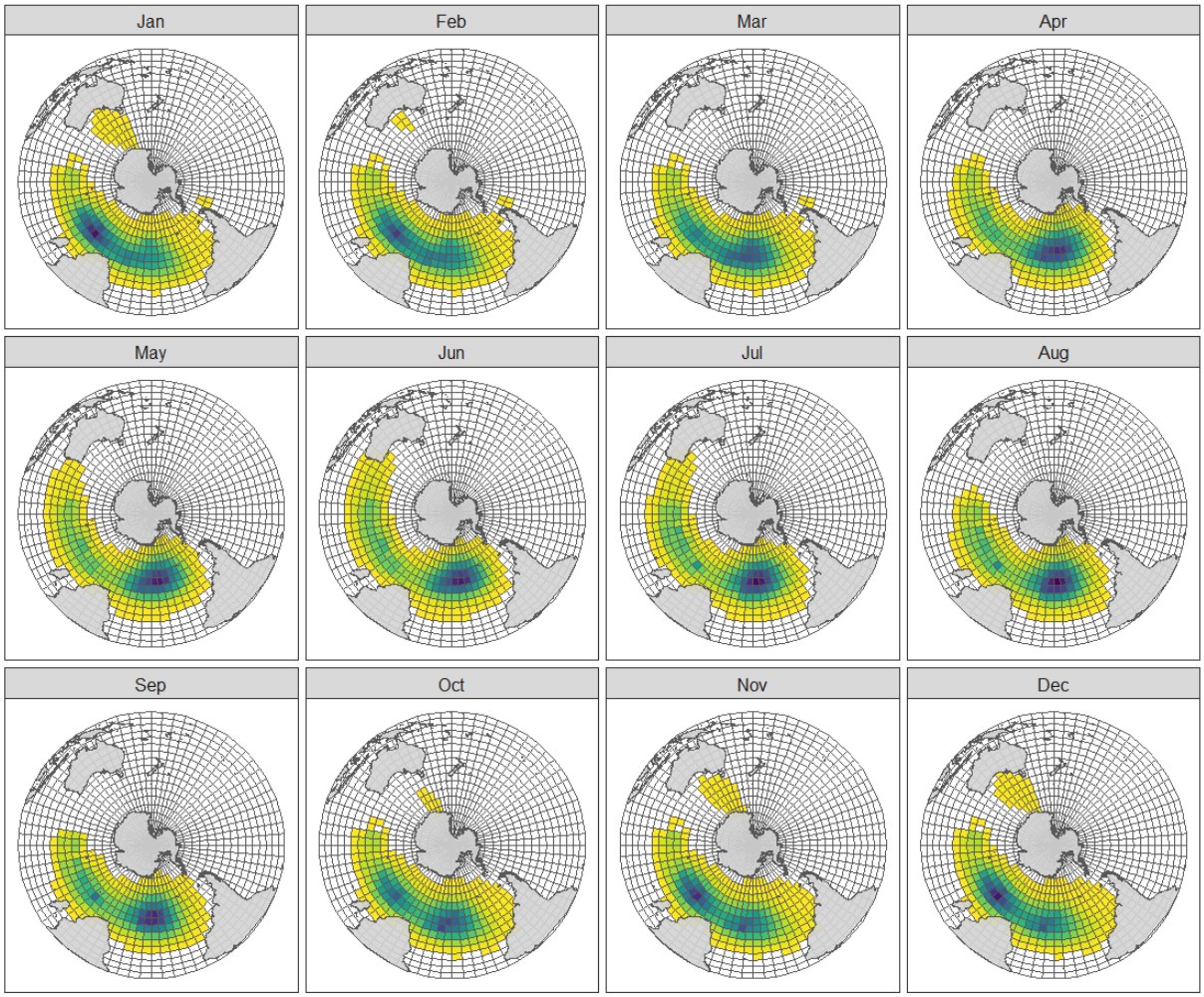

Figure 16: Sooty albatross (*Phoebetria fusca*) predicted distribution by month, after augmentation with the distribution maps of the Prince Edward Island and Tristan da Cunha colonies (Carneiro et al. 2020). Yellow indicates low densities, and dark blue indicates high densities.

3.3.12 Light-mantled sooty albatross

The review of the previous distribution mapping lacked data from the South Georgia, Crozet, and Kerguelen colonies. These data and an additional dataset from the New Zealand DOC from the Campbell colony were made available for the update (Table 2). The only dataset that was not available was from Macquarie Island, which contained only three tracks. Tracks were spare for the Marion colony in September–October. Distribution maps were augmented with the Prince Edward Island colony maps in Carneiro et al. (2020), but because it was a small colony, it made little discernible difference to the distribution maps (Figures 17–18). Light-mantled sooty albatross distributions were circumpolar in most months, but few tracks crossed the south Pacific Ocean in February and March.

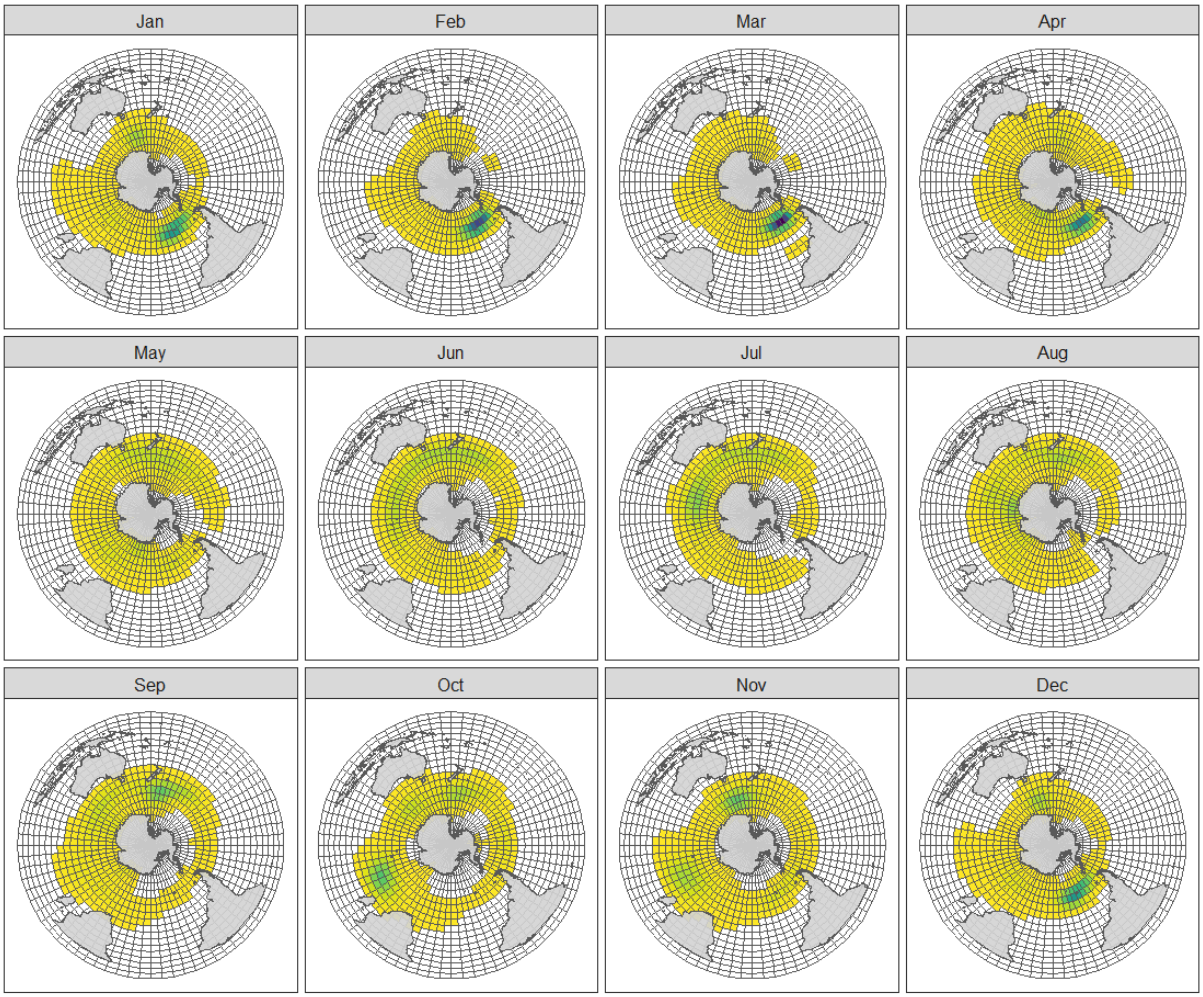

Figure 17: Light-mantled sooty albatross (*Phoebetria palpebrata*) predicted distribution by month. Yellow indicates low densities, and dark blue indicates high densities.

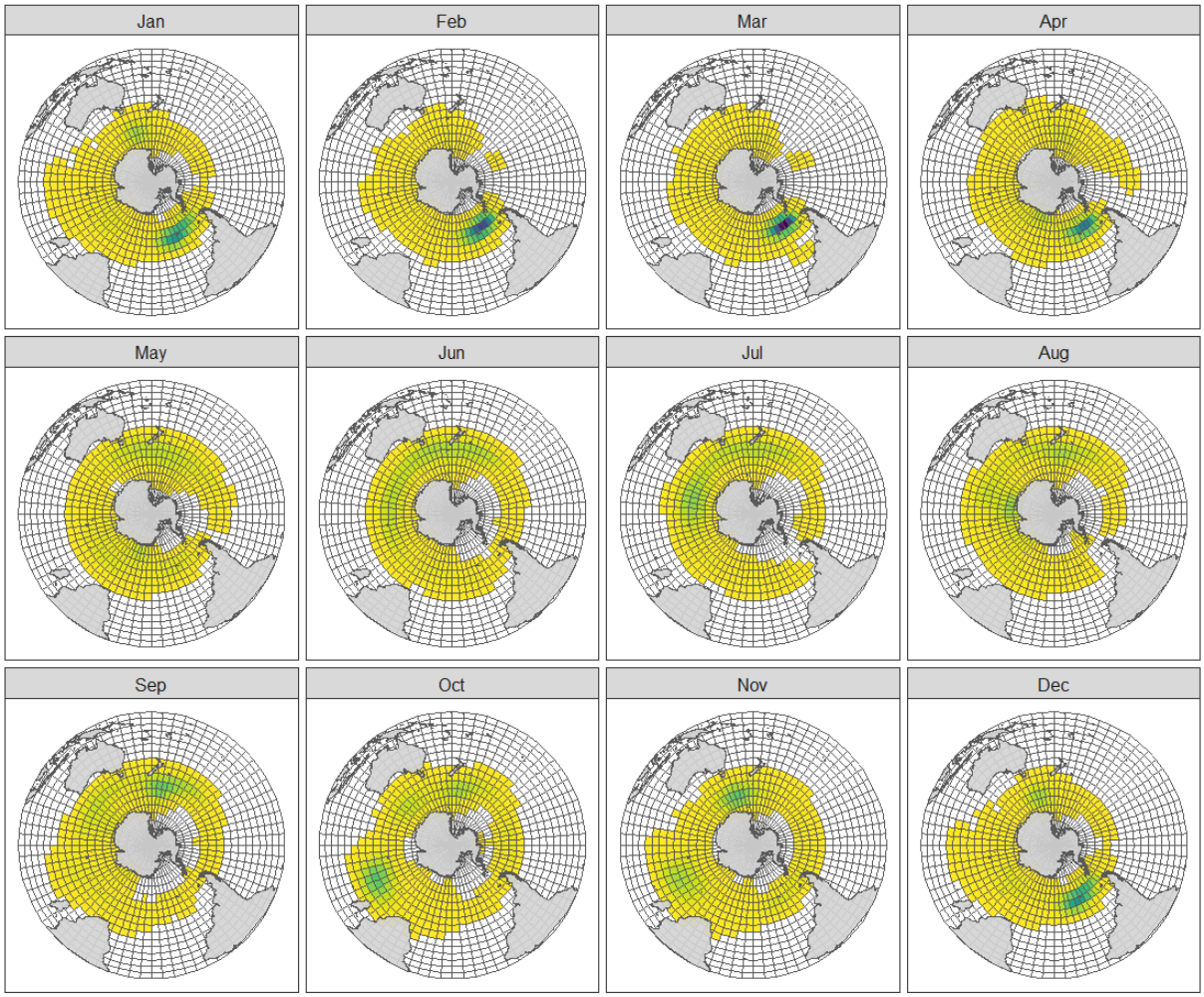

Figure 18: Light-mantled sooty albatross (*Phoebetria palpebrata*) predicted distribution by month, after augmentation with the Prince Edward Island colony distribution maps of Carneiro et al. (2020). Yellow indicates low densities, and dark blue indicates high densities.

3.3.13 Grey petrel

While no additional datasets were available for the updated analysis, the update included weighting by the mean colony size, which was not previously done. The Antipodes colony contained 70% of the population, followed by Gough Island (17%); all other colonies made up a minor proportion of the total grey petrel population (Table 3). Because of weighting the data, the distribution in the south Indian and Atlantic Oceans was de-emphasized (Figure 19). The Carneiro et al. (2020) distribution maps were not used to augment the predicted distribution.

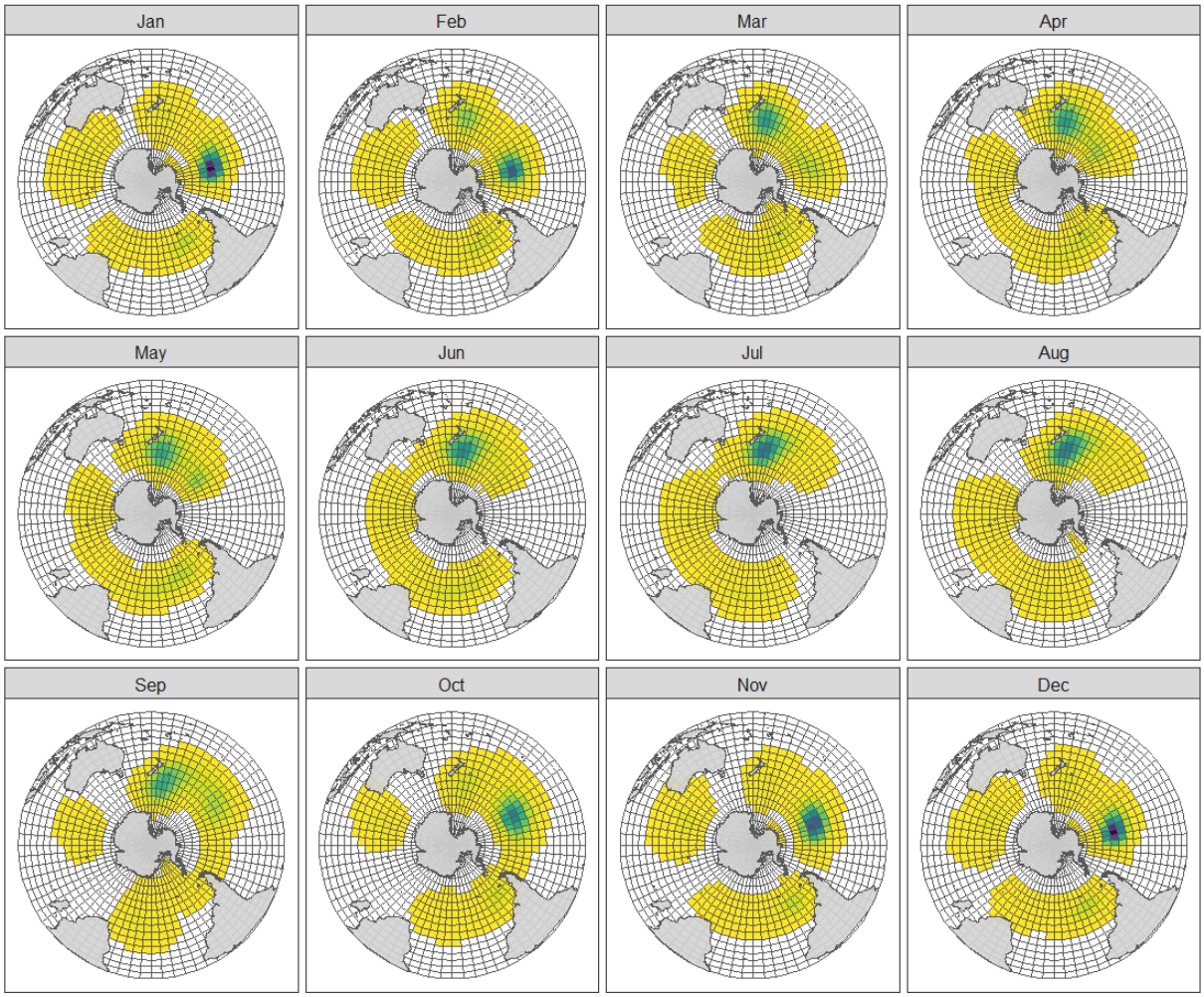

Figure 19: Grey petrel (*Procellaria cinerea*) predicted distribution by month. Yellow indicates low densities, and dark blue indicates high densities.

3.3.14 Black petrel

The external review noted that some tracks included in the previous distribution modelling may not have been black petrel tracks and that this species should be absent from New Zealand in July through September. Permission was given to use all available datasets in BirdLife International and an additional set for Aotea Great Barrier Island was provided by the New Zealand DOC (Table 2). The data identified as black petrel included tracks south of 43 °S (see Appendix N). Because these are predicting probable distribution for a species, very low relative densities were predicted around New Zealand in July, but the updated maps show that black petrels are now absent in August and September, having migrated across the south Pacific Ocean to the coast of South America and northward (Figure 20). The spatial distribution was allowed to cross the equator to simulate movement of this species into the northern hemisphere and along the coast of central America. The external review expressed concern that data had not been adequately groomed because predictions had been allowed to extend into the Caribbean Sea. Raw data were closely scrutinized. The movements were from four datasets (56 tracks) and were not associated with the equinox (as this can introduce errors); there was nothing to suggest that these data were not real, and the data were retained in the analysis. This may, however, be an issue with older GLS data and will require closer scrutiny (including working with experts) should distribution maps be updated in the future. Note that the greatest predicted density was to the Pacific

Ocean coast of South America (June–September) (Figure 20). The number of knots and model formulation had not been updated, so improvement to the distribution was due to the addition of three tracking datasets for the Great Barrier Island colony and weighting by colony size (Table 4). The Carneiro et al. (2020) distribution maps were not used to augment the predicted distribution.

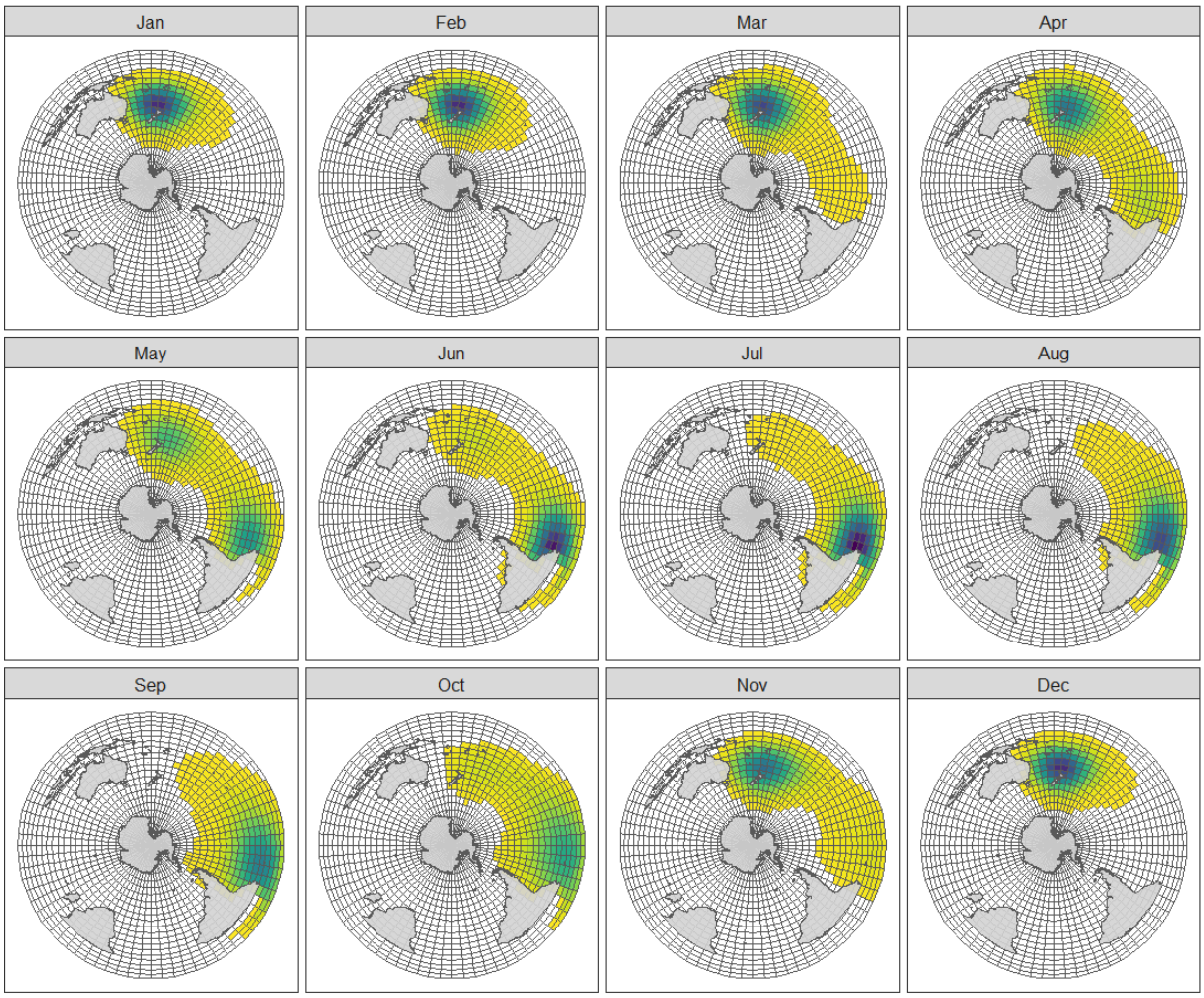

Figure 20: Black petrel (*Procellaria parkinsoni*) predicted distribution by month. Yellow indicates low densities, and dark blue indicates high densities.

3.3.15 Westland petrel

Two additional tracking datasets were provided for the updated analysis, which vastly improved the modelled distributions. Westland petrels were distributed only around New Zealand in June and July and were in high density along the South American coast (Chile and Argentina) in November–March (Figure 21). Tracking data supported the movement of birds around the tip of South America and to the Argentinian coast (see Appendix O). The external review noted that this species should not be present in New Zealand water in January–March (see Table A.6 in Edwards et al. 2025); however, the raw tracking data indicated a large number of tracks around New Zealand at that time (see Appendix O). The Carneiro et al. (2020) distribution maps were not used to augment the predicted distribution.

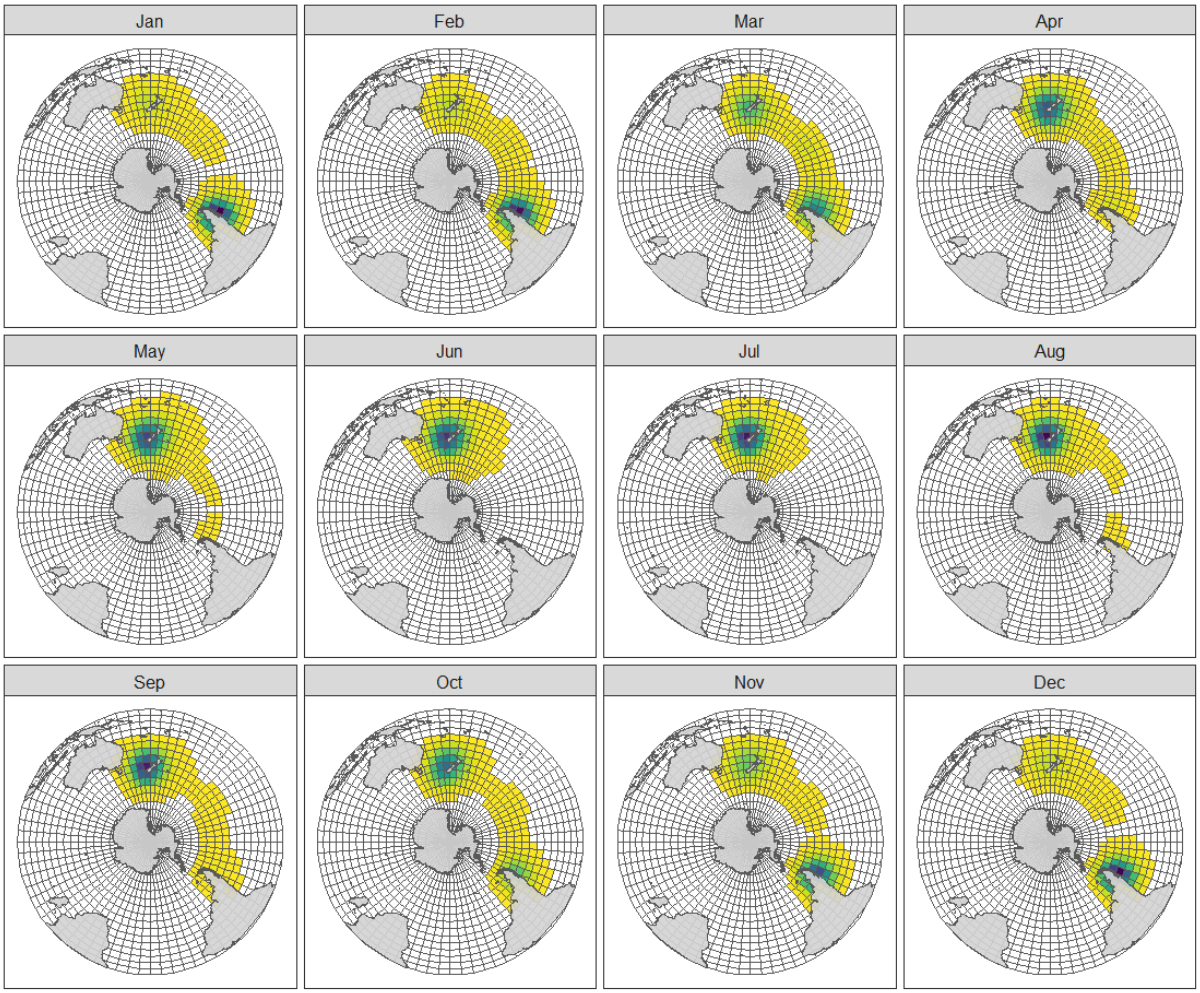

Figure 21: Westland petrel (*Procellaria westlandica*) predicted distribution by month. Yellow indicates low densities, and dark blue indicates high densities.

3.3.16 White-chinned petrel

Permission was granted to use all available tracking datasets in BirdLife International (Table 2). The external review noted that known foraging areas such as the Benguela upwelling zone were not present in the previous distributions. The current maps included an additional five datasets. Tracking data indicated movement of white-chinned petrels into this area between February and September (see Appendix P), and the predicted distributions also indicated relatively high densities here between April and August (Figure 22). However, distributions of the largest colony (South Georgia, Table 3) dominated the predicted distributions (Figure 22). The Carneiro et al. (2020) distribution maps were not used to augment the predicted distribution.

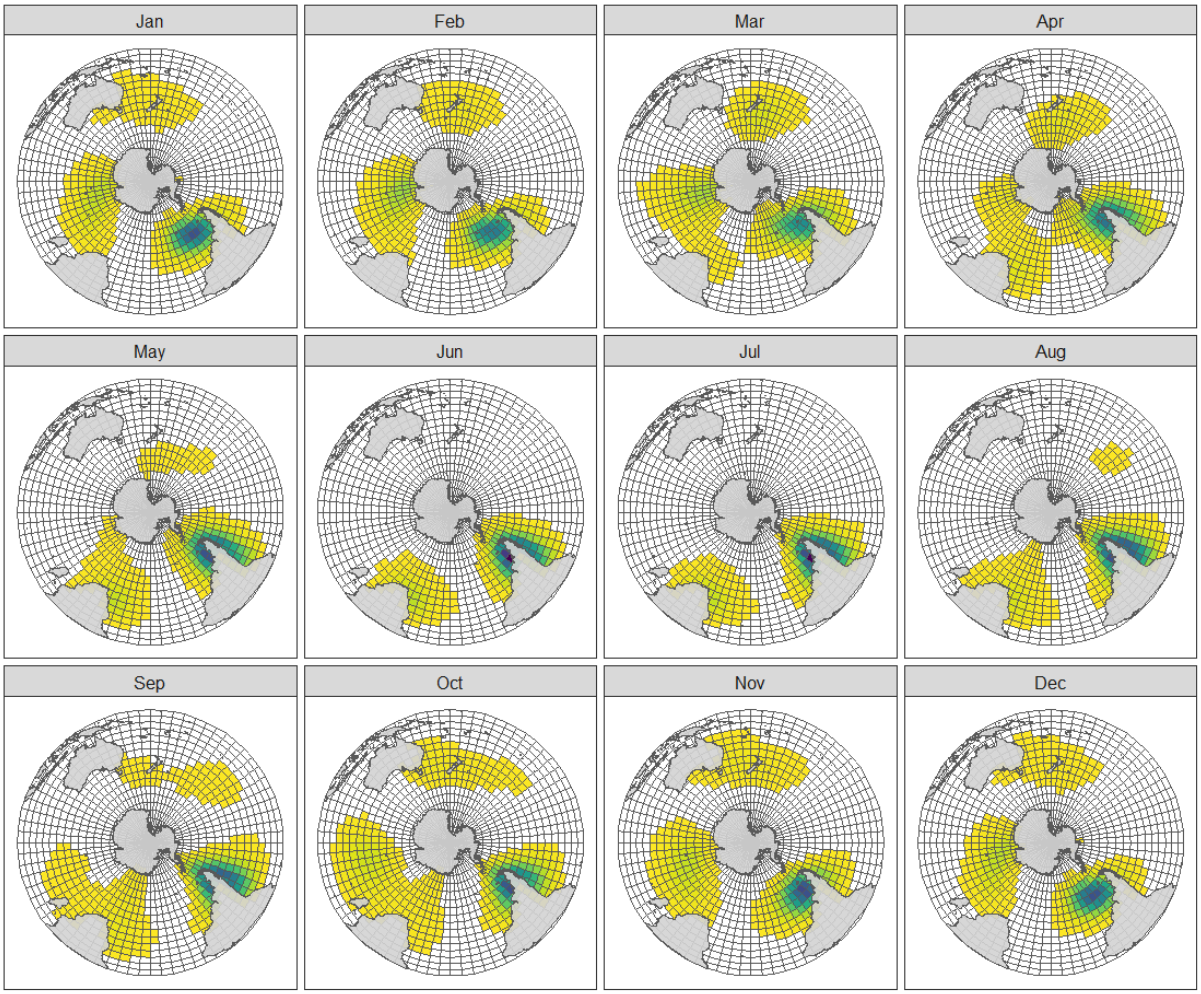

Figure 22: White-chinned petrel (*Procellaria aequinoctialis*) predicted distribution by month. Yellow indicates low densities, and dark blue indicates high densities.

4 Future wortk

Future iterations of the work presented could be improved through:

- Further inspection of older GLS tracks and potentially, where needed, reprocessing these using improved techniques (e.g., Merkel et al. 2016 A probabilistic algorithm to process geolocation data | Movement Ecology | Full Text) to reduce error. This could, for example, improve the distribution of Black Petrels and White-chinned Petrels.

- Further increase of sample sizes if and when new tracking data becomes available. This could, for example, improve the distributions of Northern and Southern Buller's Albatross. Table 3 further highlights which colonies would benefit most from future concerted tracking efforts. Wandering Albatrosses from Prince Edward Island, Atlantic Yellow-nosed Albatross from Tristan da Cunha, Grey-headed Albatross from Crozet and Kerguelen, Light-mantled Sooty Albatrosses from the Auckland Islands, Grey Petrels from Crozet, and White-chinned Petrels from Disappointment and Campbell Island appear global tracking priorities.

- Some further reprocessing of the augmentation steps using the maps from Carneiro et al. 2020 to align resolutions.

- Exploration of how tracking intensity within species, but among colonies, could be further accounted for.

5 Acknowledgements

The following list of individuals/organisations provided tracking data: Amanda Freeman, Ana Bertoldi Carneiro, Andrew Westgate, Andy Schofield, Antje Steinfurth, April Hedd, Aurore Ponchon, Azwianewi Makhado, Ben Dilley, Bindi Thomas, Chris Powell, Christina Hagen, Christopher Robertson, David Gremillet, David Nicholls, David Thompson, Dominic Rollinson, Elizabeth Bell, Ewan Wakefield, Falklands Conservation, Flavio Quintana, Graham Robertson, Henri Weimerskirch, Harry Marshall, Jacob Gonzalez-Solis, Jaime Cleeland, Javier Arata, Jean-Claude Stahl, John Arnould, Jose Pedro Granadeiro, Kalinka Rexer-Huber, Kris Carlyon, Leandro Bugoni, Leigh Torres, Lesley Thorne, Letizia Campioni, Lorna Deppe, New Zealand Department of Conservation (in particular, Kath Walker, Graeme Elliott, Graham Parker, Peter Moore, Brodie Philp, Theo Thompson, Chrissy Wickes, Jamie Darby, Mike Bell, Carlos Zavalaga, Kate Simister, Matt Charteris, Samhita Bose, Igor Debski, Graeme Taylor, Olivia Rowley, and Johannes Fischer), Paul Sagar, Paul Scofield, Paulo Catry, Peter Ryan, Pierre Pistorius, Richard Phillips, Robert Ronconi, Rosemary Gales, Ross Wanless, Scott Shaffer, Stefan Schoombie, Steffen Oppel, Susan Micol, Timothée Poupart, Todd Landers, Trevor Glass, Wildlife Management International Ltd., and William Montevecchi. The draft report was reviewed by Darren Stevens**.** This work was funded by Shearwater Analytics Ltd.

6 References

Carneiro, A.P.B.; Pearmain, E.J.; Oppel, S.; Clay, T.A.; Phillips, R.A.; Bonnet-Lebrun, A.-S.; Wanless, R.M.; Abraham, E.; Richard, Y.; Rice, J.; Handley, J.; Davies, T.E.; Dilley, B.J.; Ryan, P.G.; Small, C.; Arata, J.; Arnould, J.P.Y.; Bell, E.; Bugoni, L.; Campioni, L.; Catry, P.; Cleeland, J.; Deppe, L.; Elliott, G.; Freeman, A.; González-Solís, J.; Granadeiro, J.P.; Grémillet, D.; Landers, T.J.; Makhado, A.; Nel, D.; Nicholls, D.G.; Rexer-Huber, K.; Robertson, C.J.R.; Sagar, P.M.; Scofield, P.; Stahl, J.-C.; Stanworth, A.; Stevens, K.L.; Trathan, P.N.; Thompson, D.R.; Torres, L.; Walker, K.; Waugh, S.M.; Weimerskirch, H.; Dias, M.P. (2020) A framework for mapping the distribution of seabirds by integrating tracking, demography and phenology. *Journal of Applied Ecology 57*: 514–525.

Edwards, C.T.T.; Peatman, T.; Fischer J.; Gibson, W. (2025) Inputs to the 2024 seabird risk assessment for the Southern Bluefin Tuna surface longline fishery. *New Zealand Aquatic Environment and Biodiversity Report No. 359*. 88.

Fischer, J.; Bell, M.; Frost, P.; Sagar, P.; Thompson, D.; Middlemiss, K.; Debski, I.; Taylor, G. (2023) *Year-round GLS tracking of Northern Buller's Albatross and comparison with Southern Buller's Albatross.* Unpublished report: Department of Conservation, Conservation Services Programme POP2022-05: Northern Buller's Albatross population monitoring. 16.

Jørgensen, B. (1987) Exponential dispersion models. *Journal of the Royal Statistical Society Series B 49*: 127–162.

Marra, G.; Miller, D.L.; Zanin, L. (2011) Modelling the spatiotemporal distribution of the incidence of resident foreign population. *Statistica Neerlandica 66*: 133–160.

Reid, T.A.; Lecoq, M.; Catry, P. (2007) The white-chinned petrel *Procellaria aequinoctialis* population of the Falkland Islands," *Marine Ornithology 35*: Article 7. http://doi.org/10.5038/2074-1235.35.1.721

Wood, S.N. (2003) Thin-plate regression splines. *Journal of the Royal Statistical Society B 65*: 95–114.

Wood, S.N. (2017) *Generalized Additive Models: An Introduction with R* (2nd edition). Chapman and Hall/CRC.

Appendix A Gibson's Albatross

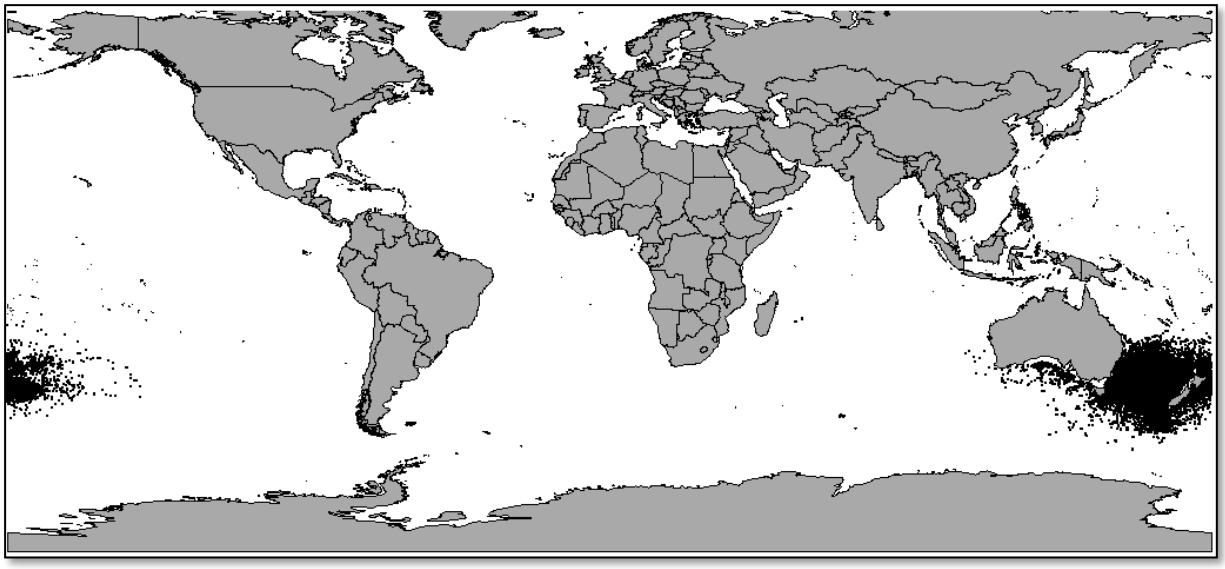

Figure A.1: Locations of ungroomed tracking data for all life stages, where different colours indicate different colonies.

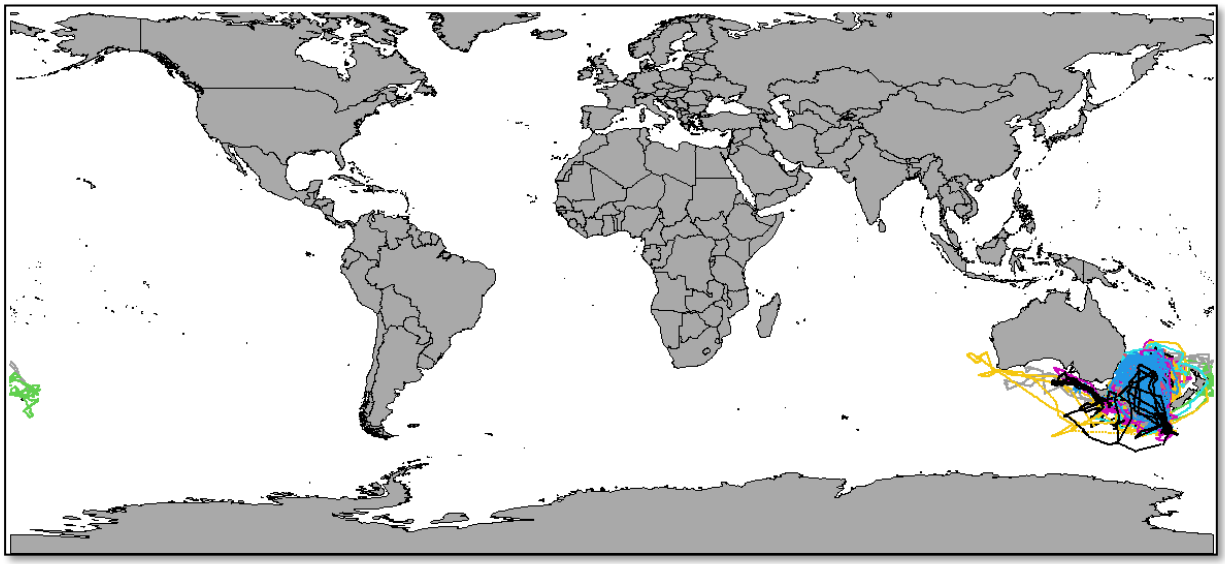

Figure A.2: Groomed and interpolated individual tracks for adult or unknown life stages, where different colours indicate different bird identifiers (noting that colours will repeat).

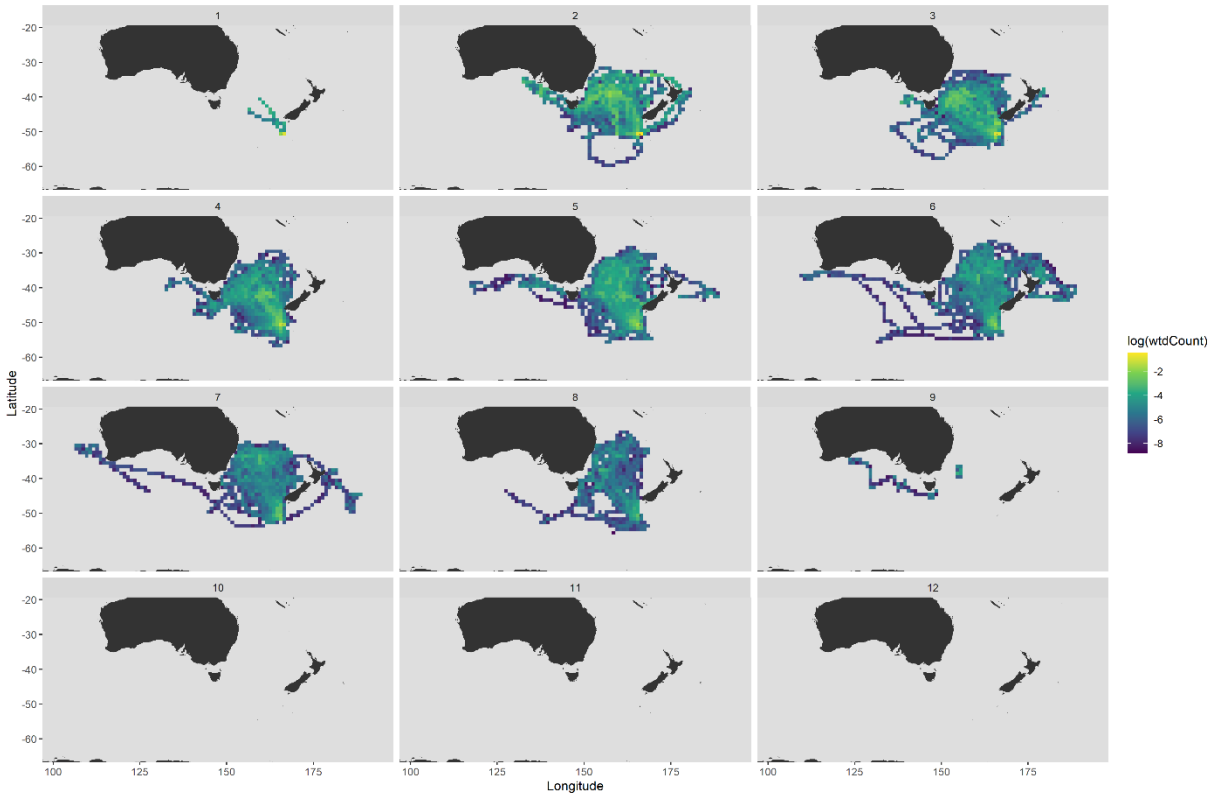

Figure A.3: Log relative density by month, aggregated by 1 ° lat-lon grid cell. Data were not weighted by mean colony size because only one colony was present.

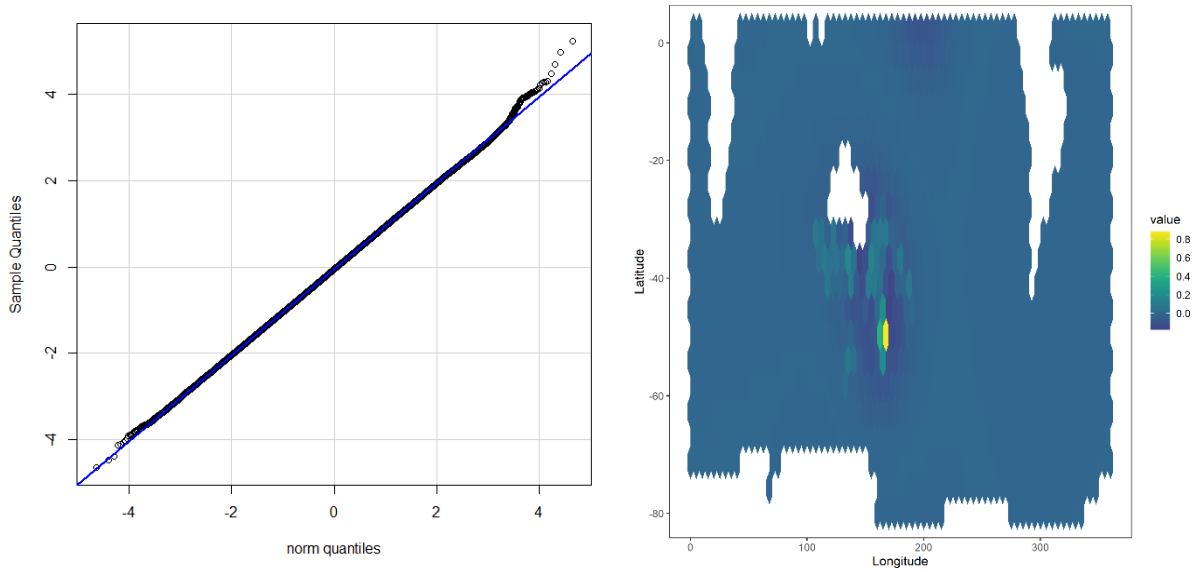

Figure A.4: Model diagnostic plots: residual QQ plot (left) and mean residual pattern by hexagonal grid cell (right).

Appendix B Wandering albatross

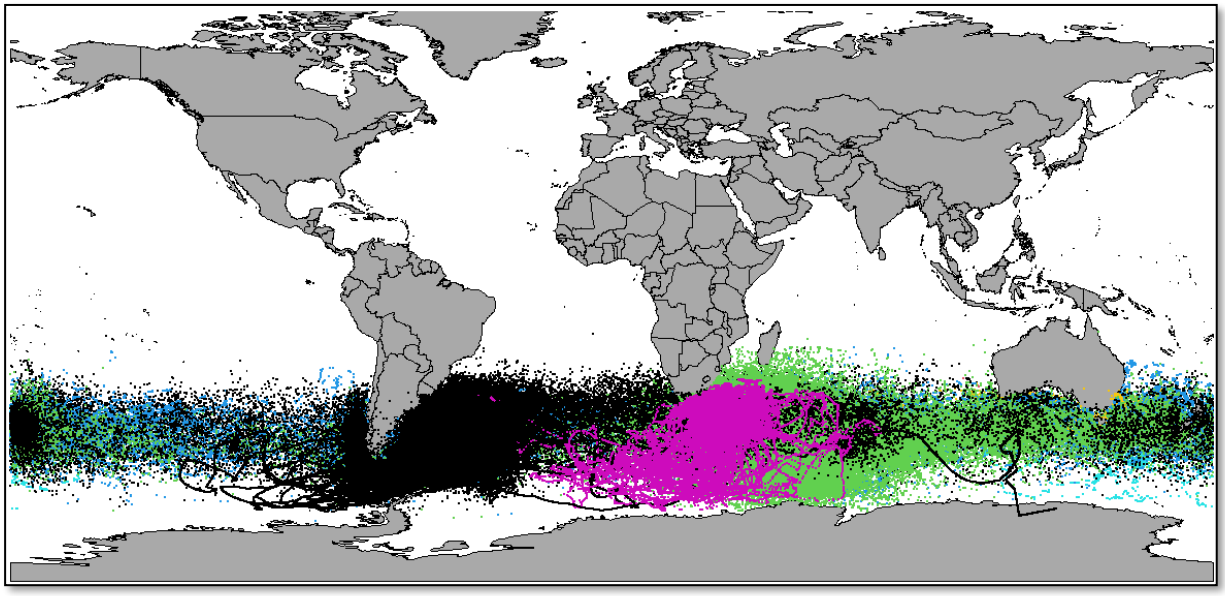

Figure B.5: Locations of ungroomed tracking data for all life stages, where different colours indicate different colonies.

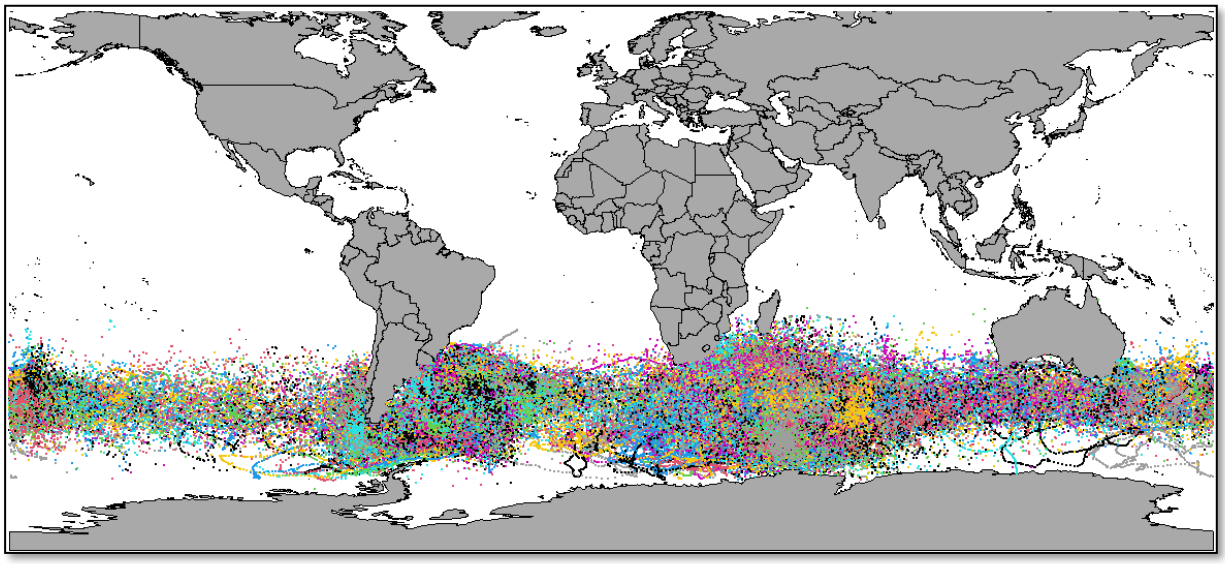

Figure B.6: Groomed and interpolated individual tracks for adult or unknown life stages, where different colours indicate different bird identifiers (noting that colours will repeat).

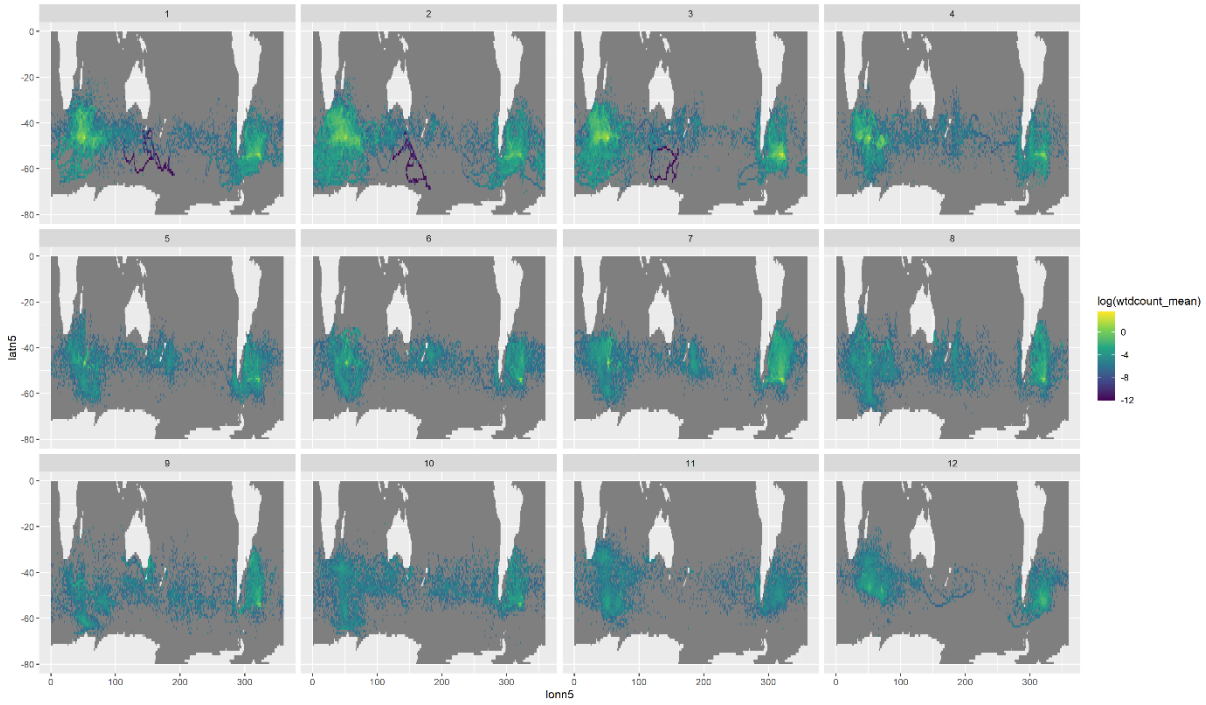

Figure B.7: Log mean weighted relative density by month, aggregated by 1 ° lat-lon grid cell.

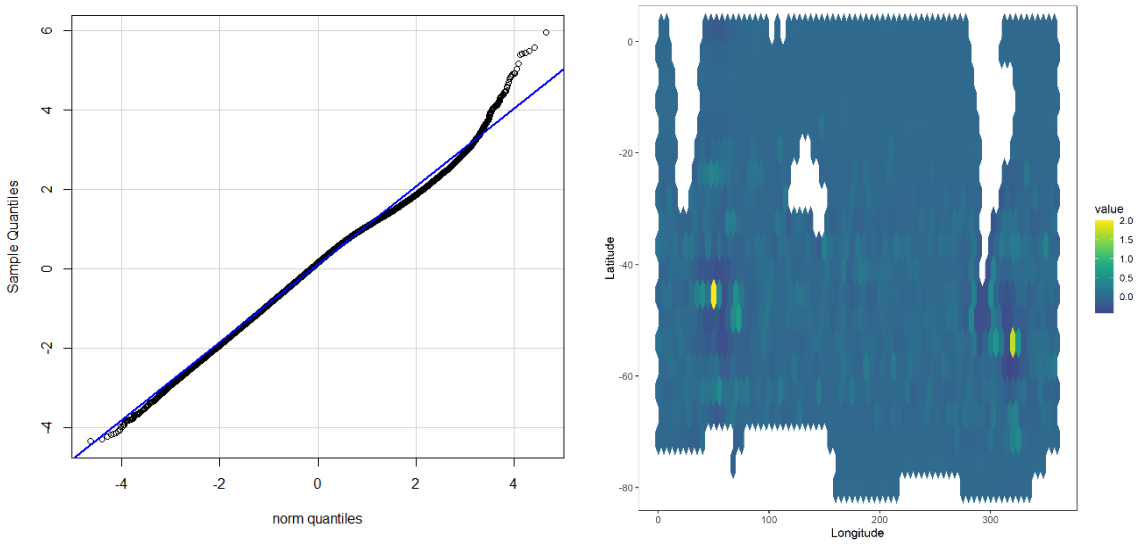

Figure B.8: Model diagnostic plots: residual QQ plot (left) and mean residual pattern by hexagonal grid cell (right).

Appendix C Southern royal albatross

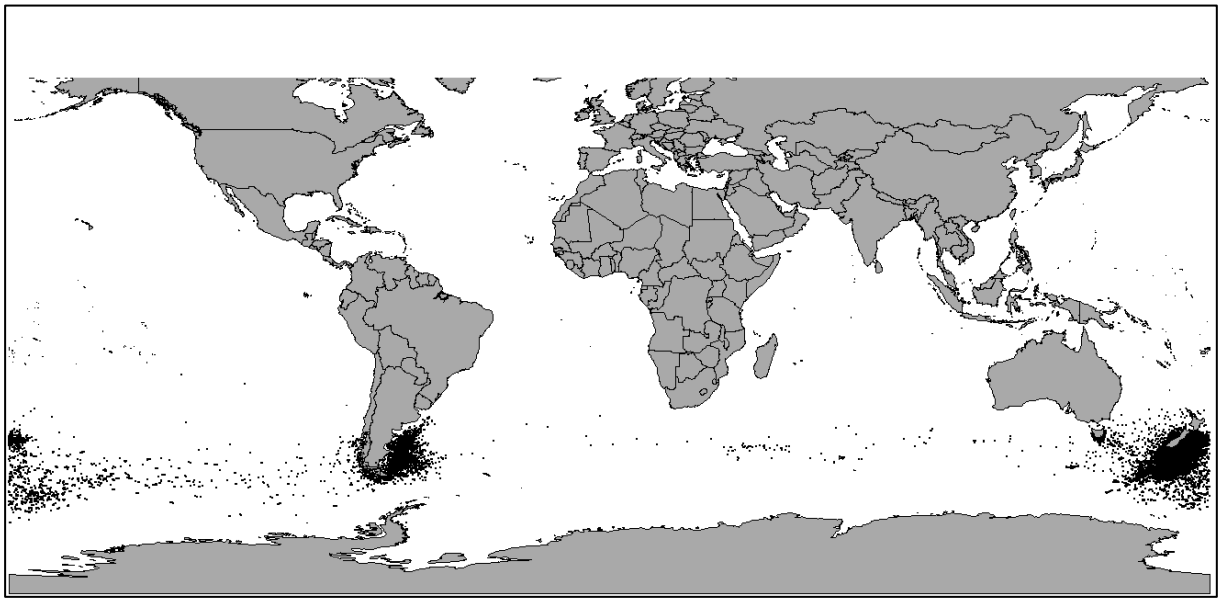

Figure C.9: Locations of ungroomed tracking data for all life stages, where different colours indicate different colonies.

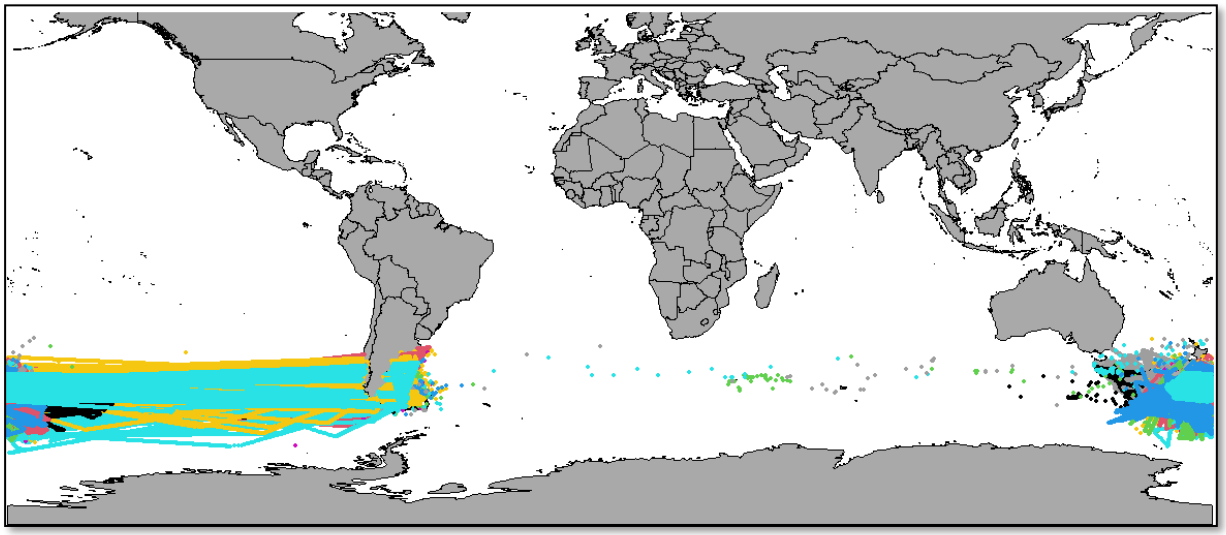

Figure C.10: Groomed and interpolated individual tracks for adult or unknown life stages, where different colours indicate different bird identifiers (noting that colours will repeat).

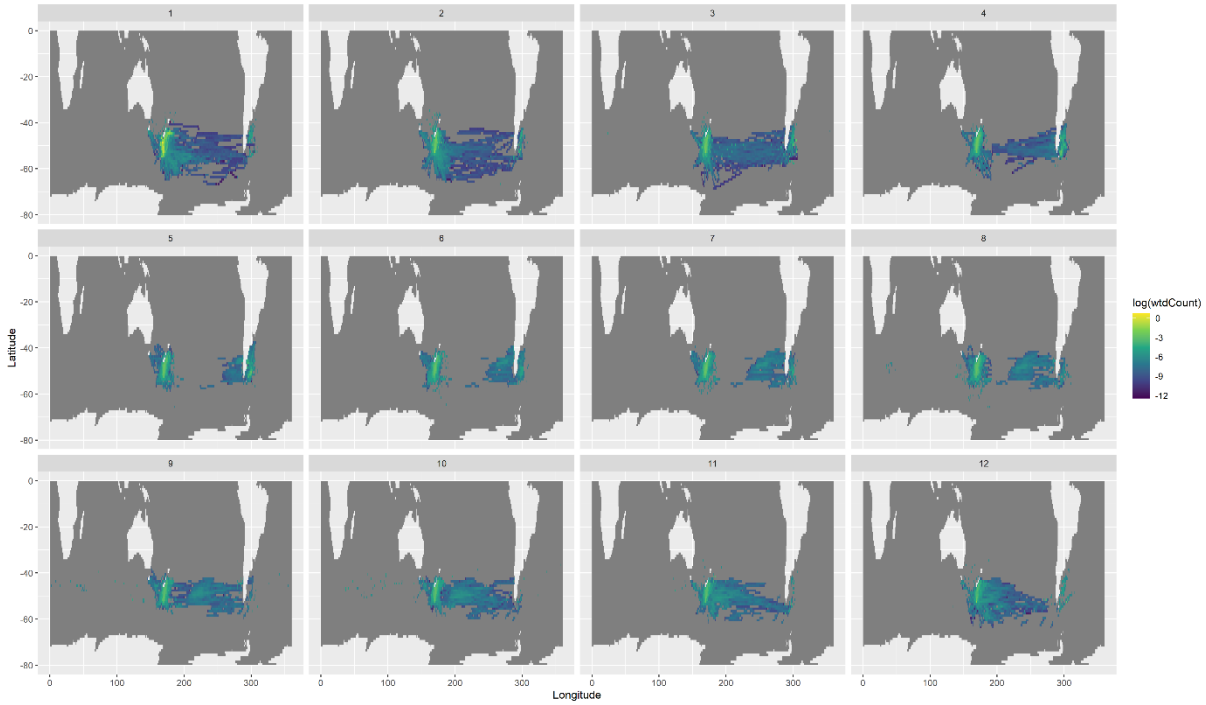

Figure C.11: Log relative density by month, aggregated by 1 ° lat-lon grid cell. Data were not weighted by mean colony size because only one colony was present.

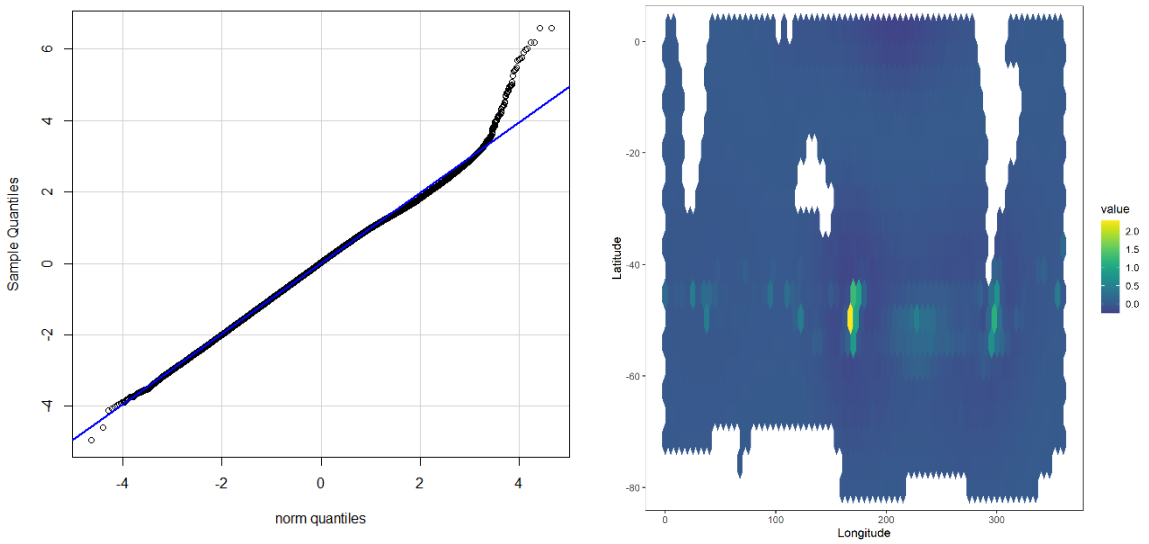

Figure C.12: Model diagnostic plots: residual QQ plot (left) and mean residual pattern by hexagonal grid cell (right).

Appendix D Atlantic yellow-nosed albatross

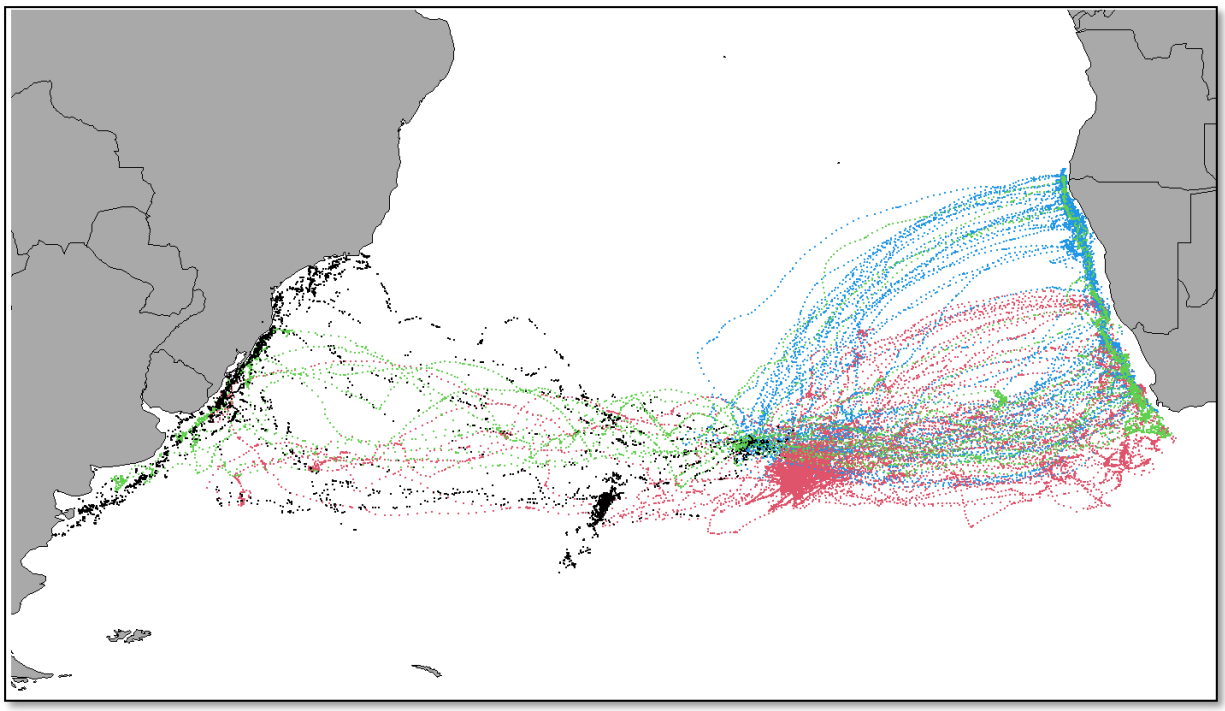

Figure D.13: Locations of ungroomed tracking data for all life stages, where different colours indicate different colonies.

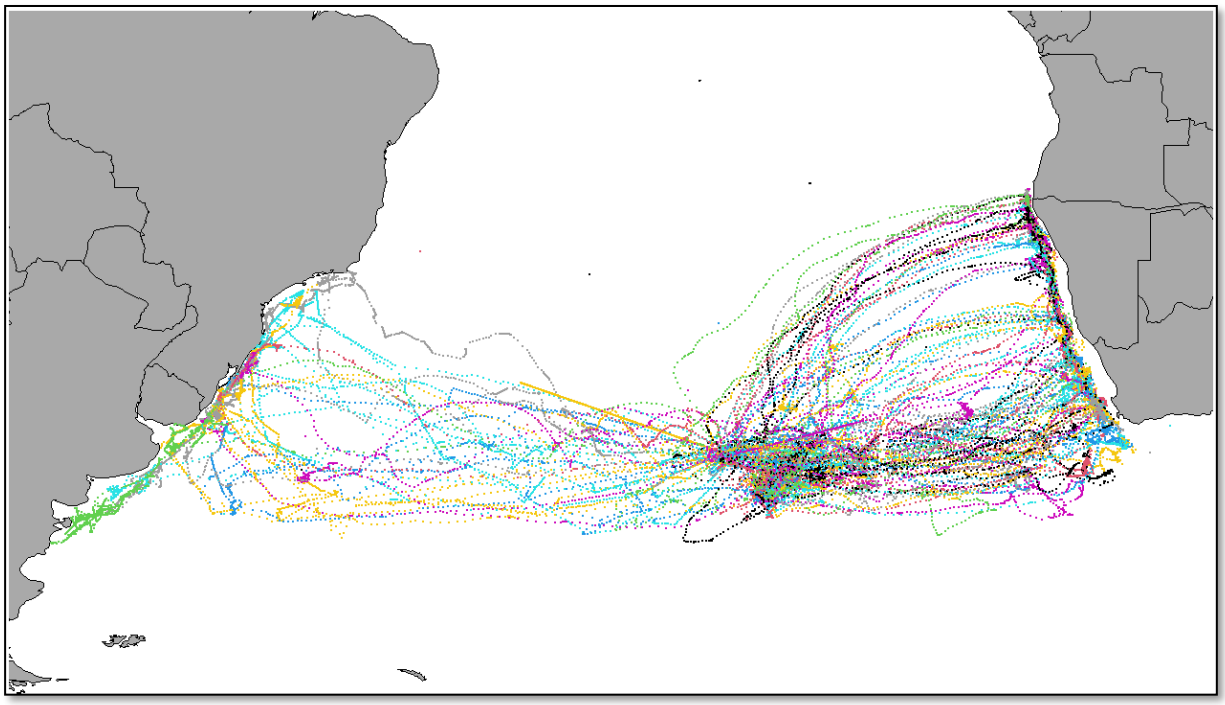

Figure D.14: Groomed and interpolated individual tracks for adult or unknown life stages, where different colours indicate different bird identifiers (noting that colours will repeat).

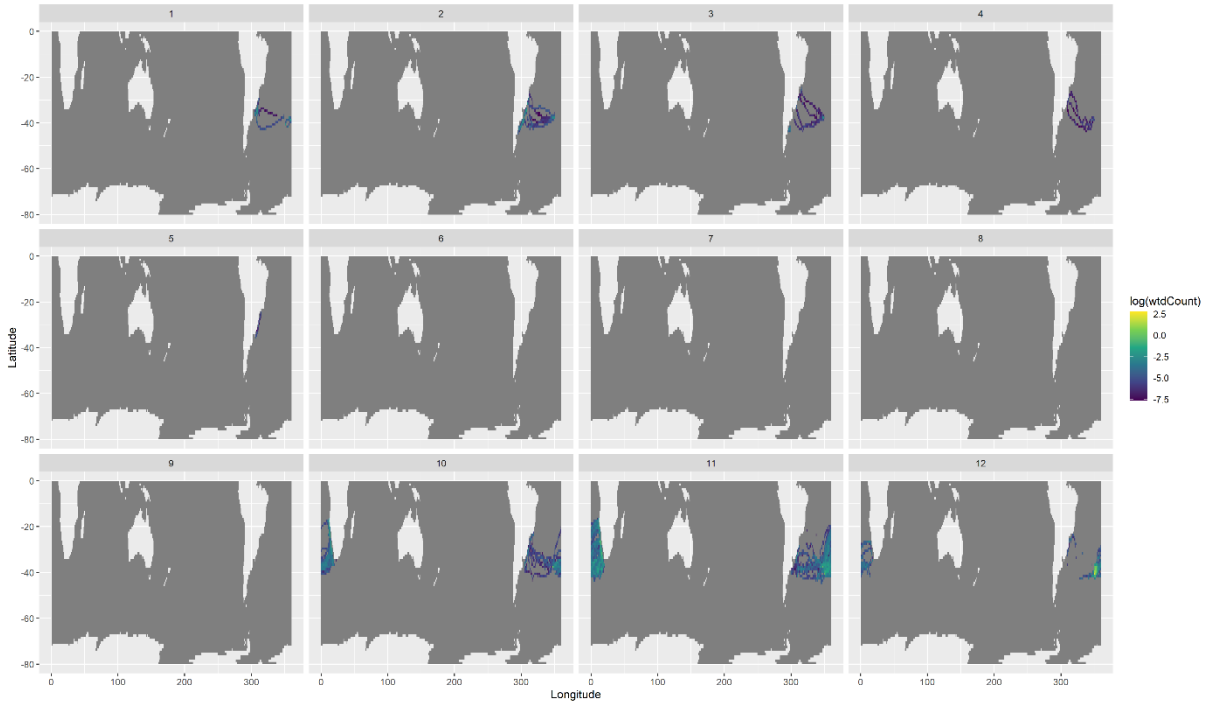

Figure D.15: Log mean weighted relative density by month, aggregated by 1 ° lat-lon grid cell.

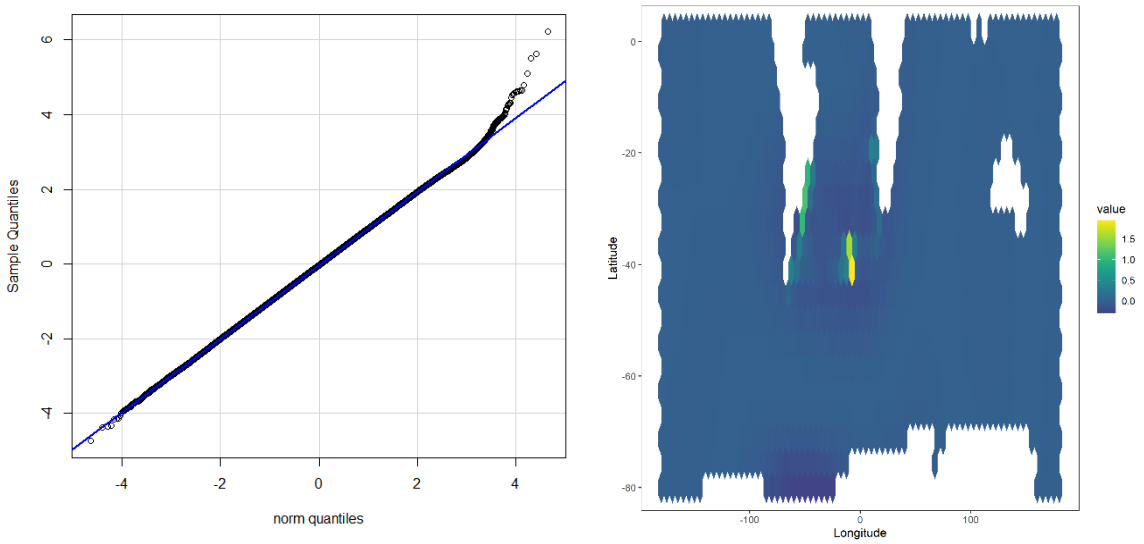

Figure D.16: Model diagnostic plots: residual QQ plot (left) and mean residual pattern by hexagonal grid cell (right).

Appendix E Black-browed albatross

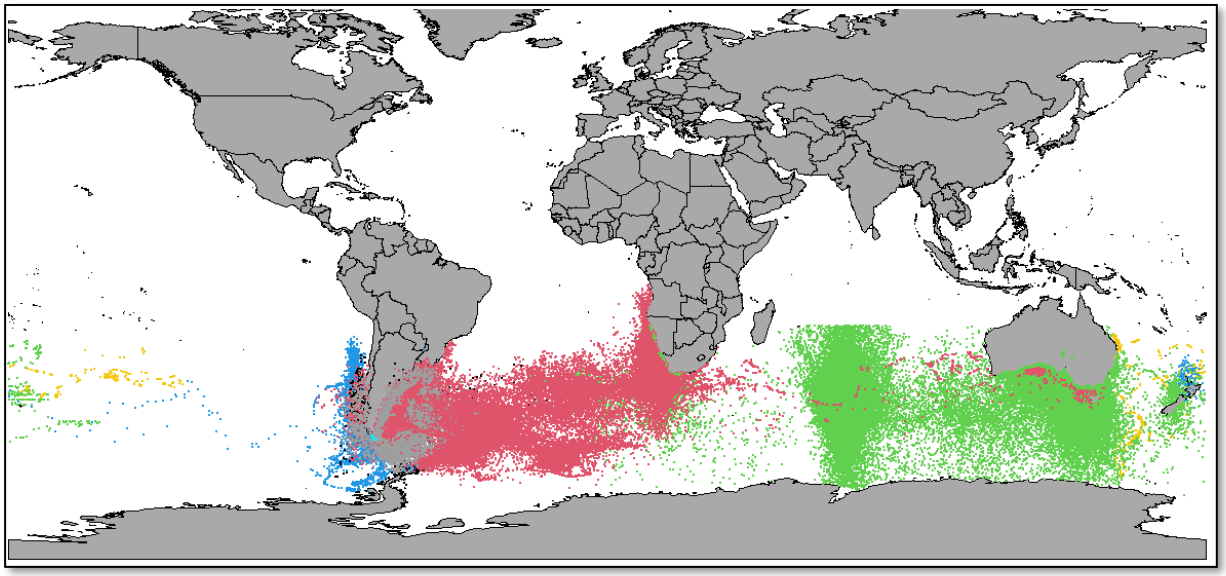

Figure E.17: Locations of ungroomed tracking data for all life stages, where different colours indicate different colonies.

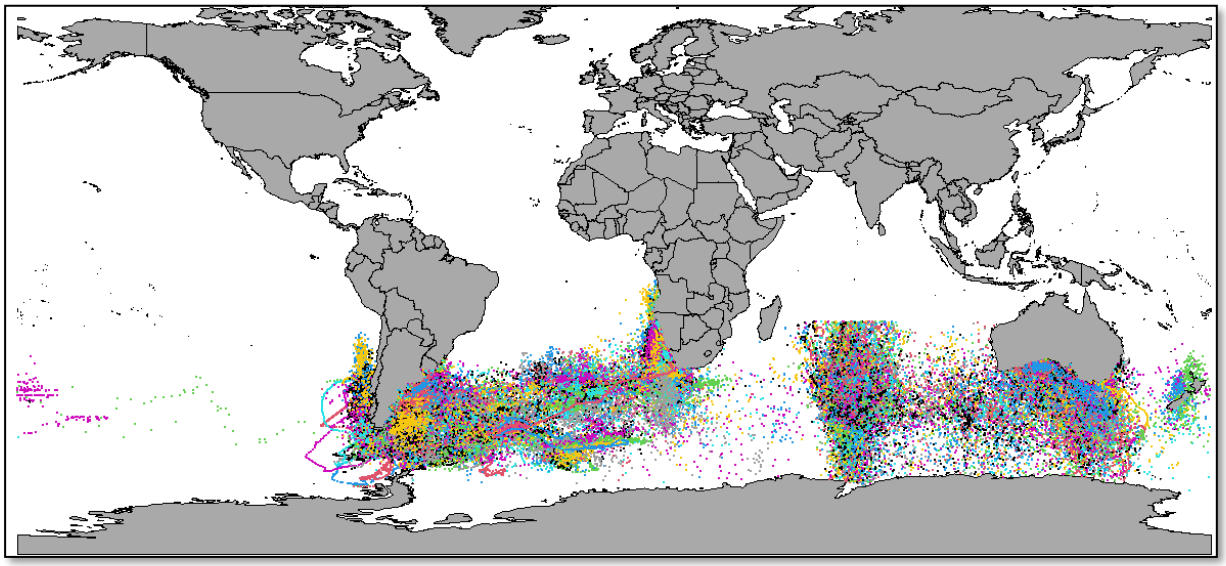

Figure E.18: Groomed and interpolated individual tracks for adult or unknown life stages, where different colours indicate different bird identifiers (noting that colours will repeat).

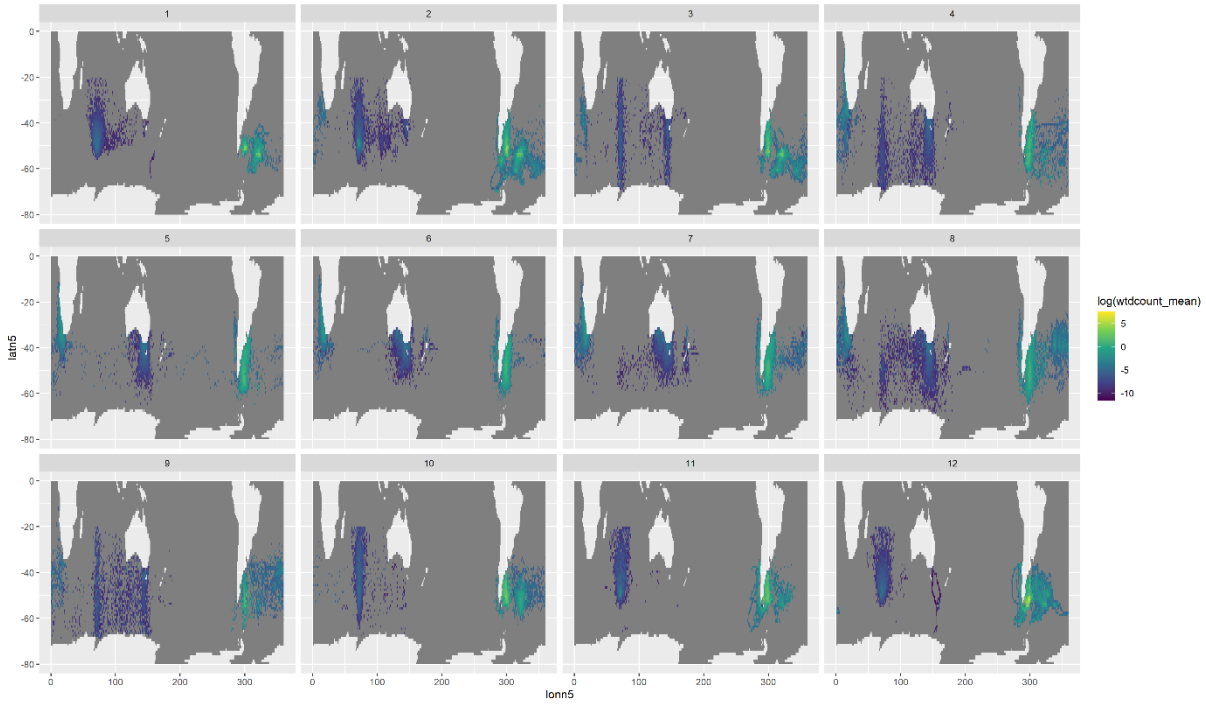

Figure E.19: Log mean weighted relative density by month, aggregated by 1 ° lat-lon grid cell.

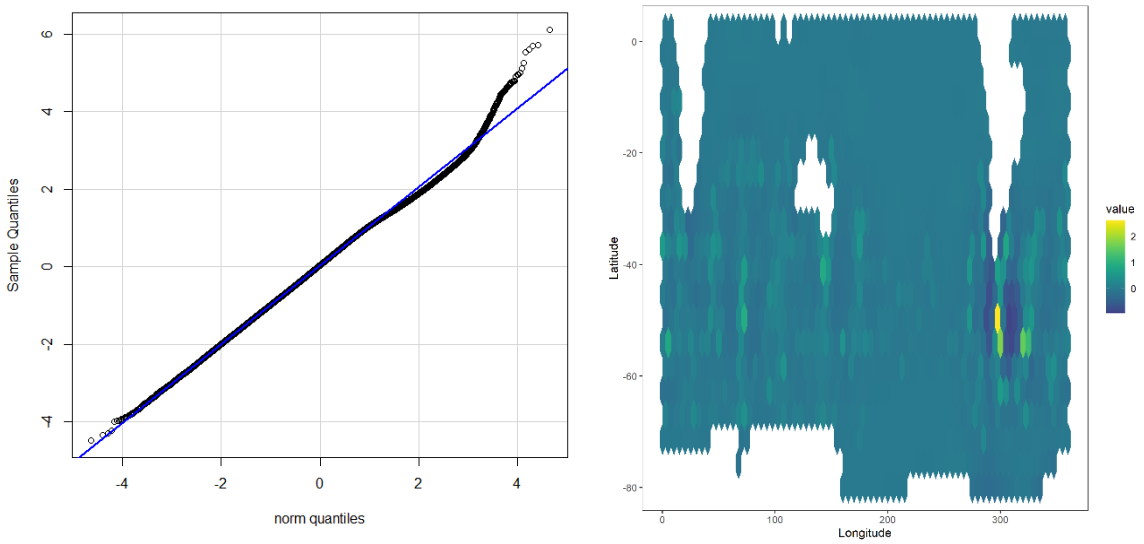

Figure E.20: Model diagnostic plots: residual QQ plot (left) and mean residual pattern by hexagonal grid cell (right).

Appendix F Campbell black-browed albatross

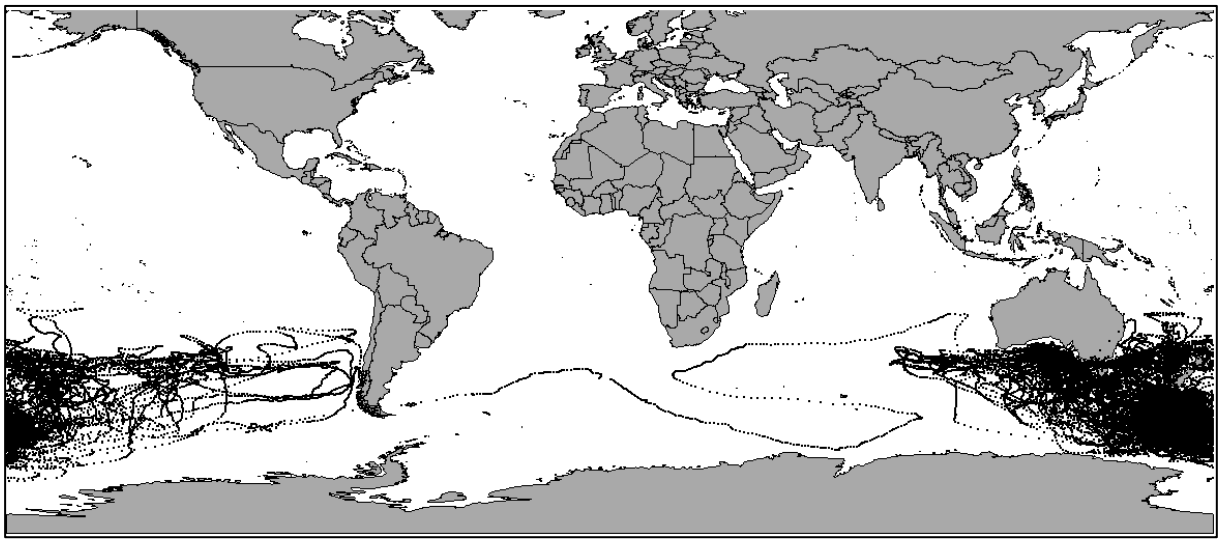

Figure F.21: Locations of ungroomed tracking data for all life stages, where different colours indicate different colonies.

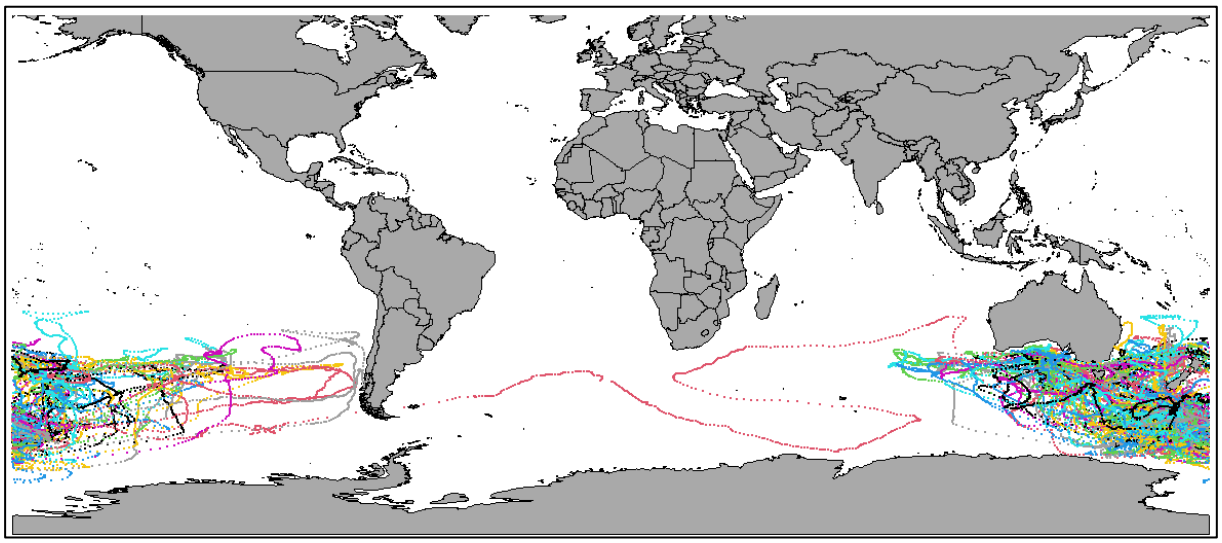

Figure F.22: Groomed and interpolated individual tracks for adult or unknown life stages, where different colours indicate different bird identifiers (noting that colours will repeat).

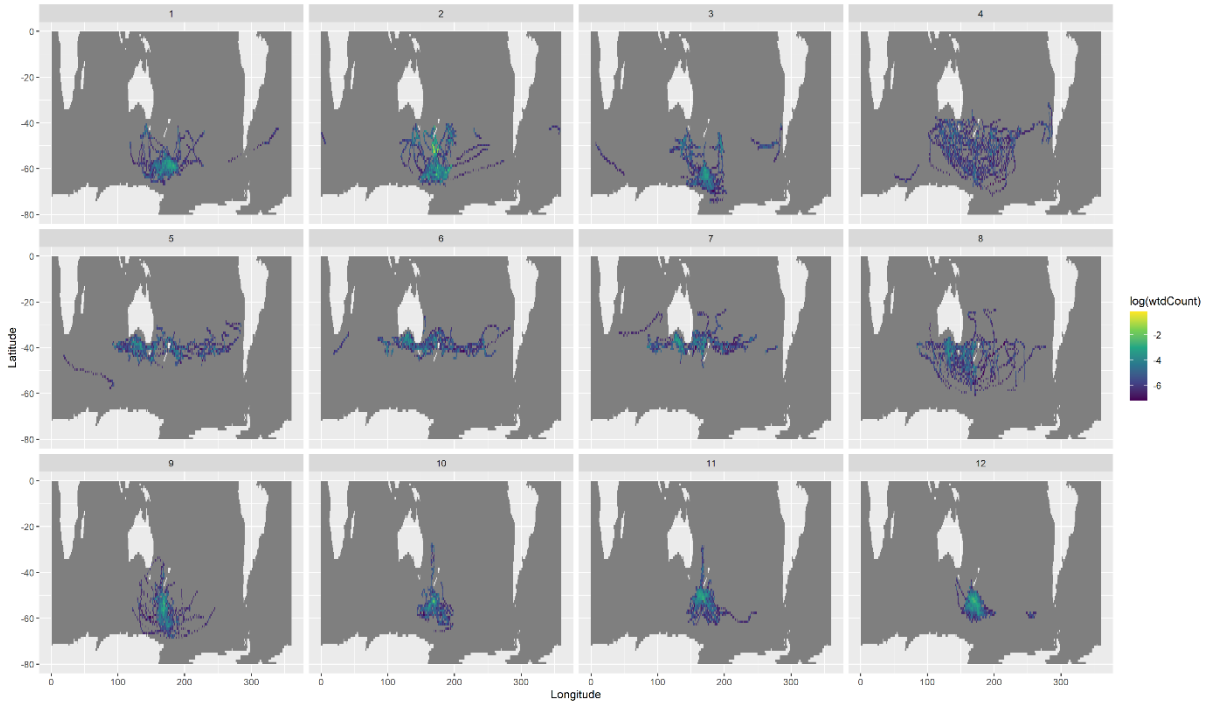

Figure F.23: Log relative density by month, aggregated by 1 ° lat-lon grid cell. Data were not weighted by mean colony size because only one colony was present.

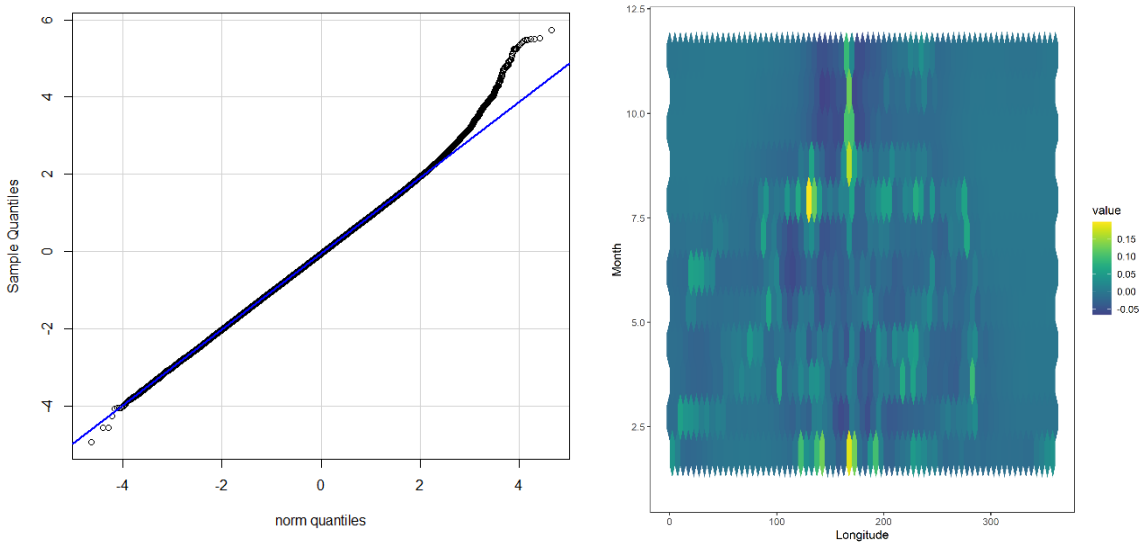

Figure F.24: Model diagnostic plots: residual QQ plot (left) and mean residual pattern by hexagonal grid cell (right).

Appendix G Shy albatross

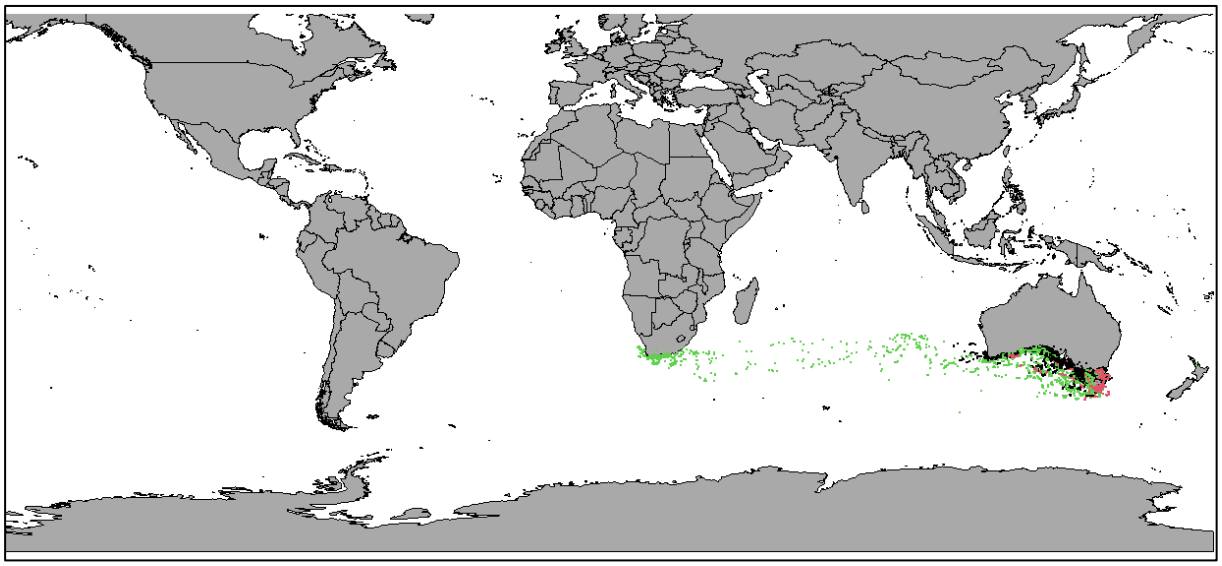

Figure G.25: Locations of ungroomed tracking data for all life stages, where different colours indicate different colonies.

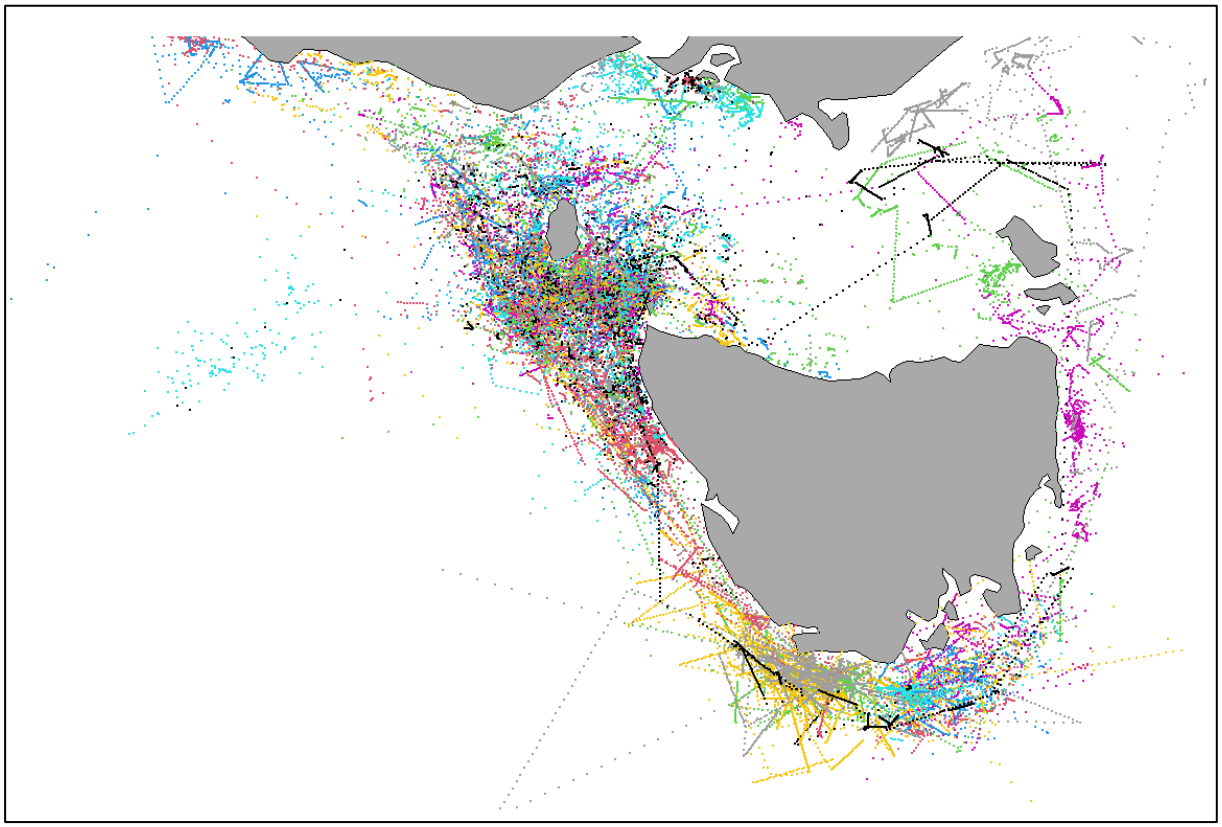

Figure G.26: Groomed and interpolated individual tracks for adult or unknown life stages, where different colours indicate different bird identifiers (noting that colours will repeat).

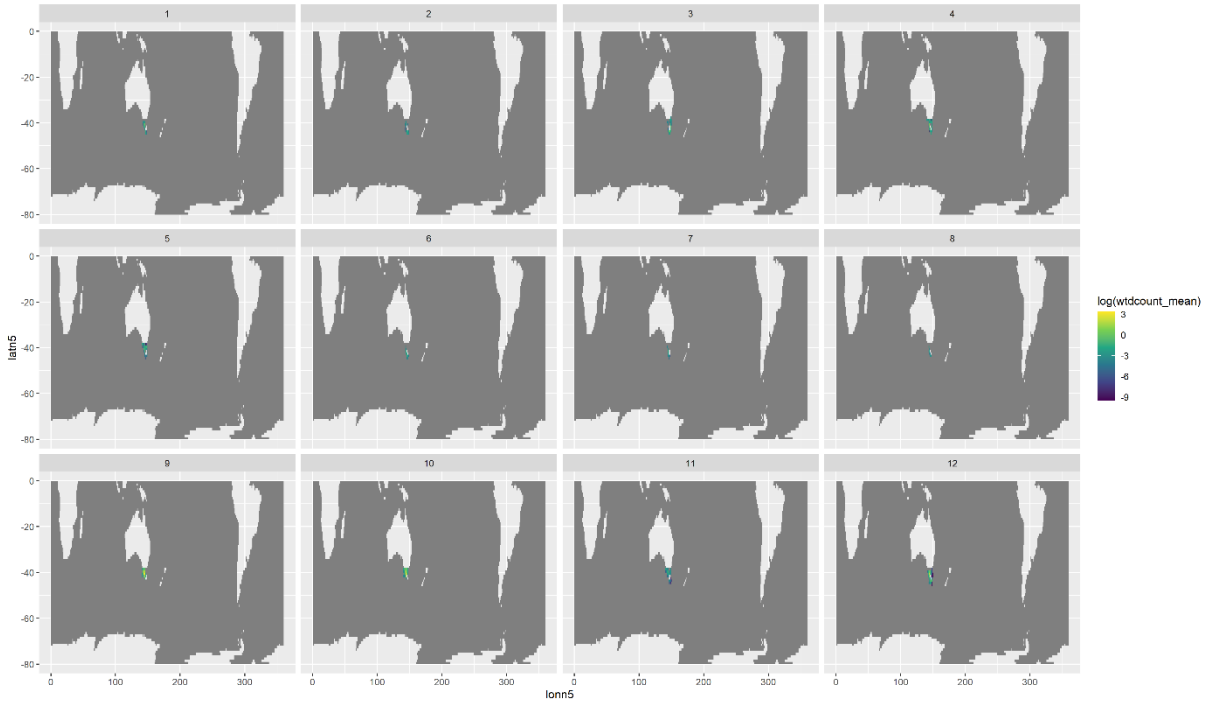

Figure G.27: Log mean weighted relative density by month, aggregated by 1 ° lat-lon grid cell.

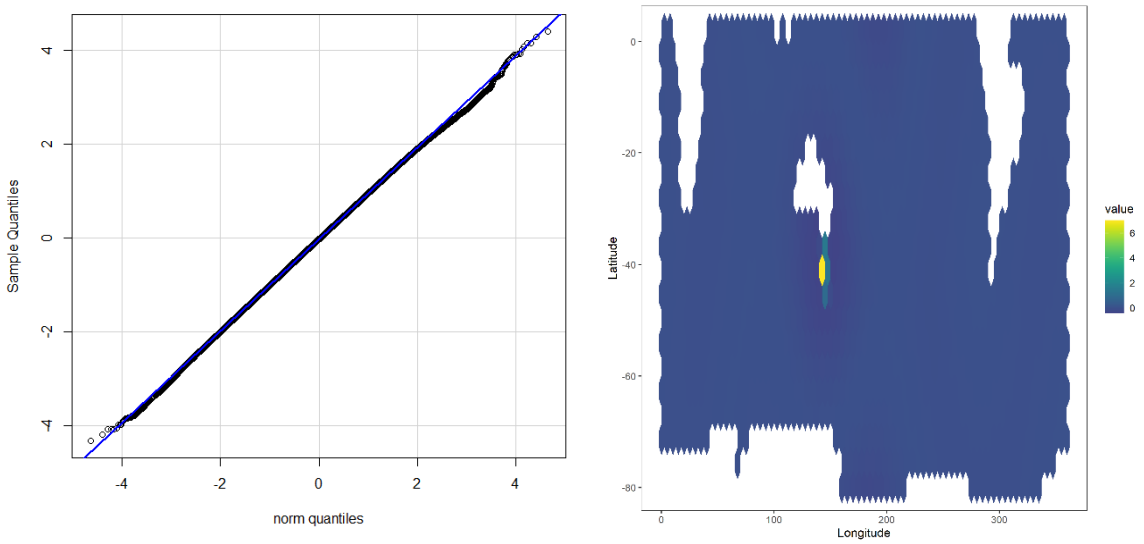

Figure G.28: Model diagnostic plots: residual QQ plot (left) and mean residual pattern by hexagonal grid cell (right).

Appendix H Grey-headed albatross

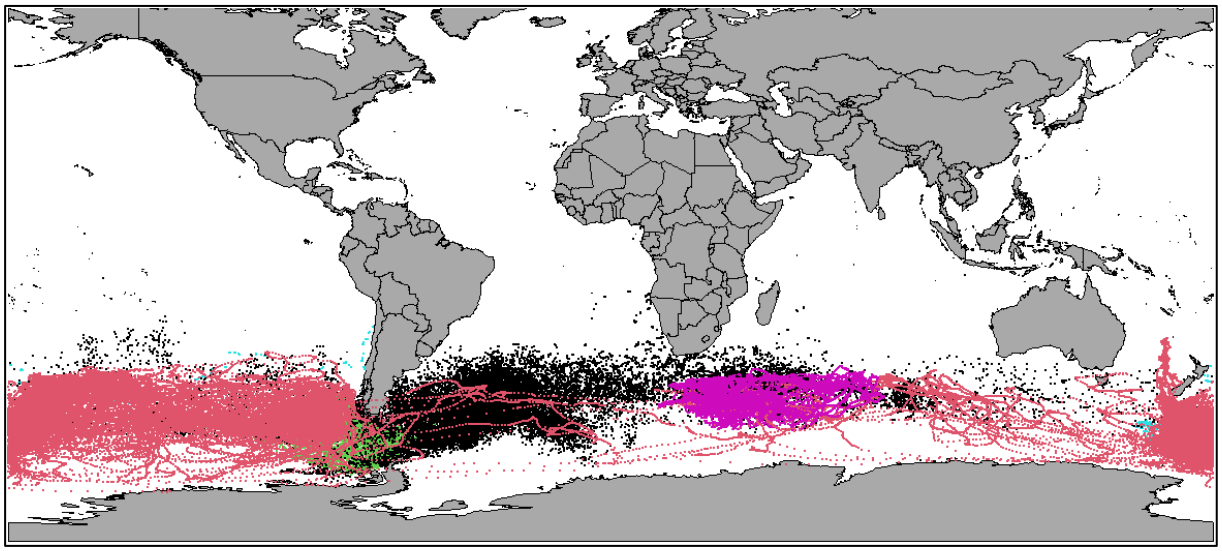

Figure H.29: Locations of ungroomed tracking data for all life stages, where different colours indicate different colonies.

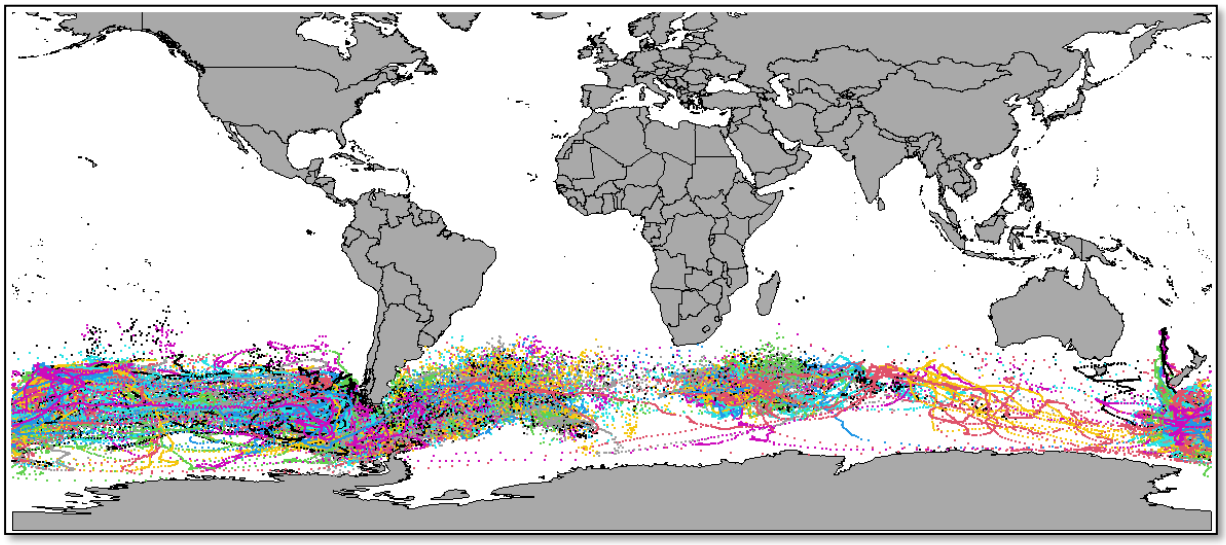

Figure H.30: Groomed and interpolated individual tracks for adult or unknown life stages, where different colours indicate different bird identifiers (noting that colours will repeat).

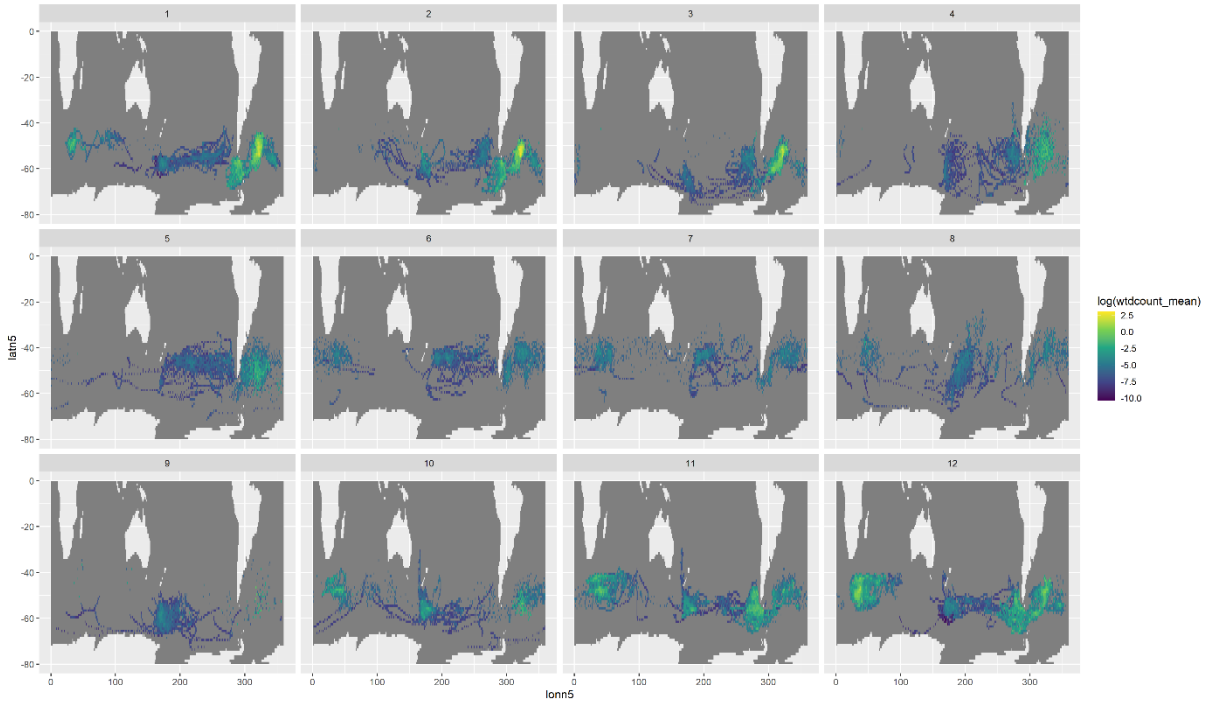

Figure H.31: Log mean weighted relative density by month, aggregated by 1 ° lat-lon grid cell.

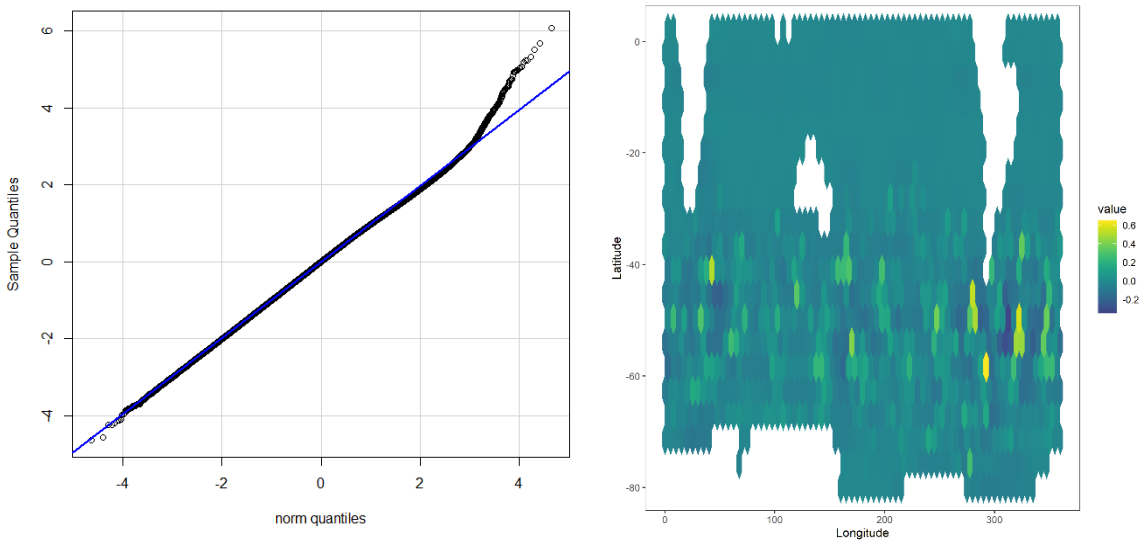

Figure H.32: Model diagnostic plots: residual QQ plot (left) and mean residual pattern by hexagonal grid cell (right).

Appendix I Southern Buller's albatross

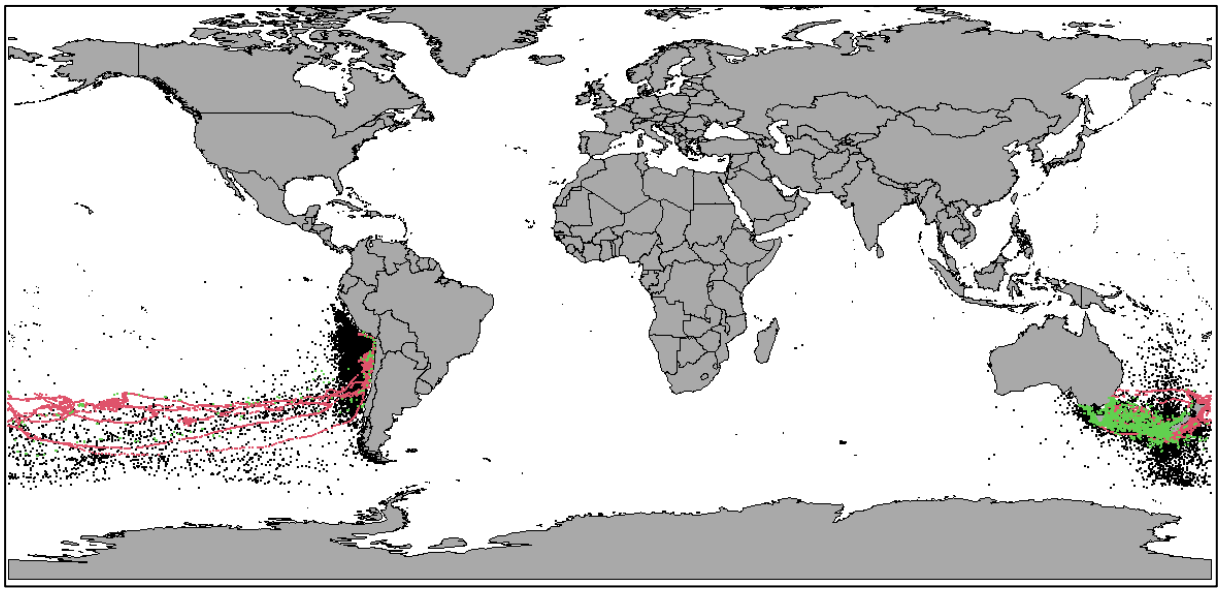

Figure I.33: Locations of ungroomed tracking data for all life stages, where different colours indicate different colonies.

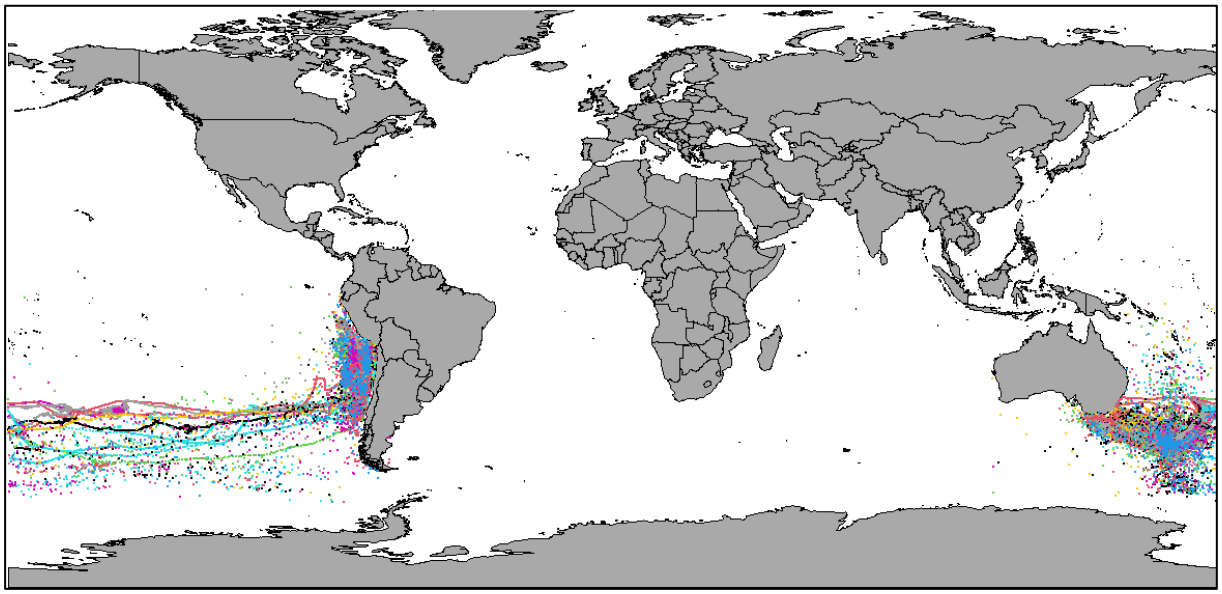

Figure I.34: Groomed and interpolated individual tracks for adult or unknown life stages, where different colours indicate different bird identifiers (noting that colours will repeat).

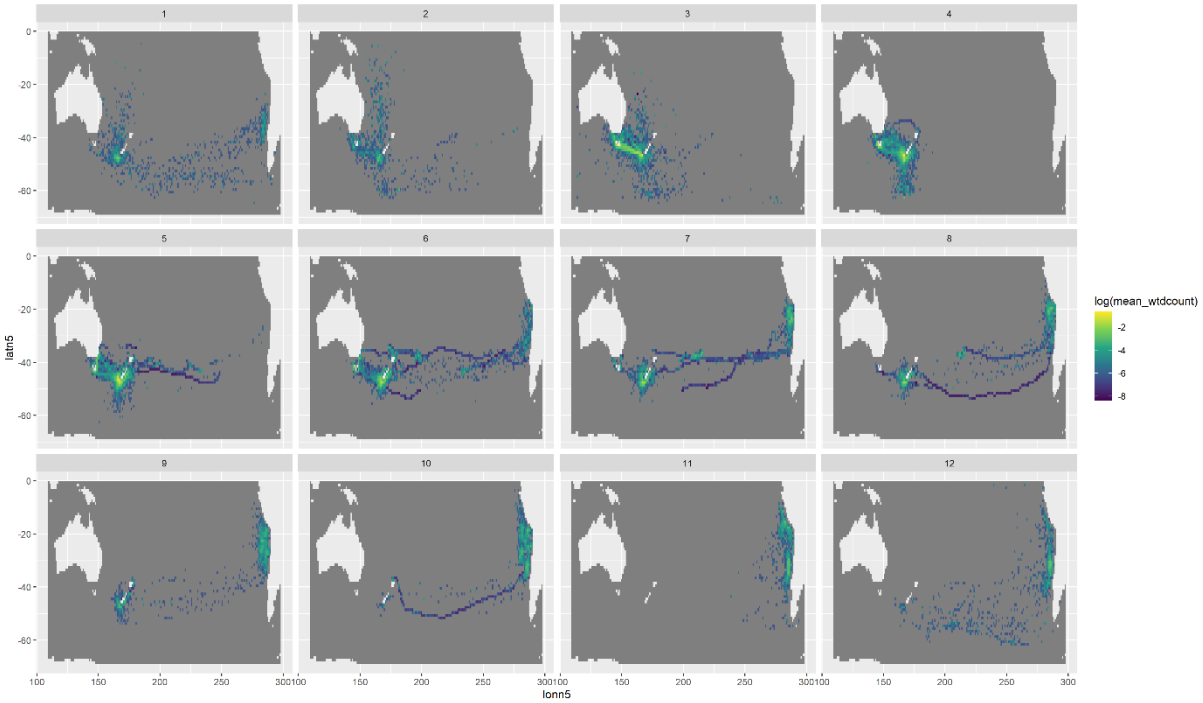

Figure I.35: Log mean weighted relative density by month, aggregated by 1 ° lat-lon grid cell.

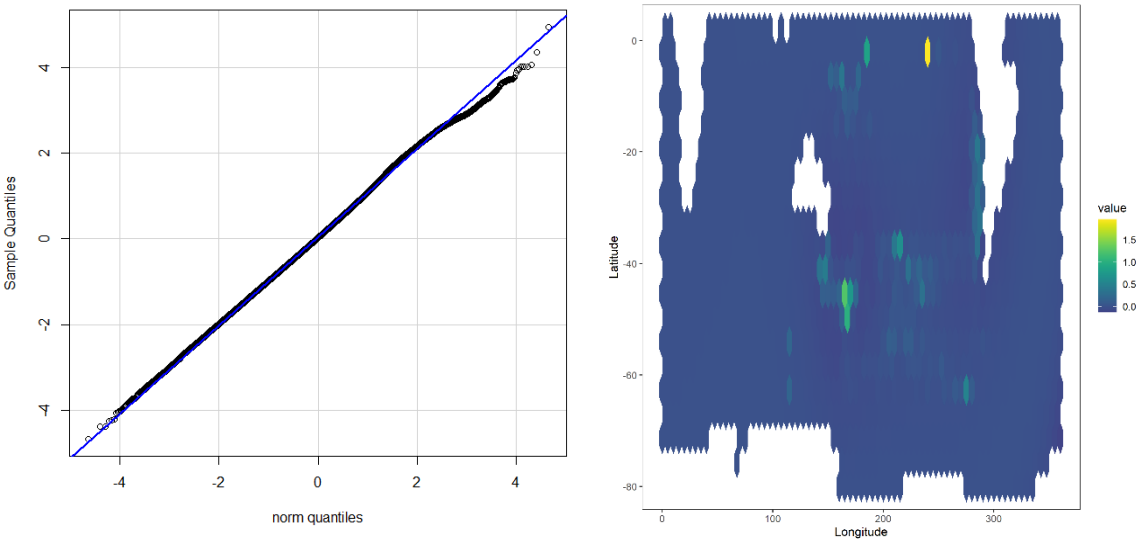

Figure I.36: Model diagnostic plots: residual QQ plot (left) and mean residual pattern by hexagonal grid cell (right).

Appendix J Northern Buller's albatross

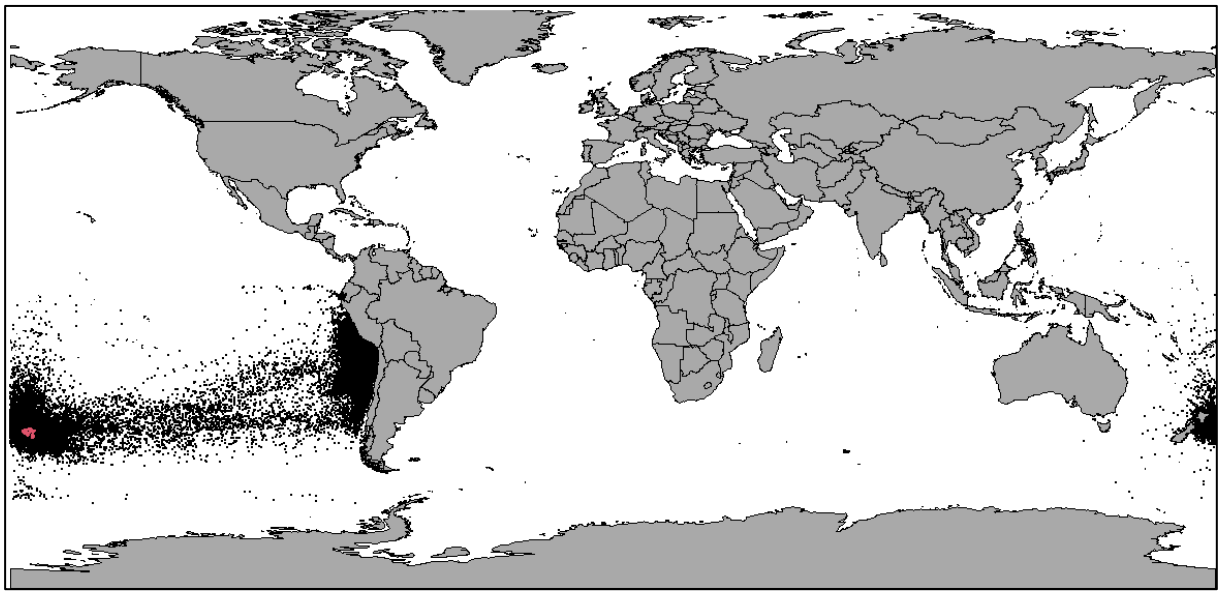

Figure J.37: Locations of ungroomed tracking data for all life stages, where different colours indicate different colonies.

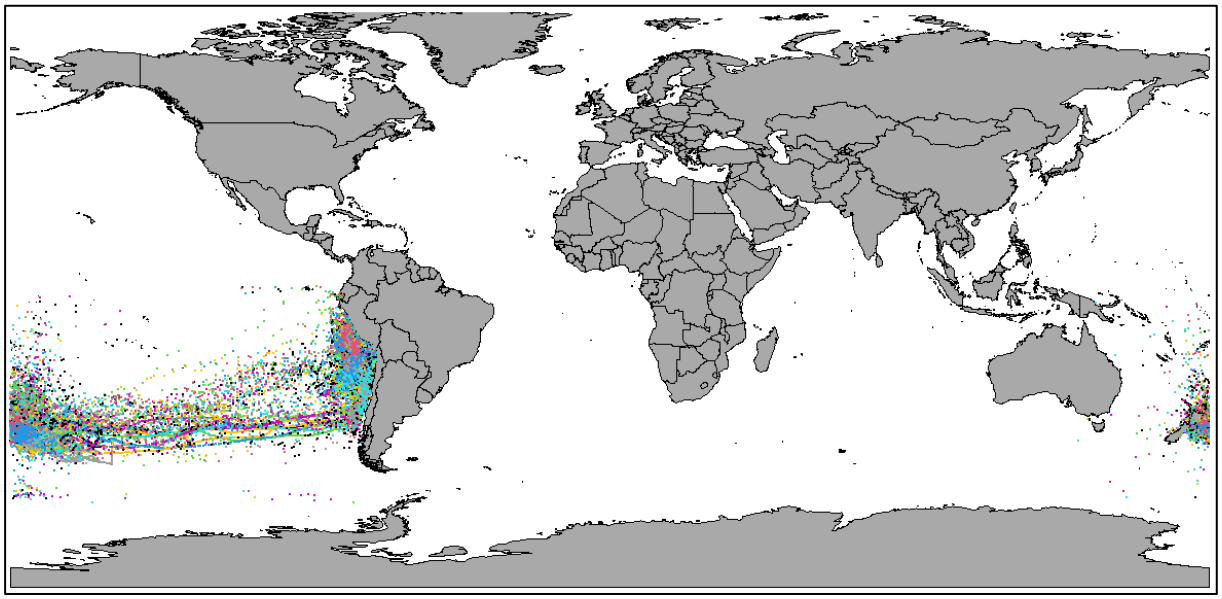

Figure J.38: Groomed and interpolated individual tracks for adult or unknown life stages, where different colours indicate different bird identifiers (noting that colours will repeat).

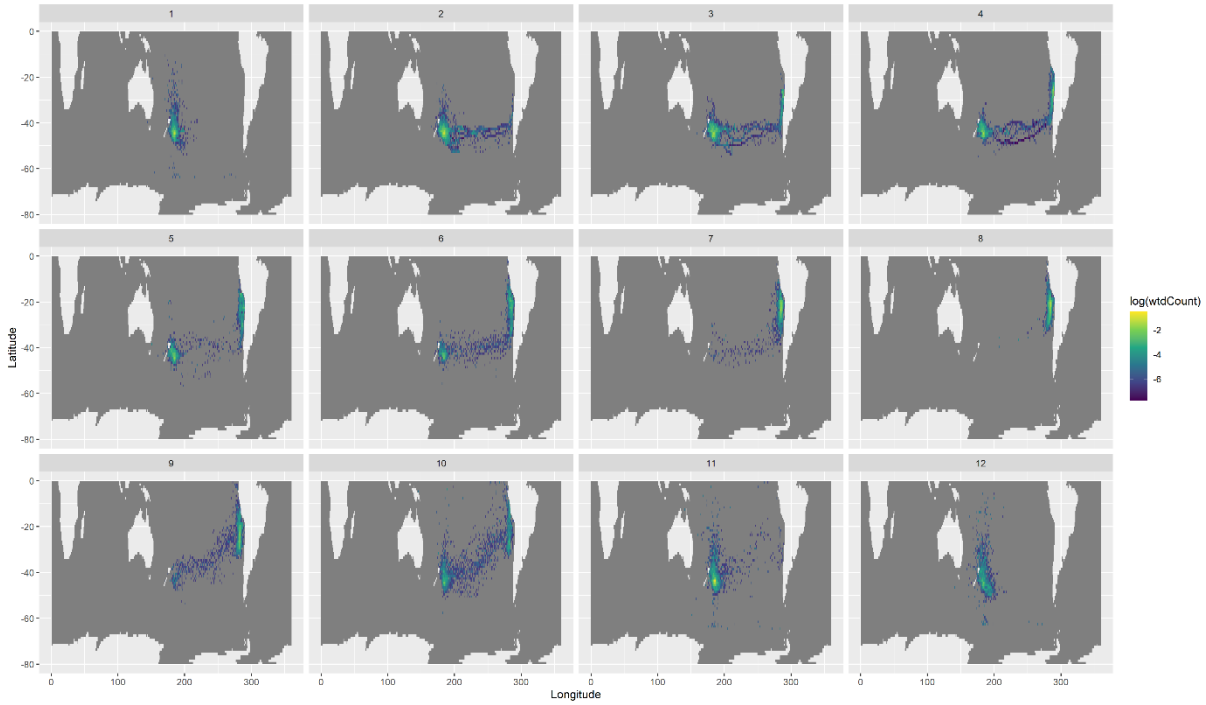

Figure J.39: Log relative density by month, aggregated by 1 ° lat-lon grid cell. Data were not weighted by mean colony size because only one colony was present.

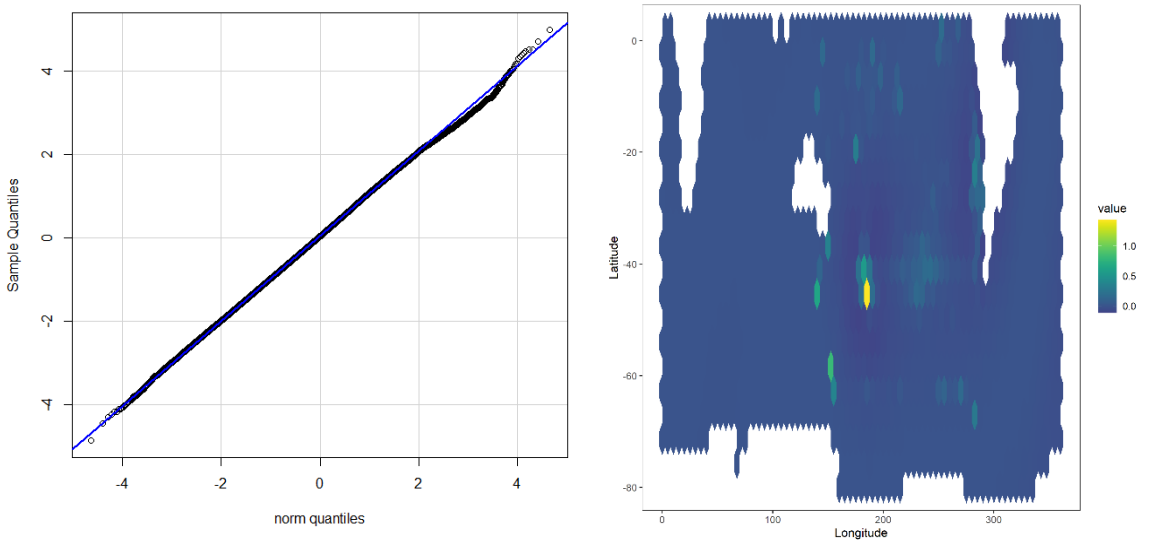

Figure J.40: Model diagnostic plots: residual QQ plot (left) and mean residual pattern by hexagonal grid cell (right).

Appendix K Sooty albatross

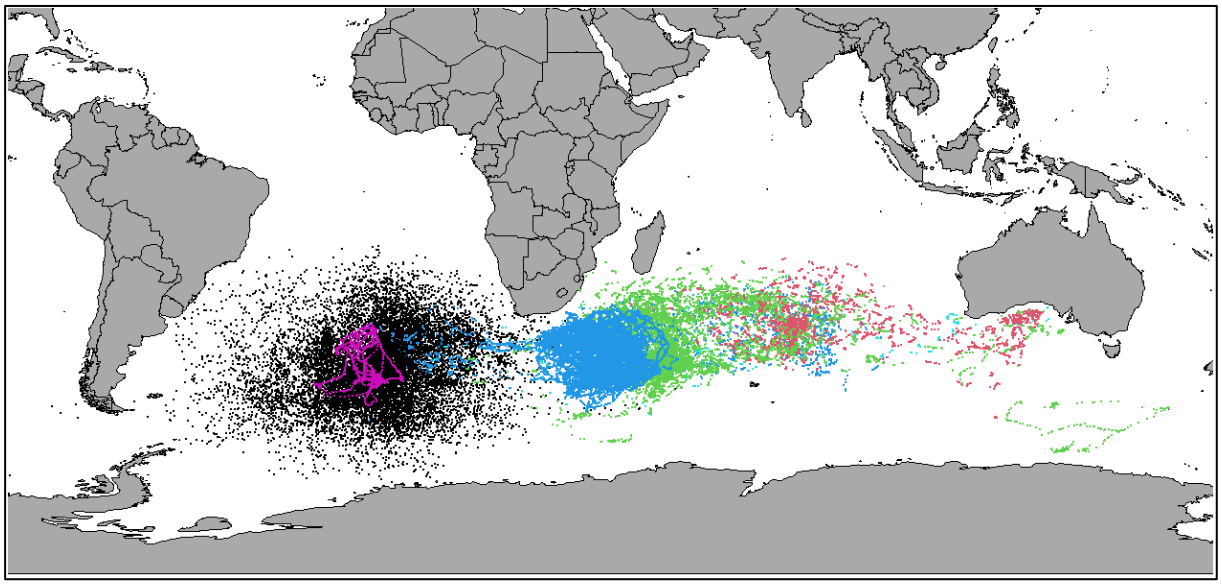

Figure K.41: Locations of ungroomed tracking data for all life stages, where different colours indicate different colonies.

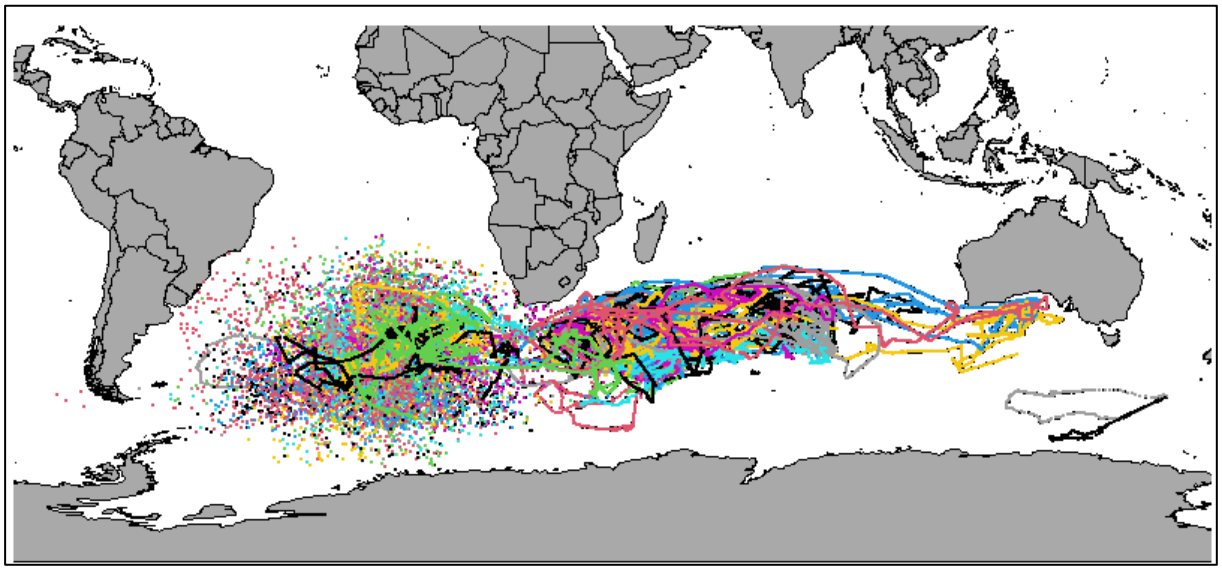

Figure K.42: Groomed and interpolated individual tracks for adult or unknown life stages, where different colours indicate different bird identifiers (noting that colours will repeat).

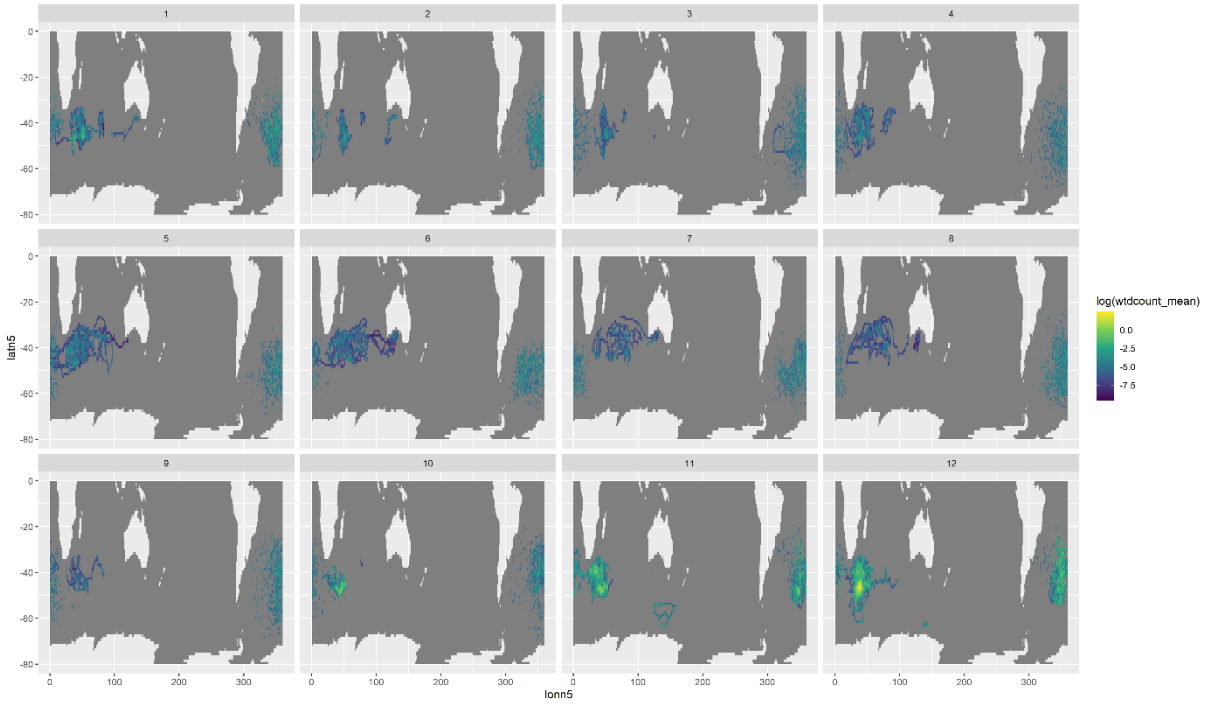

Figure K.43: Log mean weighted relative density by month, aggregated by 1 ° lat-lon grid cell.

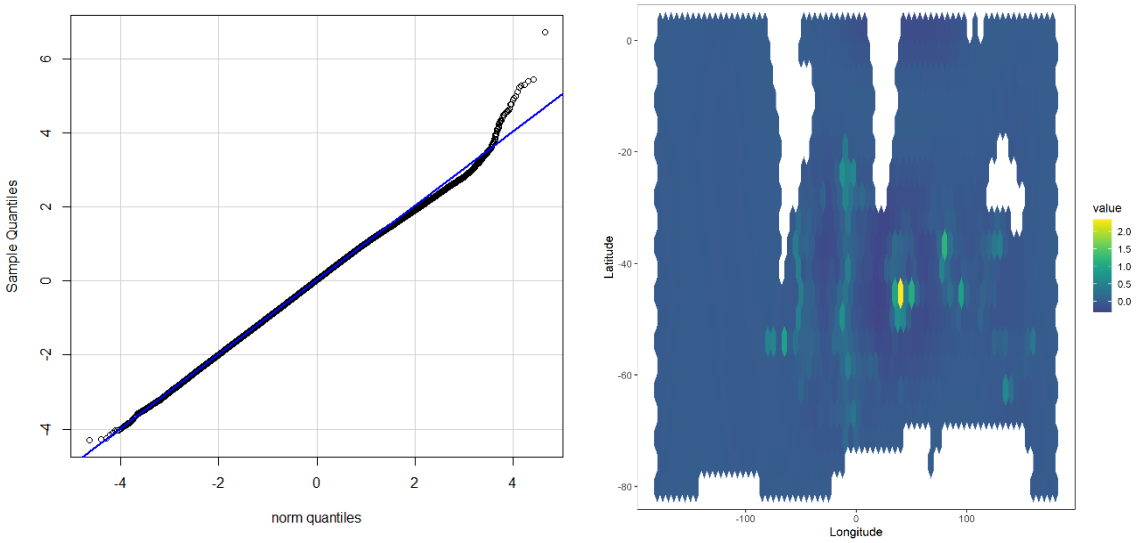

Figure K.44: Model diagnostic plots: residual QQ plot (left) and mean residual pattern by hexagonal grid cell (right).

Appendix L Light-mantled sooty albatross

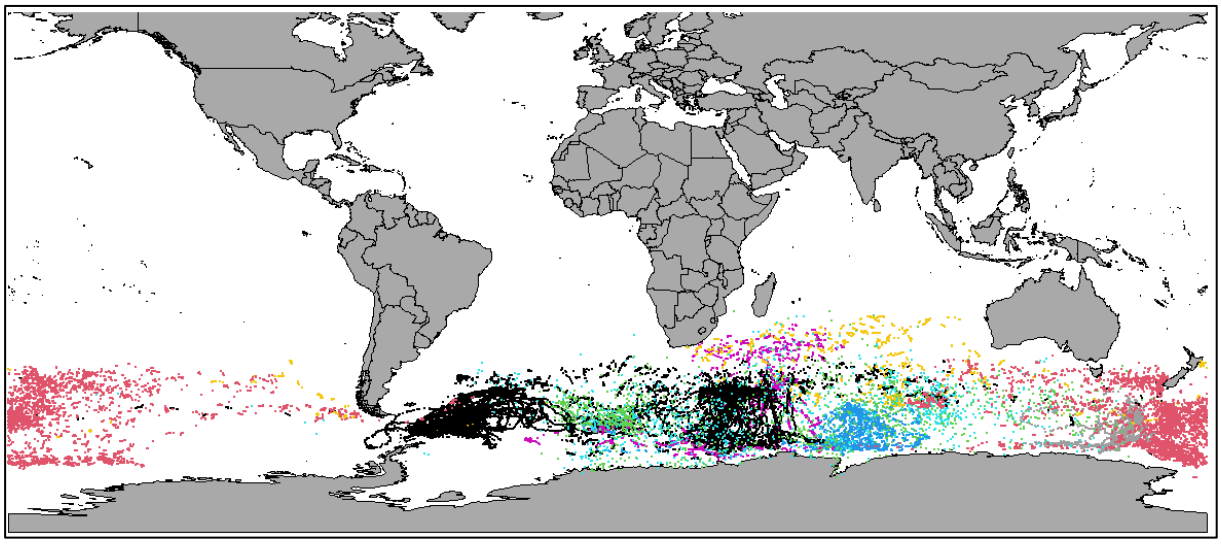

Figure L.45: Locations of ungroomed tracking data for all life stages, where different colours indicate different colonies.

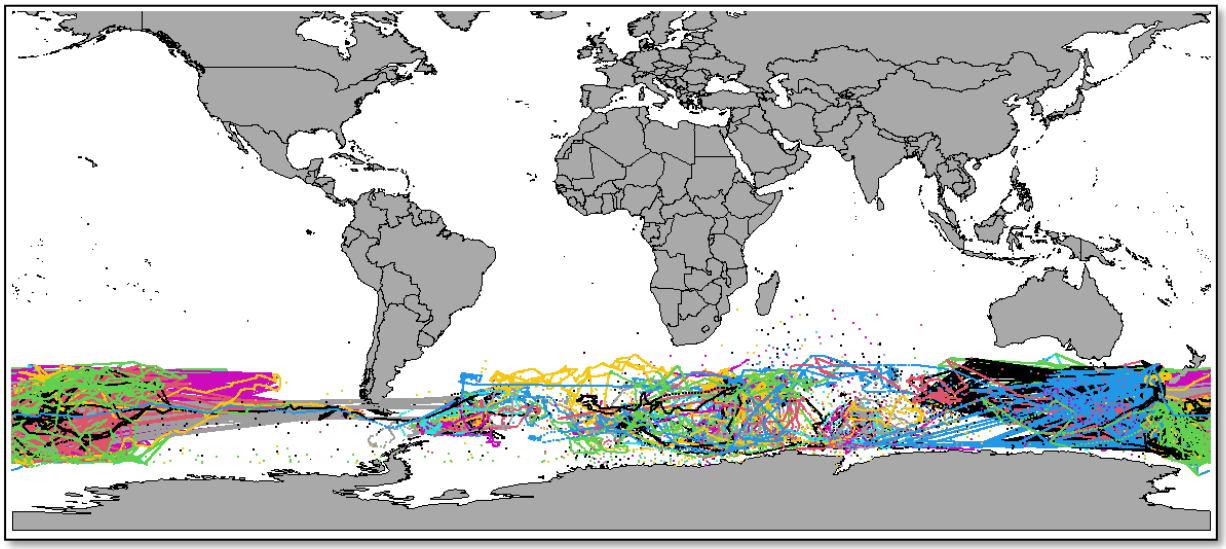

Figure L.46: Groomed and interpolated individual tracks for adult or unknown life stages, where different colours indicate different bird identifiers (noting that colours will repeat).

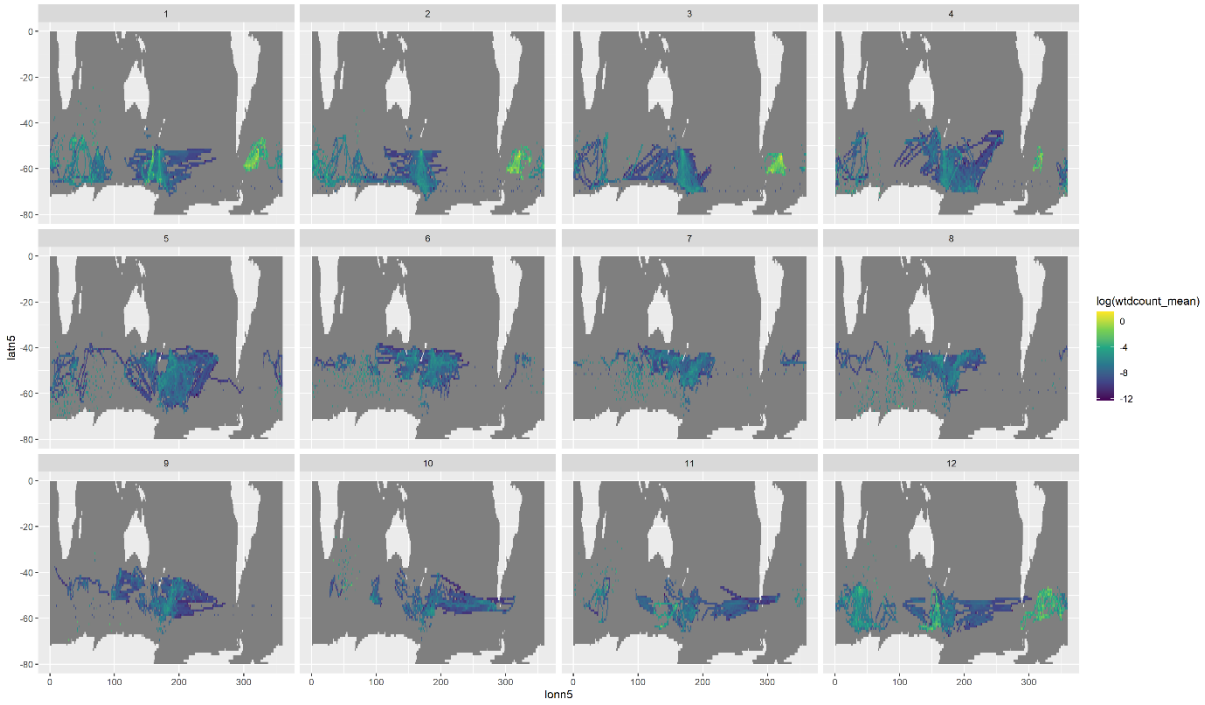

Figure L.47: Log mean weighted relative density by month, aggregated by 1 ° lat-lon grid cell.

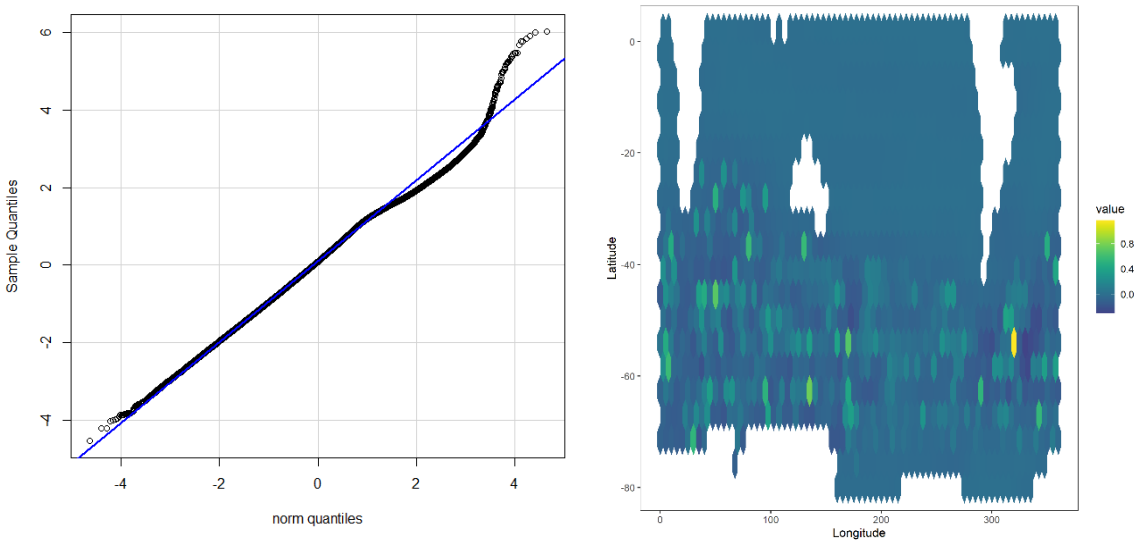

Figure L.48: Model diagnostic plots: residual QQ plot (left) and mean residual pattern by hexagonal grid cell (right).

Appendix M Grey petrel

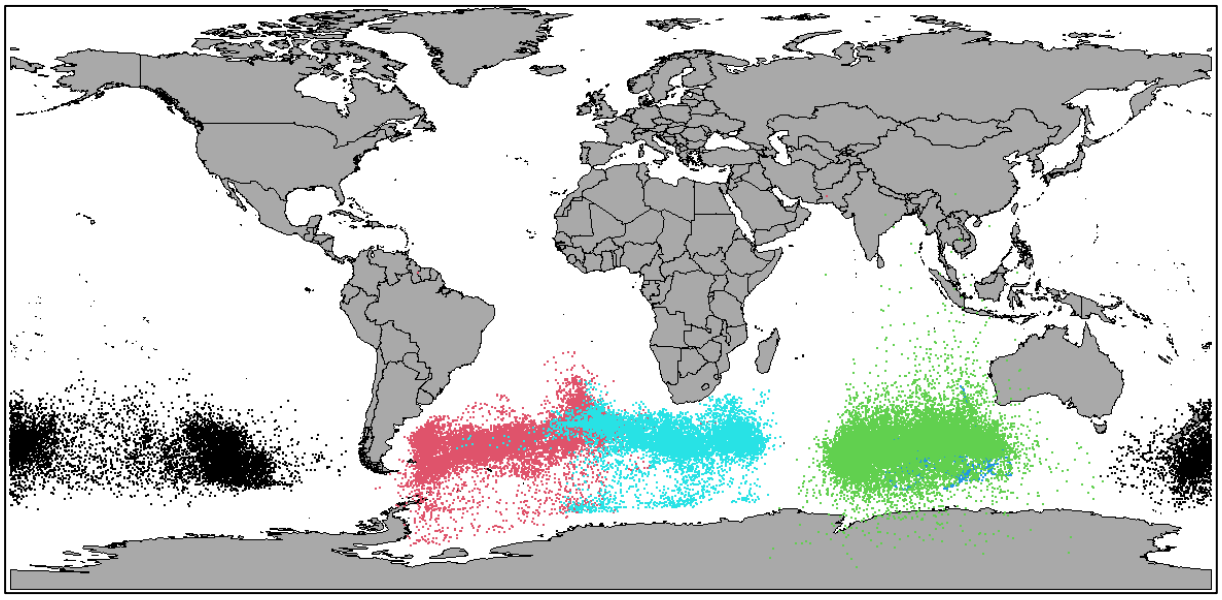

Figure M.49: Locations of ungroomed tracking data for all life stages, where different colours indicate different colonies.

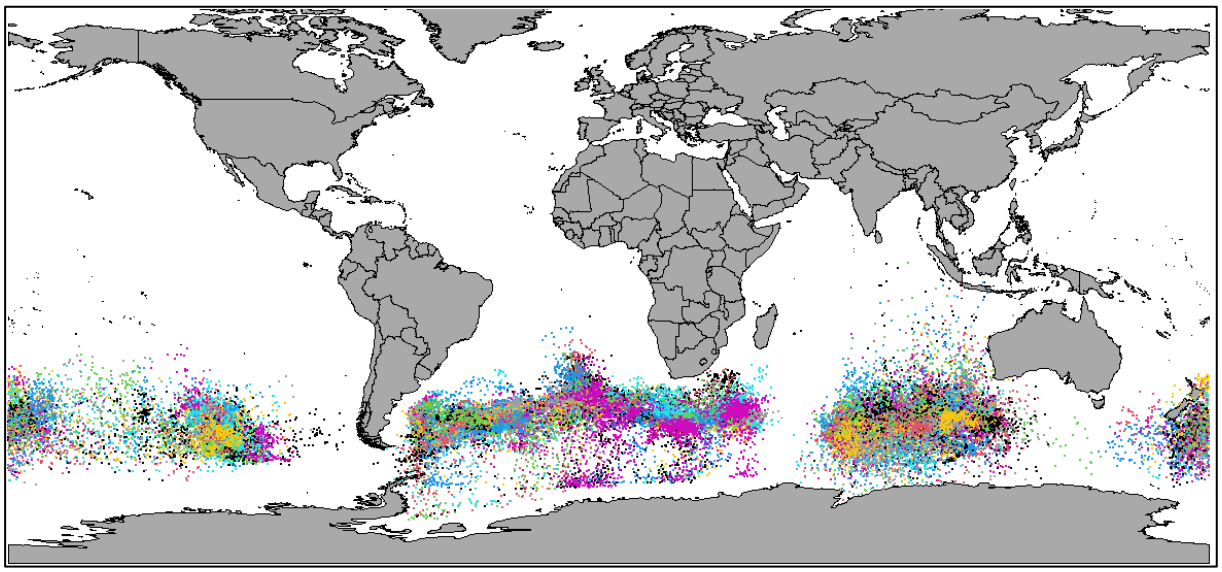

Figure M.50: Groomed and interpolated individual tracks for adult or unknown life stages, where different colours indicate different bird identifiers (noting that colours will repeat).

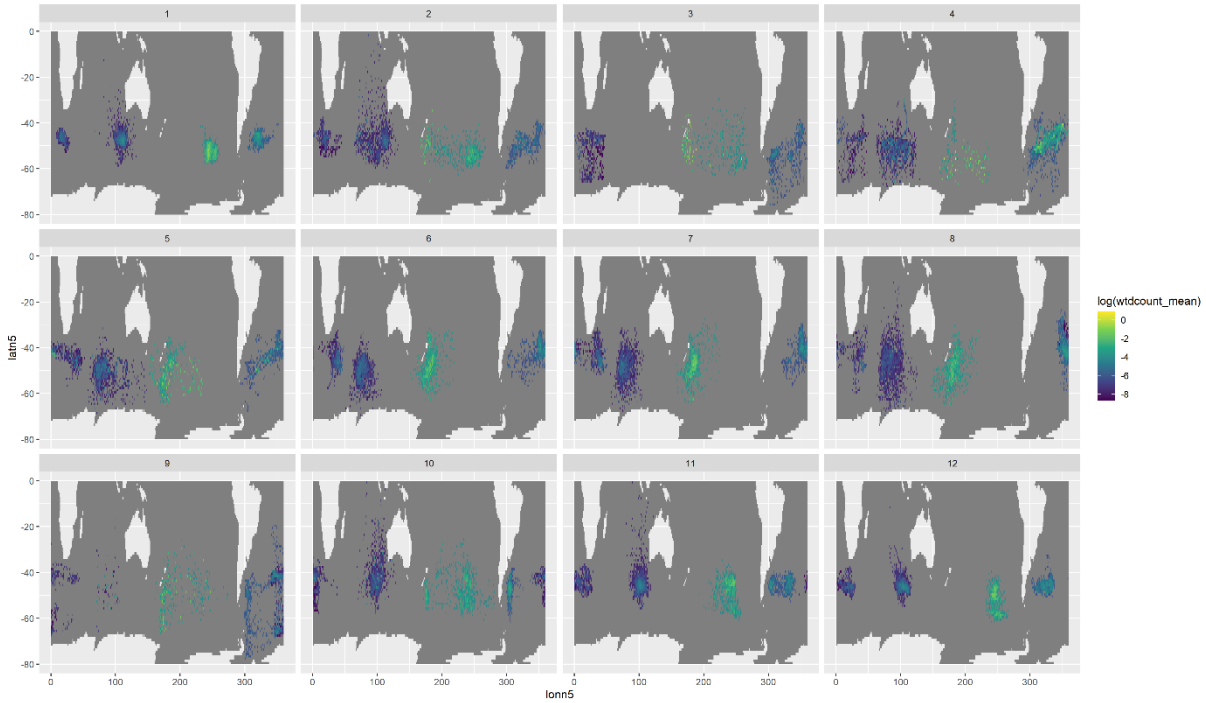

Figure M.51: Log mean weighted relative density by month, aggregated by 1 ° lat-lon grid cell.

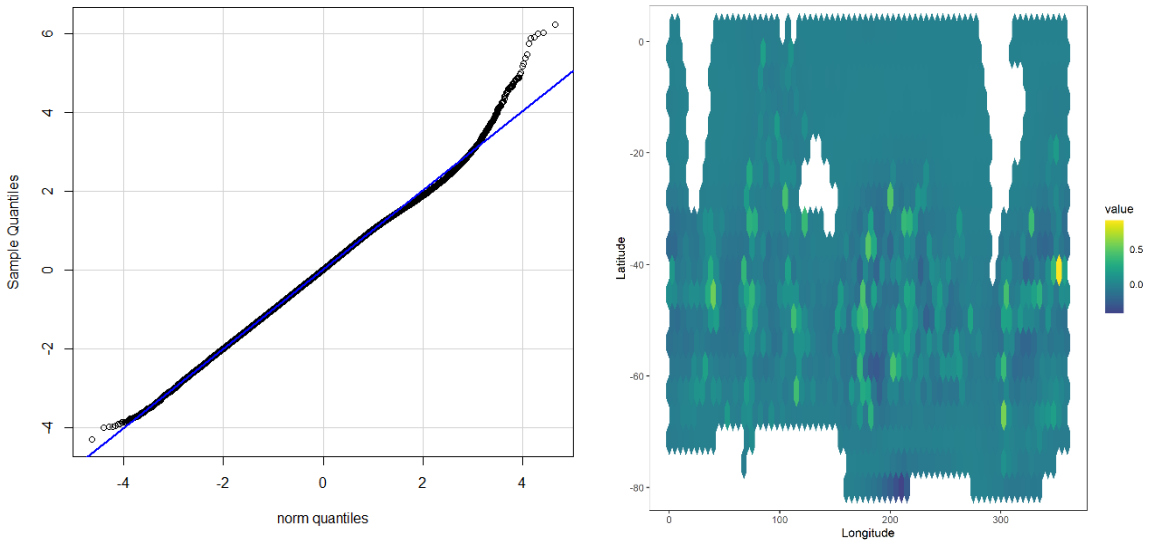

Figure M.52: Model diagnostic plots: residual QQ plot (left) and mean residual pattern by hexagonal grid cell (right).

Appendix N Black petrel

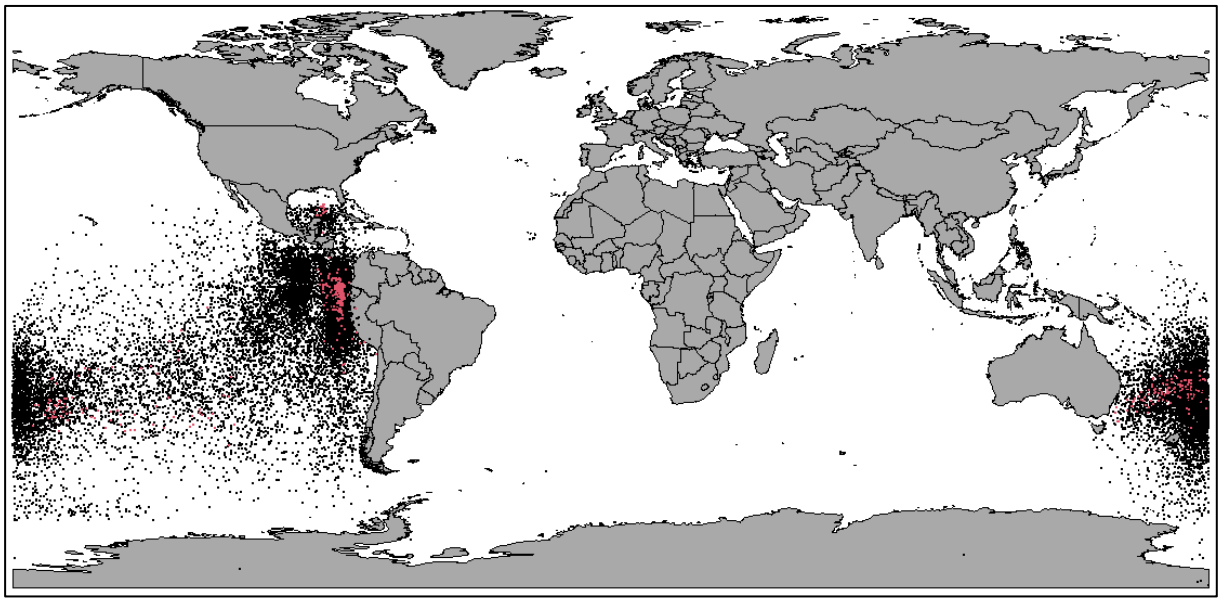

Figure N.53: Locations of ungroomed tracking data for all life stages, where different colours indicate different colonies.

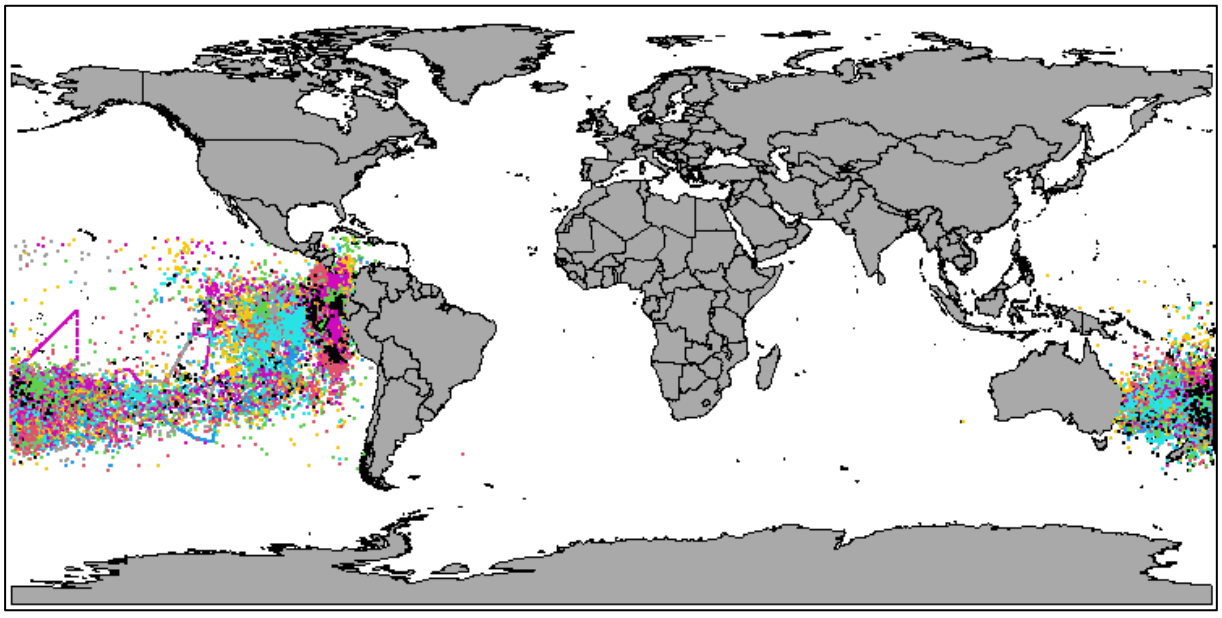

Figure N.54: Groomed and interpolated individual tracks for adult or unknown life stages, where different colours indicate different bird identifiers (noting that colours will repeat).

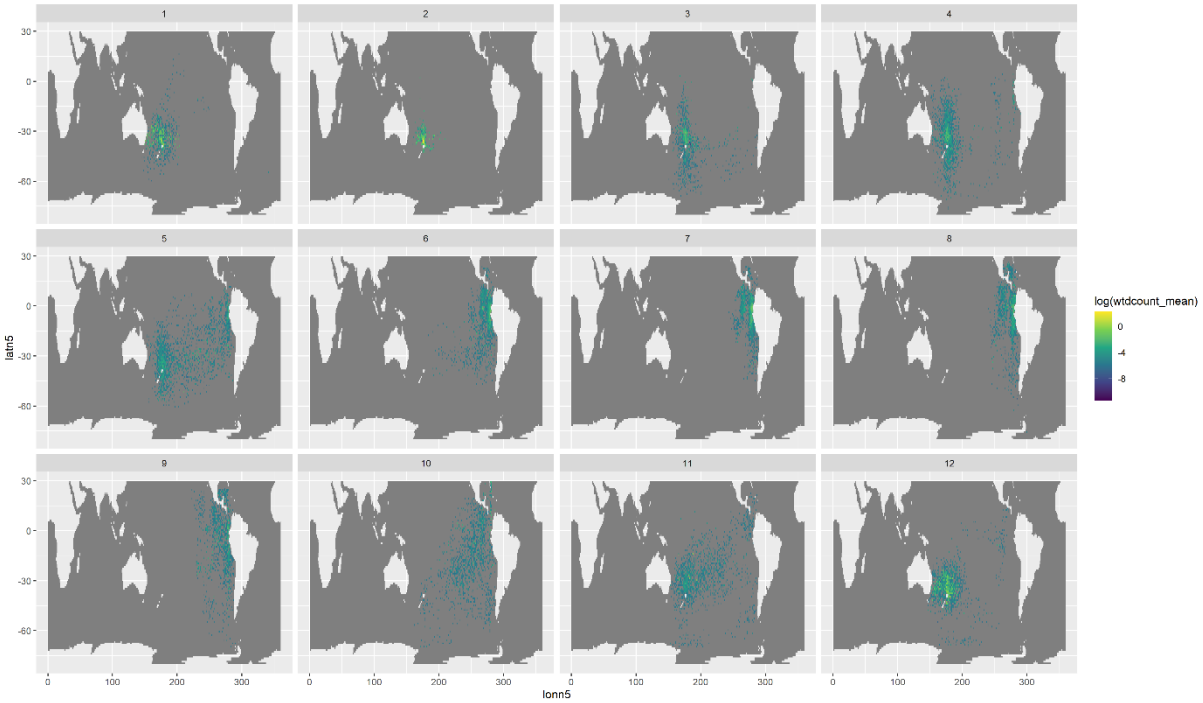

Figure N.55: Log mean weighted relative density by month, aggregated by 1 ° lat-lon grid cell.

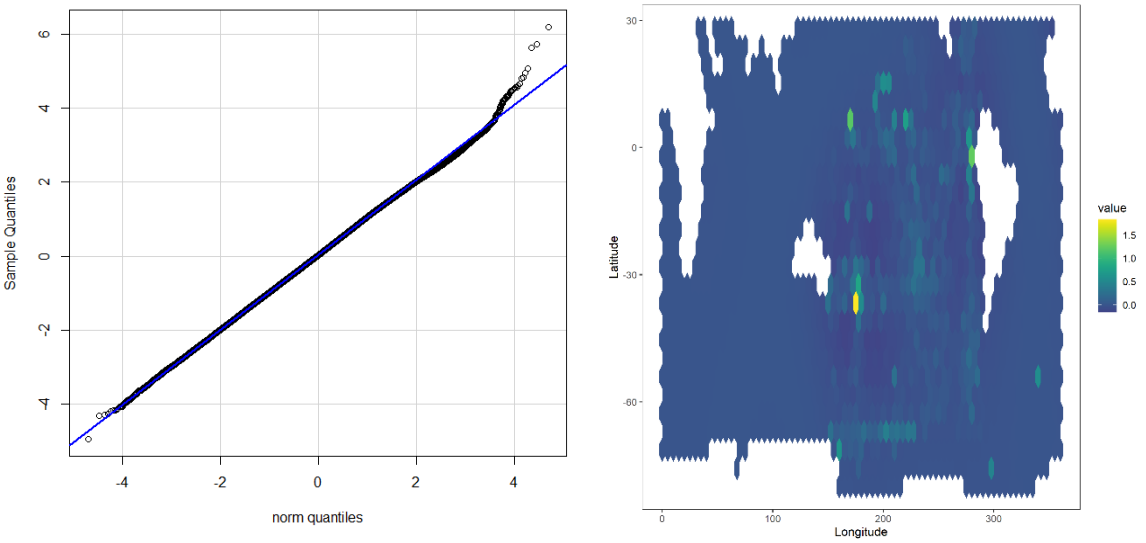

Figure N.56: Model diagnostic plots: residual QQ plot (left) and mean residual pattern by hexagonal grid cell (right).

Appendix O Westland petrel

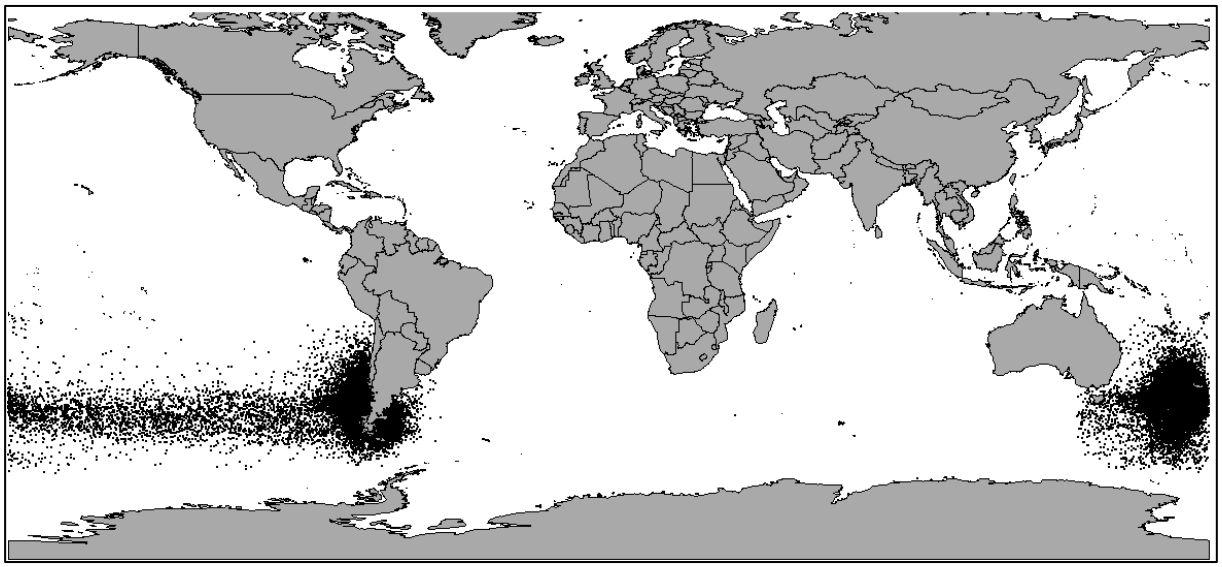

Figure O.57: Locations of ungroomed tracking data for all life stages, where different colours indicate different colonies.

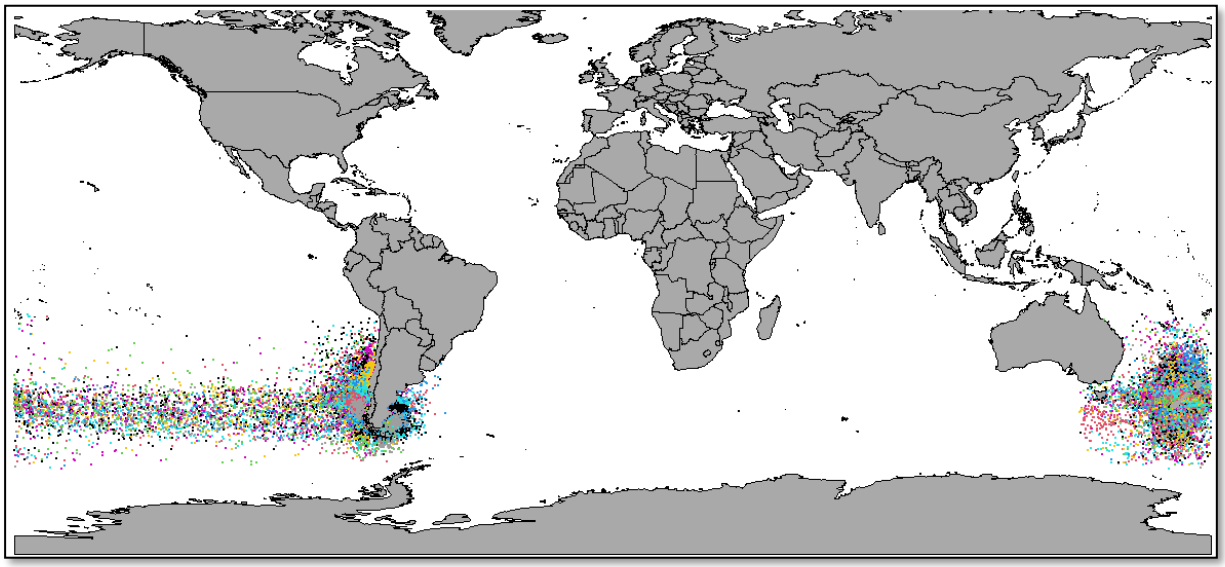

Figure O.58: Groomed and interpolated individual tracks for adult or unknown life stages, where different colours indicate different bird identifiers (noting that colours will repeat).

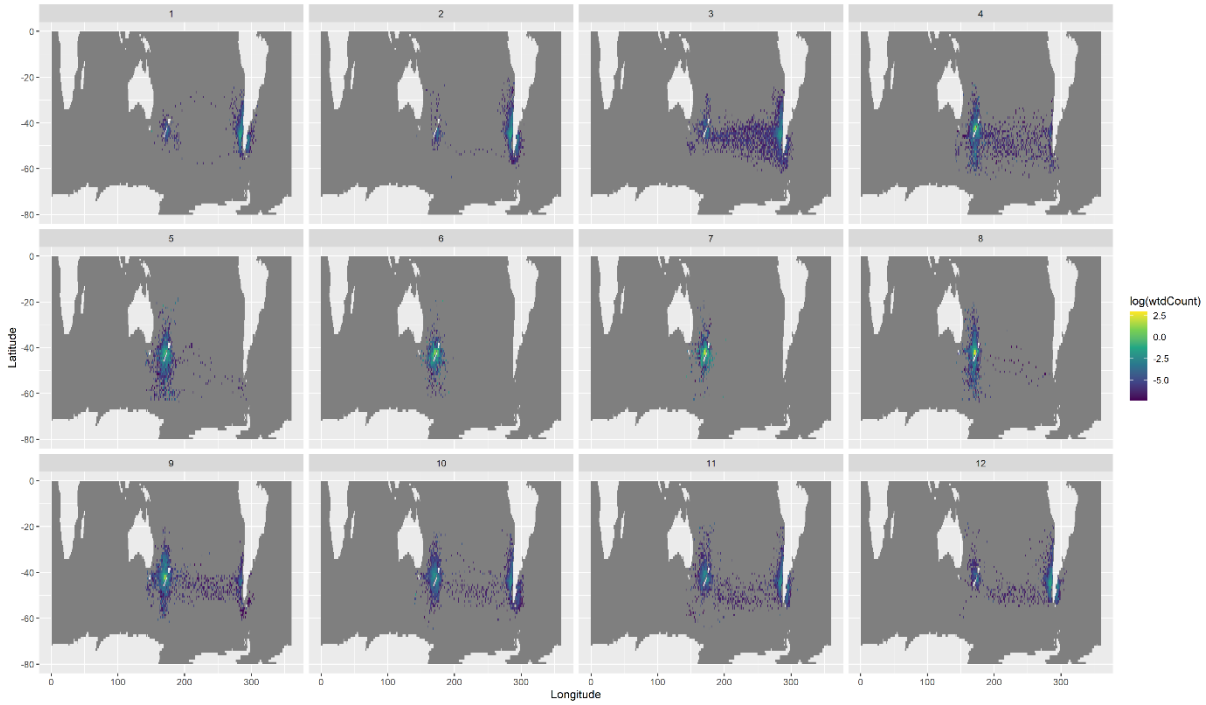

Figure O.59: Log relative density by month, aggregated by 1 ° lat-lon grid cell. Data were not weighted by mean colony size because only one colony was present.

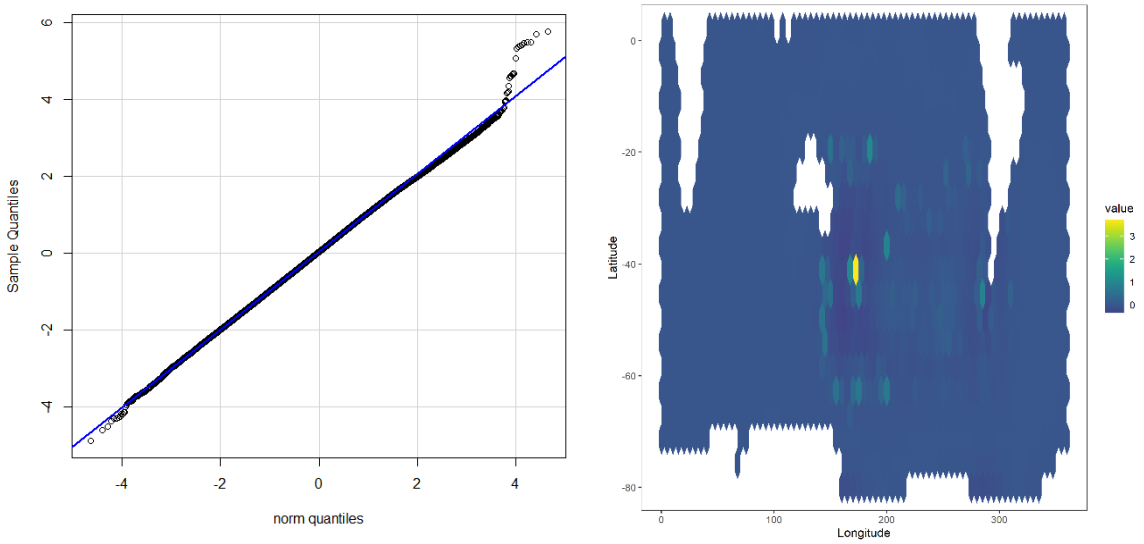

Figure O.60: Model diagnostic plots: residual QQ plot (left) and mean residual pattern by hexagonal grid cell (right).

Appendix P White-chinned petrel

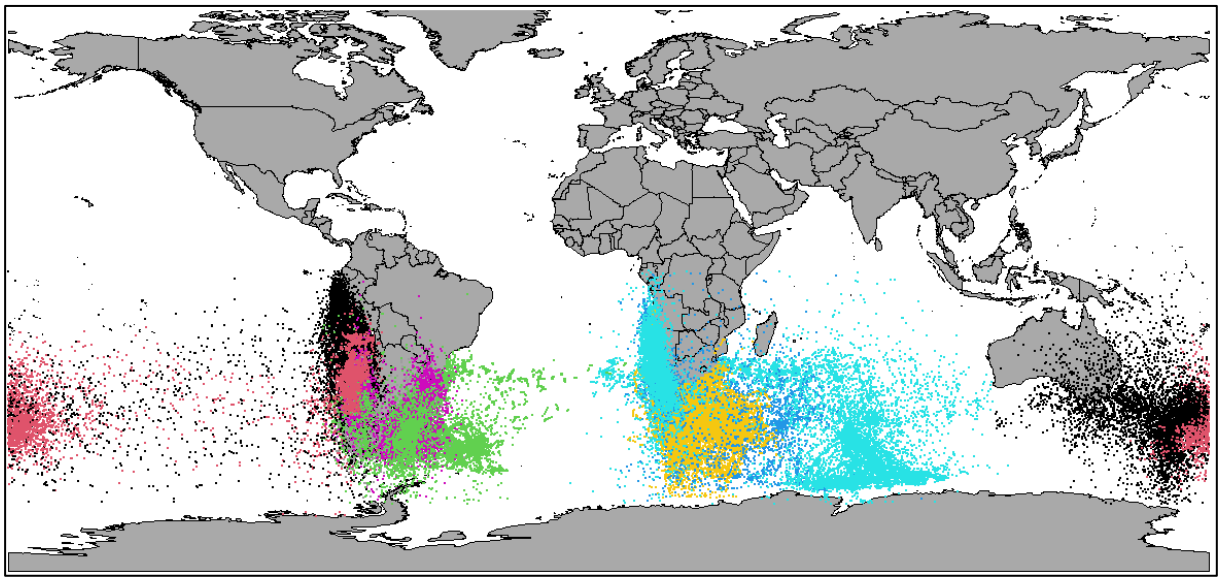

Figure P.61: Locations of ungroomed tracking data for all life stages, where different colours indicate different colonies.

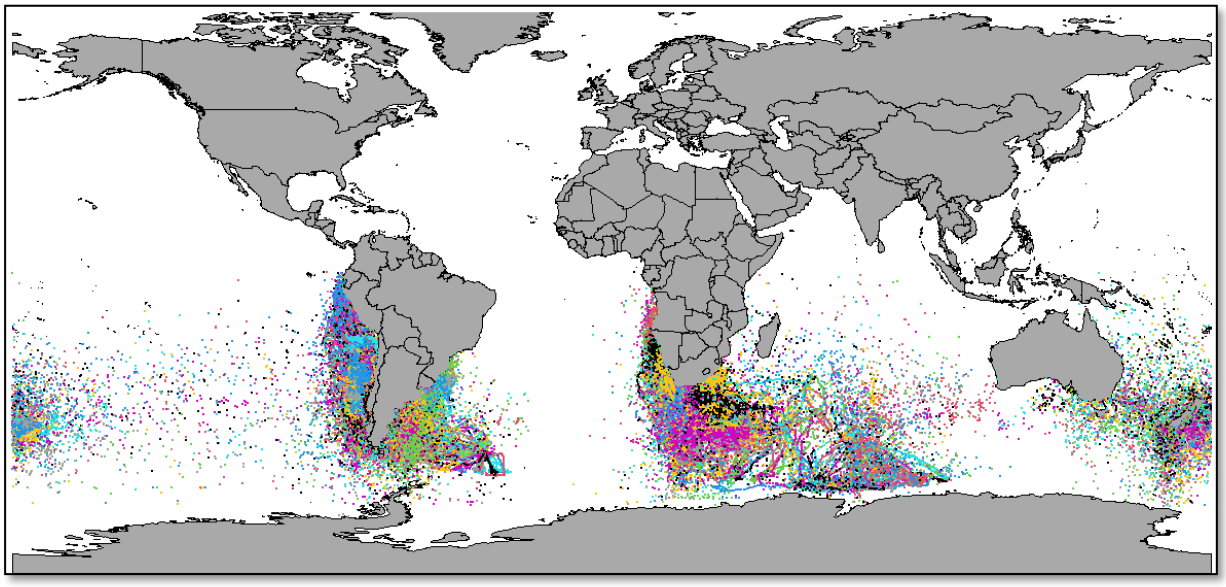

Figure P.62: Groomed and interpolated individual tracks for adult or unknown life stages, where different colours indicate different bird identifiers (noting that colours will repeat).

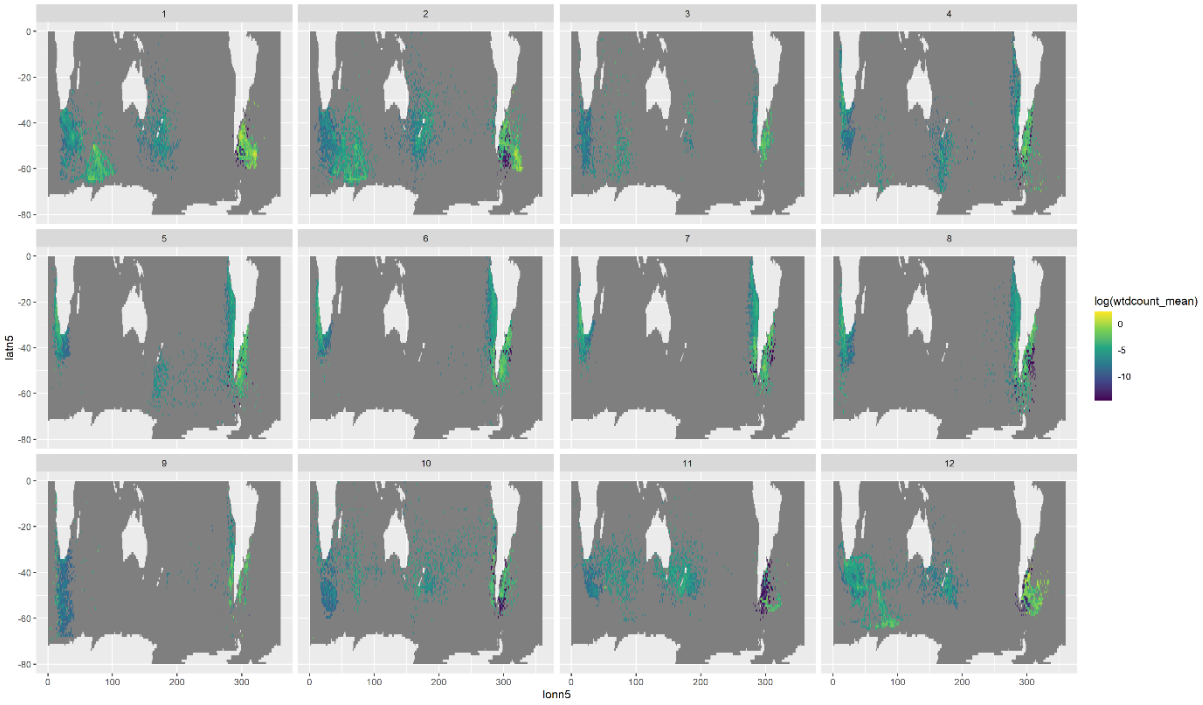

Figure P.63: Log mean weighted relative density by month, aggregated by 1 ° lat-lon grid cell.

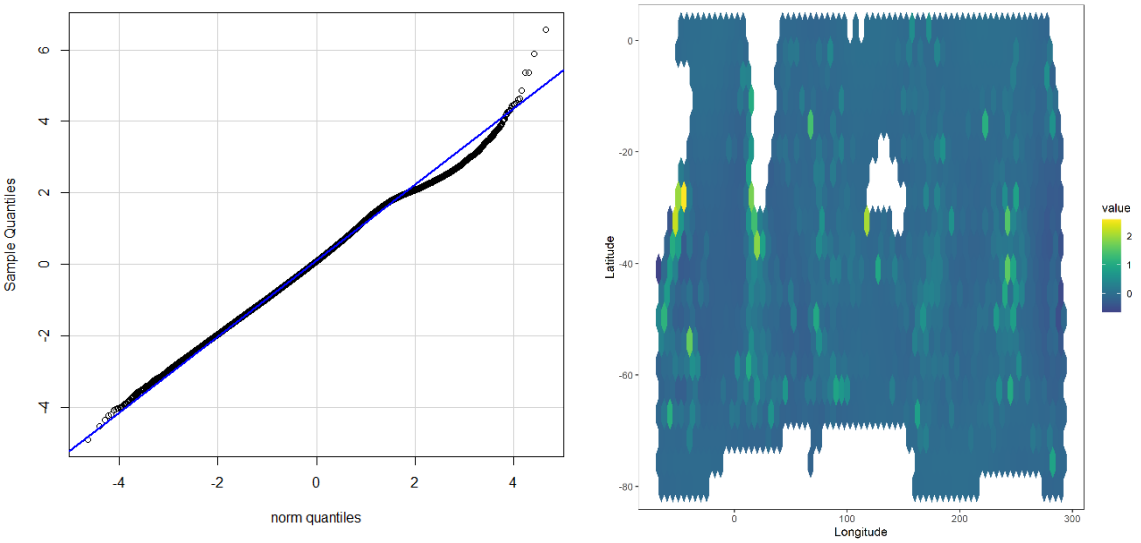

Figure P.64: Model diagnostic plots: residual QQ plot (left) and mean residual pattern by hexagonal grid cell (right).